

# **Modification of Cold Orographic Clouds**

By  
Charles F. Chappell

Department of Atmospheric Science  
Colorado State University  
Fort Collins, Colorado

**Colorado  
State  
University**

**Department of  
Atmospheric Science**

Paper No. 173

MODIFICATION  
OF  
COLD OROGRAPHIC CLOUDS

by

CHARLES F. CHAPPELL

This report was prepared with support provided by  
National Science Foundation Grants  
No. 847, 1553, 11574  
and  
Bureau of Reclamation Contract  
No. 14-06-D-6467

Department of Atmospheric Science  
Colorado State University  
Fort Collins, Colorado

December 1970

Atmospheric Science Paper 173

## ABSTRACT OF DISSERTATION

### MODIFICATION OF COLD OROGRAPHIC CLOUDS

A physical model of the cold orographic cloud system is formulated that simulates natural and seeded snowfall rates and specifies the potential for weather modification. Parameters in the model are evaluated as time-averaged quantities representative of the orographic cloud system in the area of Climax, Colorado.

The availability of weather modification potential in the model cloud is mainly controlled by cloud top temperature. The speed of the orographic updraft exerts only a minor influence on this availability, but has an important influence on the magnitude of the potential. Model theory and physical observations indicate that accretional growth of crystals and ice multiplication probably do not appreciably influence the availability of weather modification potential, only its magnitude.

The model response is compared with results from the randomized ground seeding experiments carried out in the Climax and Wolf Creek Pass areas of Colorado. The model fits reasonably well the observed natural precipitation for the Climax cloud system. Parameters associated with this fit have realistic values. The model forecasts that seeding carried out during this experiment should have caused an increase of about 5 degrees C for the temperature at which the cloud system will maintain high efficiency in producing precipitation. This was observed.

Observations suggest that seeding reduces the number of rimed crystals in the cloud system for all temperatures. In both natural and seeded clouds, accretional growth of crystals becomes significant as the growth rate of ice by vapor diffusion falls below the rate at which the vapor is supplied to the cloud system. Seeding appears to displace the onset of significant riming in the cloud system about 5 degrees C toward warmer cloud temperatures.

Evidence also indicates the dominant effect of seeding warmer Climax cloud systems is to initiate precipitation during many hours, when it would not have occurred naturally. A smaller beneficial effect is to increase precipitation rates during snowfall hours. Implications of these findings upon the existence of cold cloud micro-stability, operational and experimental program designs and precipitation forecasting are discussed. Seeding also appears to suppress precipitation for clouds with very cold temperatures and high wind speeds.

It appears that important additional water may be added to winter snowpacks in the Colorado Rockies by discriminatory cloud seeding programs. Estimates of the additional water to be available on specific mountain barriers can be computed by applying data, gathered in carefully designed field programs, to the model.

Charles F. Chappell  
Atmospheric Science Department  
Colorado State University  
Fort Collins, Colorado 80521  
December, 1970

TABLE OF CONTENTS

<u>Chapter</u>	<u>Page</u>
I. Introduction . . . . .	1
II. Modeling the Cold Orographic Cloud . . . . .	6
III. Experimental Data and Procedures . . . . .	56
IV. Testing the Model . . . . .	61
V. Cloud Microstability and the Nature of the Seeding Effect	117
VI. Overseeding and the Invalidity of the Model . . . . .	128
VII. Analyses of Weather Modification Potential . . . . .	131
VIII. Summary and Conclusions . . . . .	141
REFERENCES . . . . .	151
Appendix A: Contributions of Mean and Deviation Terms . . . . .	158
Appendix B: Fitting the Model Precipitation Equation to Observed Precipitation . . . . .	166
Appendix C: Climax and Wolf Creek Experiments . . . . .	171
Appendix D: Meteorological Analysis Programs . . . . .	190

LIST OF TABLES

<u>Table</u>	<u>Page</u>
1. Estimate of scale changes during seeded periods with respect to non-seeded periods as computed by two non-parametric statistical methods. Precipitation data are from the High Altitude Observatory near Climax and near the summit of Wolf Creek Pass. Scale changes are shown within stratifications of the 500 mb temperature. Data for Climax II (296) and Total Climax (547) samples are shown in parentheses . . . . .	74
2. Same as table 1 except scale changes are shown within stratifications of a computed vertical gradient of saturation mixing ratio below the 500 mb level (potential condensate) . . . . .	77
3. Same as table 1 except scale changes are shown within stratifications of the 700 mb equivalent potential temperature . . . . .	79
4. Same as table 1 except scale changes are shown within stratifications of the 700 mb wind direction . . . . .	81
5. Estimate of scale changes during seeded periods with respect to non-seeded periods as computed by two non-parametric statistical methods. Precipitation data are from the High Altitude Observatory near Climax for the Total Climax (623) and (547) samples. Scale changes are shown within various double stratifications of the meteorological parameters. Data for Total Climax (547) sample are shown in parentheses . . . . .	82
6. Same as table 1 except scale changes are shown within stratifications of the 700 mb wind speed . . . . .	95
7. Same as table 1 except scale changes are shown within stratifications of a convective stability index expressed as the difference in equivalent potential temperature between the 700 mb and 500 mb levels . . . . .	98
8. Same as table 1 except scale changes are shown within stratifications of a computed mean temperature advection in the 700-500 mb layer . . . . .	104

LIST OF TABLES (Continued)

<u>Table</u>	<u>Page</u>
9. Distribution of seeded experimental events among various stratifications of 700 mb equivalent potential temperature and/or 700 mb wind direction for Climax I (251) and Climax II (372) samples . . . . .	110
10. Contingency table showing the number of positive and zero precipitation hours distributed according to seeded and non-seeded conditions for the Total Climax (623) sample, when 700 mb equivalent potential temperatures were 315K through 320K . . . . .	125
11. Contingency table showing the number of positive and zero precipitation hours distributed according to seeded and non-seeded conditions for the Total Climax (623) sample, when 700 mb equivalent potential temperatures were 284K through 289K . . . . .	125
12. Distribution of non-seeded experimental days, experimental precipitation days and experimental zero precipitation days with the concurrent 500 mb temperature for the Total Climax (623) sample . . . . .	126
13. Contingency table showing the number of positive and zero precipitation hours distributed according to seeded and non-seeded conditions for the Total Climax (623) sample, when 700 mb wind speeds were 15 through 28 meters/sec . . . . .	129
14. Estimated changes in precipitation at HAO for a seeded winter season with normal precipitation . . . . .	137
15. Estimated changes in precipitation at Wolf Creek Pass for a winter season with 24 inches of total precipitation and assuming discriminatory seeding . . . . .	139
C1. Location of Climax seeding generators with respect to the primary target . . . . .	179
C2. Climatological data for Climax, Colorado, for the period November through April . . . . .	181

## LIST OF FIGURES

<u>Figure</u>	<u>Page</u>
1. Orographic cloud segment in the x-p plane with typical parcel trajectory . . . . .	7
2. Variation of the thermodynamic function ( $F_T$ ) with temperature and pressure . . . . .	16
3. Average crystal sizes observed near Climax, Colorado, as a function of 500 mb temperature. Observations are from 11 snowfall days . . . . .	17
4. Theoretical, observed and empirically deduced crystal growth rates as a function of environmental temperature . . . . .	19
5. The onset of significant accretional growth in the Climax cloud system (measured by the percentage of total crystals rimed) as a function of 500 mb temperature . . . . .	26
6. Concentrations of effective primary ice nuclei as a function of environmental temperature . . . . .	29
7. The ratio of ice crystal concentration to corresponding ice nuclei concentration as a function of cloud top temperature . . . . .	31
8. Ice crystal habit regions as a function of temperature and vapor saturation . . . . .	35
9. Relationship of ice crystal concentration, ice crystal size, vertical motion and 500 mb temperature which optimizes the efficiency of cloud water utilization. Cloud base and top are assumed to be 650 mb and 460 mb respectively . . . . .	49
10. The difference between natural and optimum ice crystal concentrations for various crystal sizes and upward speeds as a function of 500 mb temperature. Cloud base and top are assumed to be 650 mb and 460 mb respectively . . . . .	50

LIST OF FIGURES (Continued)

<u>Figure</u>	<u>Page</u>
11. Distribution of non-seeded precipitation at HAO as a function of 500 mb temperature compared to a theoretical distribution computed using the mean diffusional model. Precipitation data are from Climax I sample (251) and values are a running mean over a two-degree temperature interval . . . . .	64
12. Distribution of non-seeded precipitation at HAO as a function of 500 mb temperature compared to a theoretical distribution computed using the mean diffusional model. Precipitation data are from Climax II sample (372) and values are a running mean over a two-degree temperature interval . . . . .	65
13. Same as figure 11 except for seeded precipitation . .	67
14. Same as figure 12 except for seeded precipitation . .	68
15. Change and percentage change in mean daily precipitation during seeded days compared with non-seeded days as a function of 500 mb temperature for Climax I (251) (upper) and Climax II (372) (lower) samples. Lines are third degree polynomial curve fits to the plotted values . . . . .	70
16. Relationship of 500 mb temperature with 700 mb wind direction for non-seeded days (upper) and seeded days (lower) for Climax I sample (251). Curve is a second degree polynomial curve fit to the observed meteorological data . . . . .	83
17. Relationship of 500 mb temperature with 700 mb wind direction for non-seeded days (upper) and seeded days (lower) for Climax II sample (372). Curve is a second degree polynomial curve fit to the observed meteorological data . . . . .	84
18. Relationship of 700 mb equivalent potential temperature with 700 mb wind direction for non-seeded days (upper) and seeded days (lower) for Climax I sample (251). Curve is a second degree polynomial curve fit to the observed meteorological data . . . . .	85
19. Relationship of 700 mb equivalent potential temperature with 700 mb wind direction for non-seeded days (upper) and seeded days (lower) for Climax II sample (372). Curve is a second degree polynomial curve fit to the observed meteorological data. . . . .	86

LIST OF FIGURES (Continued)

<u>Figure</u>	<u>Page</u>
20. Relationship of 700 mb wind speed with 500 mb temperature for seeded and non-seeded days of the Climax I sample (upper) and Climax II sample (lower). Curve is a second degree polynomial curve fit to the observed meteorological data . . . . .	87
21. Relationship of 700 mb wind speed with 700 mb equivalent potential temperature for seeded and non-seeded days of the Climax I sample (upper) and Climax II sample (lower). Curve is a second degree polynomial curve fit to the observed meteorological data . . . . .	88
22. Relationship of 500 mb temperature with 700 mb wind direction for non-seeded days (upper) and seeded days (lower) for Wolf Creek sample (441). Curve is a second degree polynomial curve fit to the observed meteorological data . . . . .	91
23. Relationship of 700 mb equivalent potential temperature with 700 mb wind direction for non-seeded days (upper) and seeded days (lower) for Wolf Creek sample (441). Curve is a second degree polynomial curve fit to the observed meteorological data . . . . .	92
24. Relationship of 700 mb wind speed with 500 mb temperature for non-seeded days (upper) and seeded days (lower) for Wolf Creek sample (441). Curve is a second degree polynomial curve fit to the observed meteorological data . . . . .	93
25. Relationship of 700 mb wind speed with 700 mb equivalent potential temperature for non-seeded days (upper) and seeded days (lower) for Wolf Creek sample (441). Curve is a second degree polynomial curve fit to the observed meteorological data . . . . .	94
26. Relationship of the convective stability index with 700 mb wind direction for non-seeded days (upper) and seeded days (lower) for Climax I sample (251). Curve is a second degree polynomial curve fit to the observed meteorological data . . . . .	100
27. Relationship of the convective stability index with 700 mb wind direction for non-seeded days (upper) and seeded days (lower) for Climax II sample (372). Curve is a second degree polynomial curve fit to the observed meteorological data . . . . .	101

LIST OF FIGURES (Continued)

<u>Figure</u>	<u>Page</u>
28. Relationship of the convective stability index with 500 mb temperature for seeded and non-seeded days of the Climax I sample (upper) and Climax II sample (lower). Curve is a second degree polynomial curve fit to the observed meteorological data . . . . .	102
29. Relationship of the convective stability index with 700 mb wind direction for non-seeded days (upper) and seeded days (lower) for Wolf Creek sample (441). Curve is a second degree polynomial curve fit to the observed meteorological data . . . . .	103
30. Percentage change in average precipitation during seeded days compared with non-seeded days for 500 mb temperatures from -20C through -11C. Results are shown for Total Climax sample (623). . . . .	108
31. Same as figure 30 except for 500 mb temperatures from -18C through -11C . . . . .	108
32. Percentage change in average precipitation during seeded days compared with non-seeded days for Climax I (251) sample (left) and Climax II (372) sample (right)	109
33. Percentage change in average precipitation during seeded days compared with non-seeded days for 700 mb wind directions 190 through 250 degrees. Results are shown for Climax I (251) sample (left) and Climax II (372) sample (right) . . . . .	112
34. Percentage change in average precipitation during seeded days compared with non-seeded days for 700 mb wind directions 310 through 360 degrees. Results are shown for Climax I (251) sample (left) and Climax II (372) sample (right) . . . . .	113
35. Percentage change in average precipitation during seeded days compared with non-seeded days for equivalent potential temperatures from 308K to less than 326K and 700 mb wind directions from 310 through 360 degrees for Total Climax sample (623) . . . . .	114
36. Same as figure 35 except for 700 mb wind directions from 190 through 250 degrees . . . . .	114

LIST OF FIGURES (Continued)

<u>Figure</u>	<u>Page</u>
37. Seeded to non-seeded ratios of total precipitation change, precipitation duration change and precipitation intensity change. Ratios were generated as a function of 700 mb equivalent potential temperature by computing running means over a five-degree temperature interval. Precipitation data were measured at HAO during experimental days of the Total Climax (623) sample . . . . .	120
38. Precipitation duration and intensity change ratios as a function of the total precipitation change ratio . . . . .	123
39. Distributions of seeded and non-seeded precipitation at HAO as a function of 500 mb temperature. Precipitation data are from Climax I (251) sample and values are a running mean over a two-degree temperature interval . . . . .	133
40. Same as figure 39 except for Climax II (372) sample .	134
41. Distribution of non-seeded precipitation at Wolf Creek Pass as a function of 500 mb temperature compared to a theoretical distribution computed using the weather modification potential model. Precipitation data are from Wolf Creek (441) sample and values are a running mean over a four-degree temperature interval . . . . .	138
B1. Average number of hours of precipitation per day recorded at Climax 2NW gage during Climax I (251) experimental days and experimental precipitation days as a function of 500 mb temperature. Values were computed using a running average over a three-degree temperature interval . . . . .	170
C1. Seeding output as a function of temperature for generator used in the Climax experiment (Effective particles/gm AgI) . . . . .	174
C2. Topography of Climax experimental area . . . . .	175
C3. Climax experimental area showing location of seeding generators, snowfall observing network and snowboard grouping . . . . .	177

LIST OF FIGURES (Continued)

<u>Figure</u>		<u>Page</u>
C4.	Diurnal distribution of precipitation observed at Climax 2NW recording gage. Data are from the period November through April for the years 1953 through 1968 . . . . .	183
C5.	Cumulative frequency of snowfall at Climax 2NW recording gage as a function of hourly precipitation intensity. Data are from the period November through April for the years 1953 through 1968 . . . . .	184
C6.	Relative and cumulative percentage of snowfall at HAO as a function of 500 mb temperature . . . . .	185
C7.	Relative and cumulative percentage of snowfall at HAO as a function of 700 mb equivalent potential temperature . . . . .	186
C8.	Wolf Creek Pass Experimental Area . . . . .	189

## LIST OF SYMBOLS

### English Letters

A	coefficient in exponential equation
a	temperature function in droplet growth equation
B	coefficient in exponential equation
b	solute function in droplet growth equation
C	capacity factor in crystal growth equation
c	crystal thickness
D	diffusivity of water vapor in air
D <sub>5</sub>	500 mb wind direction
D <sub>7</sub>	700 mb wind direction
E	collection efficiency of ice crystal for cloud droplets
e	vapor pressure
E <sub>i</sub>	evaporation of ice per unit volume
e <sub>i</sub>	evaporation of ice per unit mass
e <sub>s</sub>	saturation vapor pressure over a plane water surface
E <sub>w</sub>	evaporation of liquid water per unit volume
e <sub>w</sub>	evaporation of liquid water per unit mass
e <sub>si</sub>	saturation vapor pressure over a plane ice surface
e <sub>sL</sub>	saturation vapor pressure of a lifted parcel
F <sub>1</sub>	ventilation factor of the crystal in the airflow
F <sub>2</sub>	vapor factor that corrects the vapor field to that of a supercooled cloud

LIST OF SYMBOLS (Continued)

English Letters

$F_T$	thermodynamic function in crystal growth equation
G	thermodynamic function in droplet growth equation
g	acceleration of gravity
$G^t$	thermodynamic function in crystal growth equation
K	thermal conductivity of air
$k_a$	continuous function of temperature (empirically derived)
$k_c$	continuous function of temperature (empirically derived)
L	latent heat of vaporization
l	liquid water mixing ratio
$L_i$	latent heat of sublimation
m	crystal mass
N	number of effective primary ice nuclei per unit volume
$N_c$	number of ice crystals per unit volume
$n_c$	number of ice crystals per unit mass
$N_{co}$	optimum number of ice crystals per unit volume
P	environmental air pressure
p	ambient air pressure
$P_5$	500 mb pressure
$P_7$	700 mb pressure
$P_c$	pressure at condensation level
$P_s$	snowfall intensity per unit volume
$p_s$	snowfall intensity per unit mass
q	specific humidity

LIST OF SYMBOLS (Continued)

English Letters

$Q_1, Q_2, Q_3$	thermodynamic functions in cloud supersaturation equation
$Q_w$	mass of liquid water per unit volume
$R$	gas constant for air
$r$	vapor mixing ratio crystal radius
$R_c$	ratio of ice crystal concentration to ice nuclei concentration
$r_d$	cloud droplet radius
$R_e$	Reynold's Number
$r_e$	equivalent radius of a crystal having the same droplet volume
$RH_5$	500 mb relative humidity
$RH_7$	700 mb relative humidity
$r_s$	saturation vapor mixing ratio
$R_v$	gas constant for water vapor
$s$	ice mixing ratio
$S_i$	supersaturation relative to a plane ice surface
$S_w$	supersaturation relative to a plane water surface
$T$	ambient temperature
$T_5$	500 mb temperature
$T_7$	700 mb temperature
$T_c$	temperature at condensation level
$T_{ct}$	cloud top temperature
$T_d$	dew point temperature
$T_{d7}$	700 mb dew point temperature

LIST OF SYMBOLS (Continued)

English Letters

$T_{dc}$	dew point temperature at condensation level
$T_L$	temperature of a lifted parcel
$u$	westerly wind component
$u_5$	westerly wind component at 500 mb
$u_7$	westerly wind component at 700 mb
$v$	southerly wind component
$v_5$	southerly wind component at 500 mb
$v_7$	southerly wind component at 700 mb
$V_5$	500 mb wind speed
$V_7$	700 mb wind speed
$V_c$	crystal fall speed
$V_d$	droplet fall speed
$V_T$	thermal wind speed
$w_5$	500 mb mixing ratio
$w_7$	700 mb mixing ratio
$w_L$	mixing ratio of lifted parcel
$W_a$	potential condensate
$z$	vertical distance

Greek Letters

$\alpha$	discrete function of temperature (empirically derived)
$\beta$	discrete function of temperature (empirically derived)
$\Delta N_{co}$	difference in actual and optimum ice crystal concentrations

LIST OF SYMBOLS (Continued)

Greek Letters

$\Delta z$	cloud thickness
$\theta$	potential temperature
$\theta_5$	500 mb potential temperature
$\theta_7$	700 mb potential temperature
$\theta_{e5}$	equivalent potential temperature at 500 mb
$\theta_{e7}$	equivalent potential temperature at 700 mb
$\nu$	kinematic viscosity
$\rho$	air density
$\phi_5$	500 mb wind direction
$\phi_7$	700 mb wind direction
$\phi_{VT}$	thermal wind direction
$\omega$	vertical motion in pressure coordinates

## CHAPTER I

### INTRODUCTION

#### 1. Introductory Remarks

Wegner's (1911) suggestion that ice crystals would grow rapidly within supercooled water clouds provided the initial impetus that led to the belief that artificial stimulation of precipitation might be possible. However, it was not until Schaefer (1946) demonstrated the conversion of a supercooled water cloud to ice in both a cold chamber and the atmosphere using dry ice, and Vonnegut (1947) reported a method for nucleating ice formation on a large scale in the atmosphere, that attempts at precipitation augmentation began in earnest.

A physical basis for seeding cold orographic clouds was presented by Bergeron (1949). He suggested the process of natural ice nuclei precipitation release might have an optimum effect that depended upon 1) temperature, 2) size and concentration of cloud droplets and 3) the ratio of droplet concentration to effective ice nuclei concentration. The effects of temperature and droplet size are related to the diffusional transport of water vapor from droplets to crystals, which depends upon the difference in saturation vapor pressure over the droplets compared with the crystals. He concluded that substantial potential for precipitation augmentation would exist in cloud masses produced by stationary and sufficiently strong upward motions, which surpass the 0C isotherm, but not the -10C isotherm. These conditions might be found within special orographic cloud systems as pointed out by Bergeron.

Ludlam (1955) developed further the ideas expressed by Bergeron (1949) and presented a detailed treatment on the physics of seeding cold orographic clouds. Orographic cloud efficiency was considered by comparing the growth rate of ice by vapor diffusion to the growth rate of cloud water in the cloud system, rather than emphasizing the ratio of cloud droplet concentration to effective ice nuclei concentration considered important by Bergeron. Ludlam also pointed out that any artificially induced increase in precipitation efficiency not only depended upon an increased cloud efficiency, but also was dependent upon crystal settling speed and the velocity of the wind flow over the mountain barrier. From his study, Ludlam estimated the maximum attainable annual increase in snow cover over the mountains of central Sweden might be as much as 100 percent.

The physical basis for seeding cold orographic clouds, as envisioned by Bergeron and Ludlam, considered the efficiency of the ice process in converting available liquid condensate to ice growth within the orographic cloud. It is a simple concept. Orographic induced clouds along and windward of mountain ranges are frequently composed of supercooled liquid droplets. If the number of effective natural ice nuclei does not meet cloud requirements for converting the cloud water to ice form, snow may not develop, or the precipitation process may be inefficient. Therefore, if artificial ice nuclei can be activated in the saturated orographic air stream upwind of the mountain barrier, a more efficient conversion of cloud water to ice crystals should result in increased snowfall on the mountain.

The modification potential associated with these microphysical processes is designated the "static modification potential" (S.M.P.) in

this paper. However, it is conceivable that seeding under certain conditions may alter buoyancy effects within the cloud system by changing the latent heat release in ascending parcels. In turn, this might warm the cloud system, increase cloud tops or alter the vertical motion field over the orographic barrier. The overall result could be to change the rate of condensation or cloud geometry during seeded conditions. The modification potential associated with these particular dynamic effects is called the "dynamic modification potential" (D.M.P.) in this paper.

Early attempts to increase mountain snowfall were mainly operational in nature. These were frequently plagued by either having a poor experimental design or none at all. Thus, many of the early cloud seeding endeavors yielded little information pertaining to the physical processes accompanying the modification of snowfall. Seeding results of these early programs were generally inconclusive and, with the poor experimental design inherent in most, left much of the scientific community quite skeptical. Clearly, a meaningful and well designed experiment was needed.

A study of the precipitation processes which accompany central Colorado mountain snowfall was begun in 1959 by Colorado State University. A systems approach was used that provided for a variety of observations, each relevant to the solution of the overall problem of understanding mountain snowfall and its modification. This experiment conducted near Climax, Colorado, incorporated a good statistical design and ran nearly unaltered for ten years before the initial experimental mode was altered and extended on February 1, 1970. It is mainly observations gathered during this ten-year experiment that provide basic data for testing the physical model developed here.

Grant and Mielke (1967) stratified the data gathered from the Climax experiment for the years 1960-65 with respect to 500 mb temperature. They found that the average precipitation on seeded days was 54 percent more than on the non-seeded days, when 500 mb temperatures were -20C and warmer. This positive seeding effect decreased to 12 percent for those events with 500 mb temperatures from -21C to -23C. For the coldest stratification, where 500 mb temperatures were -24C and colder, the average daily precipitation on seeded days was 15 percent less than on non-seeded days. This experimental evidence demonstrated rather convincingly that seeding effects are related to concurrent meteorological conditions. A more detailed investigation followed (Chappell, 1967) that demonstrated the consistency of Climax seeding results with several aspects of cloud physics theory. Based largely on these results, a rudimentary model delineating opportunities for cloud seeding was presented by Grant et al. (1968) that was consistent with early results of the Climax experiment.

It is now desirable to formulate a physical model of the cold orographic cloud system in a mode that is compatible with experimental data available for its testing. If the physical model can be placed in a climatological mode (time averaged over many events), testing the model would be possible since precipitation data from several randomized experiments are now available. These include the 1960-65 and 1965-70 independent samples from the Climax, Colorado, experiment, the 1964-69 State of Colorado experiment at Wolf Creek Pass, Colorado, and the Park Range, Colorado, experiment. Statistical techniques are also available in this mode to provide a measure of confidence in some of the model testing.

## 2. Objectives of this Study

The first objective of this study is to formulate a physical model of the cold orographic cloud system in a mode suitable for testing with results obtained from cloud seeding experiments in the Colorado Rockies.

A second objective of this investigation is to test the model in as many ways as the available data permits. This includes 1) testing non-seeded and seeded model precipitation equations against precipitation observed in the primary target area during the Climax experiment, 2) testing the model weather modification potential equation against observed seeding effects in the primary target area and 3) testing the internal consistency of the model theory with observed crystal growth processes and their changes from non-seeded to seeded conditions.

A third objective of this study is to investigate the nature of observed seeding effects. In this study an attempt is made to define whether the major influence of seeding, when positive results are obtained, is to initiate a precipitation release, or to improve cloud efficiency during precipitation occurrence.

Another objective of this study is to test the reality of over-seeding. Does seeding under some meteorological conditions suppress precipitation, and if so, are these conditions consistent with the cloud physics theory underlying the model equations?

A final objective of this investigation is to derive reasonable estimates of the additional water available through an optimum cloud seeding program for two locations in the Colorado Rockies.

## CHAPTER II

### MODELING THE COLD OROGRAPHIC CLOUD

#### 1. A Basis for Physical Modeling

##### a. Total Water Budget of a Parcel of Air

The physical basis for seeding cold orographic clouds may be examined and defined by investigating processes controlling the total water budget of these clouds. Based on the total water budget equation, physical models may be derived which define the modification potential in terms of precipitation intensity and which delineate meteorological conditions associated with opportunities to modify natural snowfall.

The total water budget of a parcel of air may be written

$$\frac{dr}{dt} + \frac{dl}{dt} + \frac{ds}{dt} = 0 \quad (1)$$

where  $r$  is the vapor mixing ratio,  $l$  the liquid mixing ratio and  $s$  the ice mixing ratio of the parcel.

The total water budget equation may be considered during various stages in the transit of a parcel over an orographic barrier as shown in Figure 1. For parcels moving in the sub-cloud layer, time variations of the parcel moisture quantities are given by

$$\frac{dr}{dt} = 0 \quad (2)$$

$$\frac{dl}{dt} = 0 \quad (3)$$

$$\frac{ds}{dt} = 0 \quad (4)$$

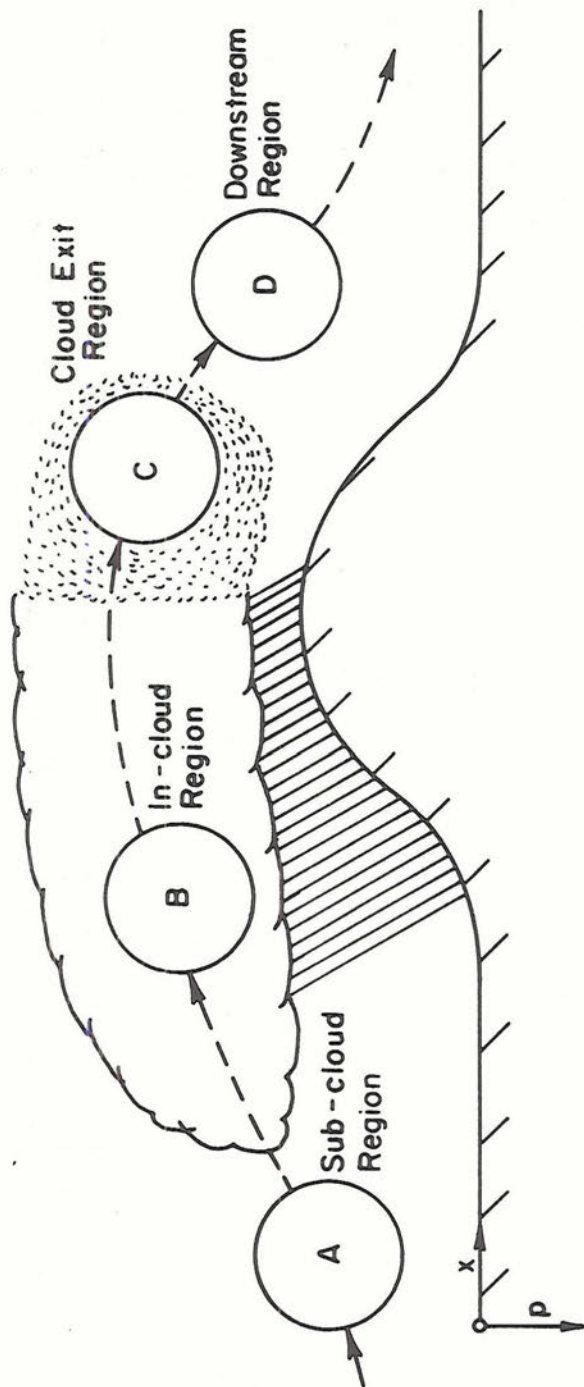


Figure 1. Orographic cloud segment in the x-p plane with typical parcel trajectory.

Equations 2 and 3 state that until saturation with respect to water is attained, the vapor mixing ratio is conserved and there is no formation of liquid water. Equation 4 assumes growth of ice particles in the sub-cloud layer is negligible. For parcels with upward trajectories in the cloud system, the time variations of the parcel moisture quantities can be written

$$\frac{dr}{dt} = \frac{dr_s}{dt} \quad (5)$$

$$\frac{dl}{dt} = - \frac{dr_s}{dt} - n_c \frac{dm}{dt} \quad (6)$$

$$\frac{ds}{dt} = n_c \frac{dm}{dt} \quad (7)$$

where  $r_s$  is the saturation vapor mixing ratio,  $n_c$  is the number of ice crystals per unit mass,  $m$  is the ice crystal mass, and (5) and (6) apply best for zero supersaturation with respect to water.

Equation 5 states that time variations of the vapor mixing ratio during the in-cloud stage are equivalent to changes in the saturation vapor mixing ratio of the parcel. Equation 6 gives the time variation of the liquid water content of the parcel as an imbalance between the vapor supply rate and the rate of ice growth in the parcel. Equation 7 gives the rate of ice growth in the parcel as the time change in crystal mass multiplied by the number of ice crystals per unit mass.

When parcels begin their downward trajectories prior to departing the cloud system, time variations of the parcel moisture quantities can be expressed by the following equations which apply until all liquid and solid condensates have evaporated.

$$\frac{dr}{dt} = \frac{de_w}{dt} + \frac{de_i}{dt} \quad (8)$$

$$\frac{dl}{dt} = - \frac{de_w}{dt} \quad (9)$$

$$\frac{ds}{dt} = - \frac{de_i}{dt} \quad (10)$$

In these equations  $de_w/dt$  and  $de_i/dt$  are the rates of evaporation of liquid water and ice form in the parcel, respectively.

#### b. Basic Equations

The following equations apply over a parcel trajectory that originates in the sub-cloud layer, extends through the cloud updraft and downward to a point where all liquid and solid condensates have evaporated. This final point delineates the downstream edge of the cloud exit region.

$$\frac{dr}{dt} = \frac{dr_s}{dt} + \frac{de_w}{dt} + \frac{de_i}{dt}$$

$$\frac{dl}{dt} = - \frac{dr_s}{dt} - n_c \frac{dm}{dt} - \frac{de_w}{dt}$$

$$\frac{ds}{dt} = n_c \frac{dm}{dt} - \frac{de_i}{dt}$$

If it is now assumed that precipitation fallout from the parcel is in ice form, the following conservation equations apply over the trajectory.

$$\frac{dr_s}{dt} + \frac{de_w}{dt} + \frac{de_i}{dt} + \frac{dp_s}{dt} = 0 \quad (11)$$

$$\frac{dl}{dt} = - \frac{dr_s}{dt} - n_c \frac{dm}{dt} - \frac{de_w}{dt} = 0 \quad (12)$$

$$n_c \frac{dm}{dt} - \frac{de_i}{dt} - \frac{dp_s}{dt} = 0 \quad (13)$$

The net rate of ice growth over the parcel trajectory or equivalently, the snowfall intensity following the parcel is given by  $dp_s/dt$ .

Both (11) and (13) give expressions for this quantity.

$$\frac{dp_s}{dt} = n_c \frac{dm}{dt} - \frac{de_i}{dt} = - \frac{dr_s}{dt} - \frac{de_w}{dt} - \frac{de_i}{dt} \quad (14)$$

From (12) the following relation is designated the "rate" equation.

$$\frac{de_w}{dt} = - \frac{dr_s}{dt} - n_c \frac{dm}{dt} \quad (15)$$

where  $\frac{de_w}{dt} > 0$  for  $n_c \frac{dm}{dt} < - \frac{dr_s}{dt}$

and  $\frac{de_w}{dt} = 0$  for  $n_c \frac{dm}{dt} \geq - \frac{dr_s}{dt}$

Equation 15 shows that if the rate of vapor supplied to the ascending parcel is greater than the extraction rate due to ice crystal growth, there is an evaporation of liquid water in the cloud exit region. This evaporative loss arises due to accumulation of liquid water in the parcel through cloud droplet growth during its ascension. Subsequent evaporation of these cloud droplets in the subsiding airstream to the lee of the mountain barrier therefore represents a loss of precipitation on the mountain due to an inefficient ice process. On the other hand, if the extraction rate of liquid cloud droplets by ice crystal growth is equal to or greater than the rate of liquid water formation in the ascending parcel, there is no net accumulation of liquid water and consequently, no evaporation of liquid droplets.

#### c. Optimum Conditions for Crystal Growth

From (15) it follows that a desirable condition, for minimizing losses and maximizing the cold cloud precipitation process, is for ice growth to occur at a rate equivalent to the vapor supply rate. Further, it is advantageous to have this conversion of cloud water to ice form

at water saturation, since this degree of cloud supersaturation provides for highest diffusional growth rates of crystals without a net growth of liquid water droplets. Thus, a process is envisioned wherein the vapor is converted to ice using liquid droplets as a "buffer" or "catalyst" in the reaction.

#### d. Simplification of Basic Equations

Equations 14 and 15 express important relationships about the precipitation process in orographic clouds. At this point the equations are general in that the manner of crystal growth is not specified and local and advective changes in saturation mixing ratio are retained. They apply to parcels traversing through the orographic cloud system.

The ultimate in cloud seeding operations would be to individually treat the various cloud parcels as they traverse through the orographic cloud system according to their immediate requirements. However, the technology to accomplish this does not exist, nor would it be economically feasible to attempt this, even if cloud requirements could be specified in such accurate detail. It would be more compatible with present technology to treat a cloud segment of unit width normal to the orographic barrier (as shown in Figure 1) in its entirety. This approach may be followed if it is required that 1) steady state conditions apply, 2) temperature changes due to horizontal advection are small, and 3) equations 14 and 15 are satisfied when averaged over the cloud segment.

Converting equations 14 and 15 into terms of unit volume, and averaging over the cloud segment, they may be written

$$\overline{\frac{dP_s}{dt}} = N_c \overline{\frac{dm}{dt}} - \overline{\frac{dE_i}{dt}} = -\omega \overline{\frac{\partial r_s}{\partial p}} - \overline{\frac{dE_w}{dt}} - \overline{\frac{dE_i}{dt}} \quad (16)$$

$$\overline{\frac{dE_w}{dt}} = -\overline{\omega \rho \frac{\partial r_s}{\partial p}} - \overline{N_c \frac{dm}{dt}} \quad (17)$$

where the bar signifies an average over the cloud segment and the capitalized letters indicate quantities per unit volume.

In (16)  $\overline{dP_s/dt}$  is the snowfall intensity averaged over the cloud segment,  $\overline{N_c (dm/dt)}$  is the growth rate of ice averaged over the cloud segment,  $\overline{-\omega \rho (\partial r_s / \partial p)}$  is the condensation rate averaged over the cloud segment, and  $\overline{dE_w/dt}$  and  $\overline{dE_i/dt}$  are the evaporation rates of liquid water and ice respectively, averaged over the cloud segment. Henceforth, these individual terms will be designated as average terms for ease of reference.

From (16) it is apparent that there may be three possibilities for increasing the average precipitation intensity of the cloud system. These include 1) increasing the average rate of condensation of the cloud system (dynamic potential), 2) decreasing the average evaporation rate of liquid droplets in the cloud exit region (static potential) and 3) decreasing the average evaporation rate of ice crystals in the cloud exit region (elimination of overseeding). Before discussing more fully the possibilities of modifying snowfall, (16) is developed in greater detail in order to bring out important aspects of seeding cold orographic clouds.

First, however, it is important to review microphysical processes that control the growth rate of ice in the cloud segment. In the next two sections the growth of ice crystals by vapor diffusion and accretion are considered.

## 2. The Growth of Ice by Vapor Diffusion

Equations 16 and 17 were derived without specifying the nature by which ice crystals grow in the cold orographic cloud system. In such a cloud system, there are two possible processes by which ice crystals may grow; vapor diffusion or accretion wherein the falling ice crystals capture the cloud droplets directly. In this section the diffusional growth of ice crystals is investigated and the resulting equation tailored for conditions representative of the Climax cloud system.

### a. Diffusional Growth Equation

If around a growing ice crystal there is a steady state diffusion of water vapor and steady state thermal conduction, the rate of ice crystal growth by vapor diffusion can be expressed (Mason, 1965)

$$\left(\frac{dm}{dt}\right)_d = 4\pi S_i G' C F_1 F_2 \quad (18)$$

where

$$G' = \left( \frac{R_v T}{D e_{si}} + \frac{L_i^2}{K R_v T^2} \right)^{-1} \quad (19)$$

and  $m$ , the ice crystal mass

$S_i$ , the supersaturation relative to a plane ice surface

$C$ , the electrostatic capacity factor

$F_1$ , the ventilation factor of the crystal in the airflow

$F_2$ , the vapor factor that corrects the vapor field to that of a supercooled cloud

$L_i$ , the latent heat of sublimation

$R_v$ , the gas constant for water vapor

$D$ , the diffusivity of water vapor in air

$K$ , the thermal conductivity of air

$e_{si}$ , the saturation vapor pressure over a plane surface of ice at the ambient temperature,  $T$

Mason (1965) has written the ventilation factor for spheres as a function of the Reynold's number or

$$F_1 = 1 + 0.22(R_e)^{1/2} \quad (20)$$

which is quite similar to that obtained empirically by Frössling (1938) for the rate of evaporation of liquid droplets.

The Reynold's number for ice crystals may be estimated from its equivalent radius

$$R_e = 2r_e V_c / \nu \quad (21)$$

where  $V_c$  is crystal velocity relative to the environment,  $r_e$  the equivalent radius of a crystal having the same volume as a droplet, and  $\nu$  the kinematic viscosity.

The equivalent radius of a crystal may then be determined from the relation

$$r_e = 0.91r^{2/3}c^{1/3} \quad (22)$$

where  $r$  and  $c$  are the crystal radius and thickness, respectively.

Combining (20), (21), and (22) the ventilation factor may be expressed as

$$F_1 = 1 + 0.31 (V_c r^{2/3} c^{1/3} / \nu)^{1/2} \quad (23)$$

From (23) it is seen that the ventilation factor in the growth equation is a function of crystal habit, size and fall speed and the kinematic viscosity. Through the habit and viscosity terms the ventilation factor is dependent upon pressure and temperature.

Marshall and Langleben (1954) derived a factor that corrects the vapor field to that of a supercooled cloud. An expression for this vapor factor may be written

$$F_2 = 1 + r \left( 4\pi \sum_1^{N_d} r_d \right)^{1/2} \quad (24)$$

where  $r$  is ice crystal radius and  $r_d$  the cloud droplet radius. The vapor factor is a function of the size of the growing crystal and the sum over unit volume of all cloud droplet radii.

The electrostatic capacity factor is a function of the crystal shape. Three simple cases generally serve as approximations for the majority of ice crystal forms (McDonald, 1963); sphere of radius  $r$ ,  $C = r$ ; disk of radius  $r$ ,  $C = 2r/\pi$ ; and prolate spheroid with major and minor semiaxes  $a$  and  $b$  respectively,  $C = 2ae/\ln [(1 + e)/(1 - e)]$  where  $e = (1 - b^2/a^2)^{1/2}$ .

In the case of a crystal growing in an environment at water saturation, the quantity  $(S_1 G')$  may be solved as a function of temperature and pressure (Mason, 1953; Marshall and Langleben, 1954). This function has been evaluated for different pressures and temperatures and is shown in Figure 2. It is henceforth denoted as  $F_T$ . If pressure is lowered at constant temperature, the decrease in diffusivity dominates the function resulting in an increase in the crystal growth rate. It is also noted that the maximum growth rate shifts slightly toward colder temperatures at lower pressures.

For purposes of immediate simplification, the effect of the vapor factor on crystal growth may be shown to be rather unimportant for continental type cold orographic clouds representative of the Climax area. Assuming a snow crystal radius of 400 microns, mean cloud droplet radius of 6 microns and a cloud droplet concentration of 200 per  $\text{cm}^3$ , the vapor factor is computed to be about 1.05. Figure 3 shows average crystal sizes observed near Climax are well below a radius of

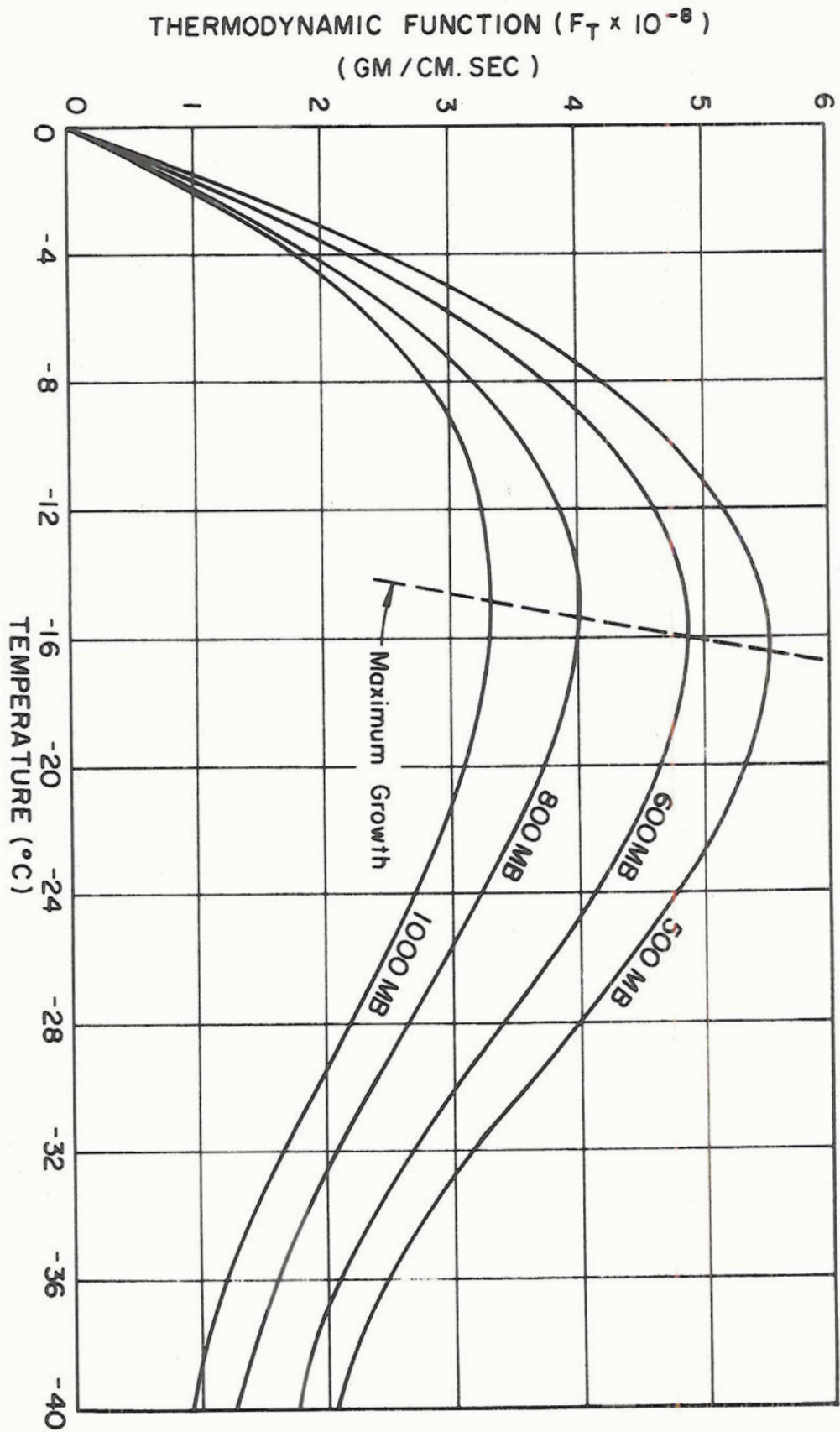


Figure 2. The variation of the thermodynamic function ( $F_T$ ) with temperature and pressure.

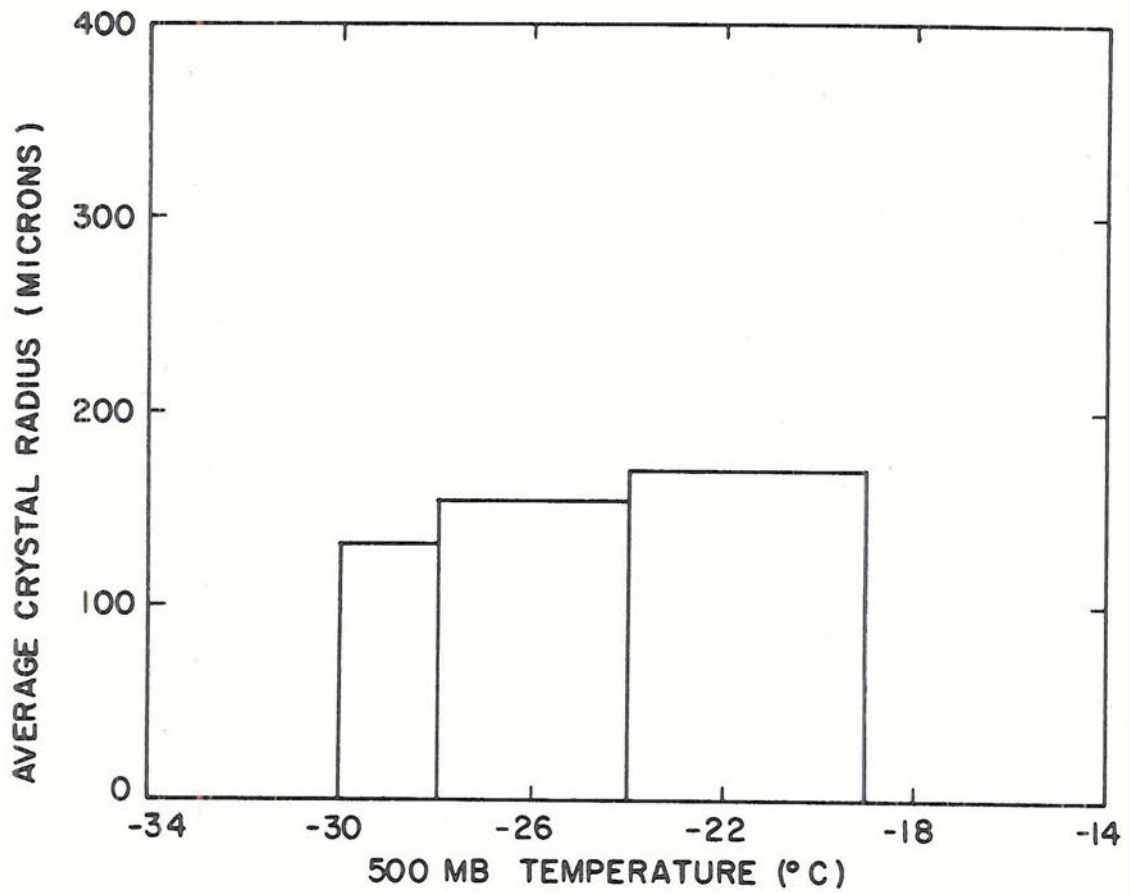


Figure 3. Average crystal sizes observed near Climax, Colorado, as a function of 500 mb temperature. Observations are from 11 snow-fall days.

400 microns and over 90 percent of all crystal sizes observed had radii less than 400 microns. The effect of the vapor factor may therefore be neglected for these cloud systems.

Based on typical temperatures found in winter orographic clouds, it is reasonable to consider that the electrostatic capacity factor may be approximated by that of a circular disk, or  $C = 2r/\pi$ . Substituting this expression for  $C$  and neglecting the vapor factor, (18) may now be written

$$\left(\frac{dm}{dt}\right)_d = 8rF_T F_1 \quad (25)$$

#### b. Comparison of Growth Equation with Observations

Fukuta (1969) integrated (18) over short periods of time and compared these results with carefully measured rates of ice crystal growth. He neglected the vapor and ventilation factors from the equation and assumed a spherical ice crystal ( $C = r$ ). Figure 4 shows the comparison between results obtained through measurements and by integration of the growth equation. It is seen that the growth equation gives values higher than observed at the warmer temperatures and lower than observed at the colder temperatures. In an actual cloud system, however, the ice crystal growth rate should be integrated over existing cloud temperatures. It appears from Figure 4, for cloud top temperatures around  $-18\text{C}$  to  $-20\text{C}$  and cloud base temperatures around  $-2\text{C}$  to  $-4\text{C}$ , the areas under the theoretical and observed curves are nearly equal and the theoretical equation would be adequate in this case. For the colder cloud systems the theoretical growth rates appear to be somewhat conservative.

Todd (1964) through an empirical study of ice crystals attempted to determine ice crystal growth rates as a function of temperature. He extracted crystal growth rate information from tables, scatter diagrams

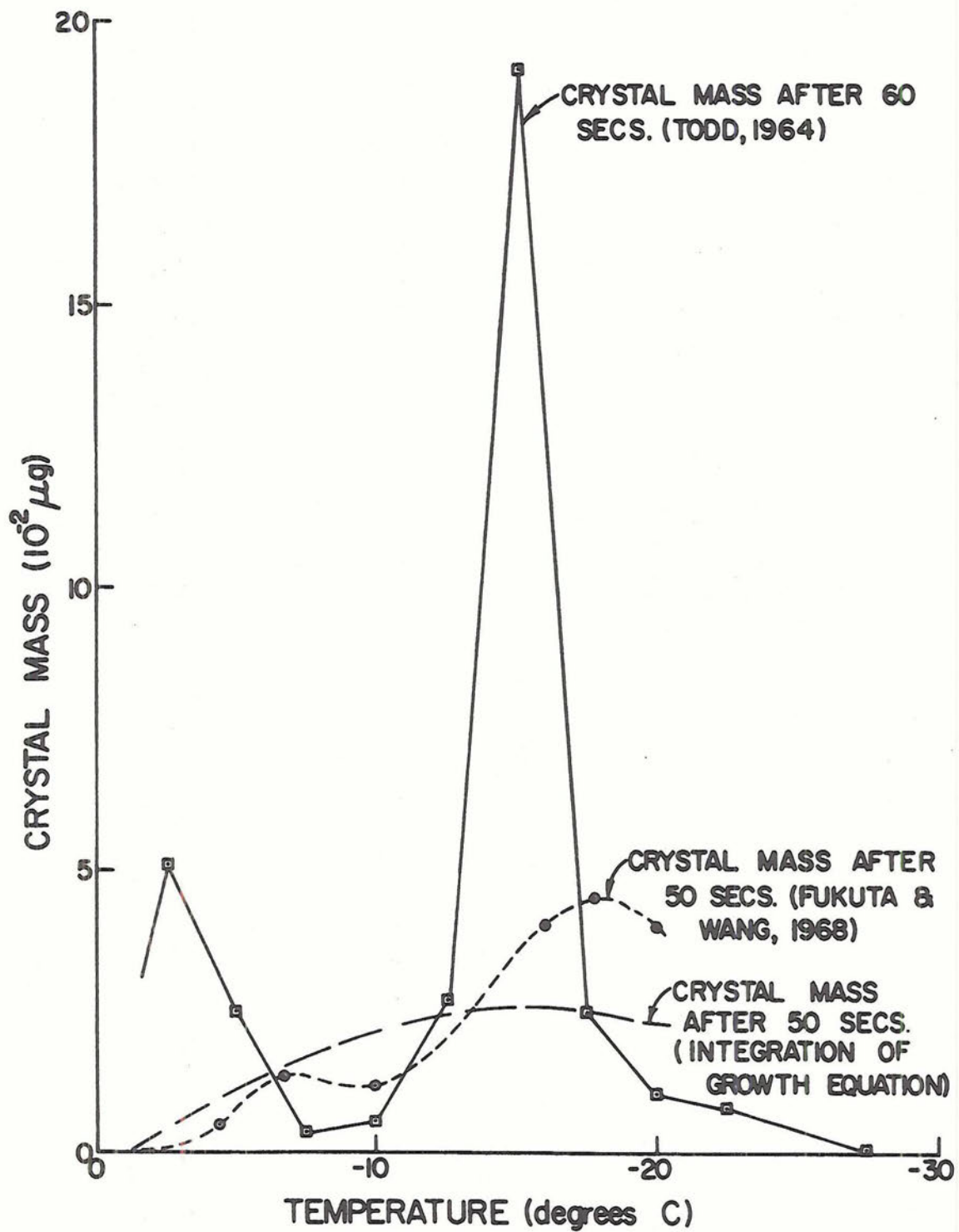


Figure 4. Theoretical, observed and empirically deduced crystal growth rates as a function of environmental temperature.

and micrographs. Ice crystal dimensions were then related to growth time and it was found that growth of the crystal axes (a and c) could be fitted to equations of the type;  $a = k_a t^\alpha$  and  $c = k_c t^\beta$  where  $\alpha$  and  $\beta$  are discrete functions of temperature, and  $k_a$  and  $k_c$  are continuous functions of temperature. The results of this investigation are also shown in Figure 4. It is seen that the crystal growth rates determined by Todd are not well explained by the diffusional growth equation. Around  $-15^\circ\text{C}$  there is nearly an order of magnitude difference in the two curves.

Braham (1968) combined observations on the relative rate of ice crystal growth as reported by Hallet (1965) with laboratory measurements of actual crystal growth rates reported by Mason (1957) to derive crystal growth rates as a function of environmental temperature. These values are generally less than those found by Todd.

It is apparent that the growth rate of ice crystals is still not well established. On this basis, (25) will be adopted as being representative of ice crystal growth by vapor diffusion. Cloud water can also be extracted from the cloud system by accretional growth of ice crystals and this important process is discussed in the next section.

### 3. Ice Crystal Growth by Accretion

#### a. Accretional Growth Equation

The rate of increase of mass of a falling crystal by accretion of supercooled cloud droplets is commonly given by

$$\left(\frac{dm}{dt}\right)_a = \pi r^2 (V_c - V_d) E Q_w \quad (26)$$

where  $r$  is crystal radius,  $E$  the collection efficiency,  $Q_w$  the liquid water content and  $(V_c - V_d)$  the relative velocity between the crystal

and the collected droplets. Since droplet fall velocities are much less than crystal settling speeds (26) is usually simplified to

$$\left(\frac{dm}{dt}\right)_a = \pi r^2 V_c E Q_w \quad (27)$$

where  $V_c$  is the crystal settling speed.

The growth rate due to accretion depends upon the mass of droplets lying in the path of a falling crystal and its ability to collect them. This process is complicated by 1) the air flow around the crystal which allows some of the droplets to escape collection by the falling crystal, and 2) the tendency for small water droplets to evaporate upon approaching a larger ice crystal due to the vapor pressure gradient that exists between them. These effects give rise to a critical droplet size for which a given crystal cannot collect droplets of a smaller size.

#### b. Observations of Rimed Crystals and Accreted Droplets

Kumai (1951) found traces of condensation nuclei scattered over the surface of ice crystal replicas and suggested the accretion of small cloud droplets might contribute significantly to crystal growth. However, since Kuroiwa (1955) found that small droplets tend to evaporate when approaching a larger ice crystal, it is unlikely that accretion of very small droplets contributes importantly to crystal growth. He showed that only droplets larger than a micron in diameter could reach a typical small crystal without evaporating. The aerodynamic effects which were not considered by Kuriowa make it quite likely that droplets of a few microns cannot be collected.

Ludlam (1955) suggested the critical droplet radius for collection is about 8 microns. Observations of Ono (1969) indicated that dendritic crystals of 1000 micron radius captured cloud droplets with 7 to 20

micron radii. Column crystals with major axes from 200 to 400 microns and minor axes from 100 to 150 microns captured cloud droplets ranging in radii from 10 to 35 microns. Observations of rimed crystals by Marwitz and Auer (1968) in cap clouds over southern Wyoming showed hexagonal crystals with radii less than 175 microns were never rimed, while 1000 micron crystals exhibited moderate to heavy riming. In all cases the lower threshold radius for accreted droplets was not less than 8 microns. From the above observations it is estimated that only cloud water existing in droplets of radii greater than 7 or 8 microns is likely to contribute significantly to accretional growth of ice crystals.

c. Control of Accretional Growth by Cloud Residence Time

It follows from the existence of a critical drop size, that the limited geometry of some orographic cloud systems may control somewhat the amount of cloud water available for accretional growth by limiting cloud residence time available for droplet growth. In addition, continental type orographic clouds, having cloud nuclei that favor growth of smaller droplets and a narrower droplet size distribution than maritime type clouds, would be inherently slower to exhibit accretional growth. Howell (1949) showed for a continental type cloud nuclei spectrum and an ascension rate of about 30 cm/sec, that only a relatively few droplets attained an 8 micron radius at the end of 20 minutes of growth. Since this time interval is of the same order as that required for transit of parcels through the Climax orographic cloud, it seems likely that accretional growth would frequently be subordinate to diffusional growth processes in this cloud system. While there are effects operating to suppress accretional growth of crystals in the Climax orographic cloud system, the dominant control on accretional

growth inevitably must be traced to cloud supersaturation which is discussed in the next section.

d. Effect of Cloud Supersaturation on Accretional Growth

The presence of the ice phase in cold orographic clouds has important effects on the ability of the cloud system to contribute to ice crystal growth by accretion. This can be seen from considering supersaturation in a mixed cloud system. The time rate of change of cloud supersaturation may be written

$$\begin{aligned} \frac{dS_i}{dt} = & Q_1 \frac{dz}{dt} - Q_2 (4\pi G) \sum_1^{N_d} r_d \left( S_w - \frac{a}{r_d} + \frac{b}{r_d^3} \right) - Q_3 (4\pi F_2 S_i G') \sum_1^{N_c} CF_1 \\ & - Q_3 (\pi Q_w) \sum_1^{N_c} r^2 EV_c \end{aligned} \quad (28)$$

where  $Q_1$ ,  $Q_2$ ,  $Q_3$ ,  $G$  and  $G'$  are thermodynamic functions and other quantities not yet defined are:

$S_w$ , the supersaturation relative to a plane water surface

$a$ , a function of temperature equal to  $3.3(10^{-5})/T$

$b$ , a function of droplet solute equal to 4.3 times the moles of solute contained in a droplet

$z$ , the vertical distance

Equation 28 shows the time rate of change in cloud supersaturation is due to imbalances between the cooling rate associated with the up-draft speed, rate of droplet growth, and the rates of crystal growth by vapor diffusion and accretion. The droplet growth rate term tends to act as a stabilizing influence on cloud supersaturation since it takes on both negative (evaporation) and positive (growth) values.

It is interesting to consider (28) under two differing conditions. In the first case, it is assumed that a supercooled cloud is at water saturation and that cloud system temperatures are cold so that the magnitude of the diffusional growth rate term exceeds that of the cooling rate term ( $N_c$  is large). In this event the droplet growth rate term becomes negative and droplet evaporation tends to maintain the cloud supersaturation at the level of water saturation. Eventually, the reservoir of liquid droplets is depleted by evaporation and cloud supersaturation falls. However, as cloud supersaturation decreases the diffusional growth rate also is reduced and cloud supersaturation attains a steady state at some value near ice saturation. In this steady state condition, the liquid water content ( $Q_w$ ) is near zero and there is an extremely low probability of accretional growth of ice crystals.

In contrast to the above case, if the magnitude of the cooling rate term exceeds that of the diffusional growth rate term ( $N_c$  is small), a net droplet growth tends to relieve the increase in cloud supersaturation. Since the droplet mass growth rate is directly proportional to the droplet size (radius), cloud supersaturation attains a steady state at some value above the level of water saturation. There is, therefore, a specific probability that a given cloud droplet will continue to grow. The greater the difference between the cooling rate term and the diffusional growth rate term, the larger this probability becomes. Thus, the probability increases that more of the cloud water will be found in droplets exceeding 7 or 8 microns radius, and will therefore be available for the accretional growth process.

The above theory has important implications concerning cold orographic precipitation processes. Significant accretional growth of

ice crystals is to be expected under conditions of steady state cloud supersaturation only when the diffusional growth rate term is less than the cooling rate term. In other words, the occurrence of significant numbers of rimed crystals reflects an inefficiency of the diffusional ice growth process within the cloud system. Since the accretional growth rate cannot be counted upon to make up the total deficit between the vapor supply rate and the diffusional growth rate, static modification potential is likely to exist and will be crudely delineated by those meteorological conditions for which significant accretion is observed.

e. Accretional Growth in the Climax Cloud System

A strong dependence of accretional growth upon cloud temperature for the Climax cloud system is shown in Figure 5. This figure depicts the percentage of all crystals (columns, prisms, plates, stellars and dendrites) rimed for 16 different days at the High Altitude Observatory and Chalk Mountain (located near Climax, Colorado) as a function of cloud system temperature. It is seen that the percentage of crystals rimed on both seeded and non-seeded days is exceedingly small for the colder cloud systems, but increases rapidly as 500 mb temperatures become warmer than about  $-21^{\circ}\text{C}$  to  $-22^{\circ}\text{C}$  for unseeded events and about  $-16^{\circ}\text{C}$  to  $-17^{\circ}\text{C}$  for seeded events. This strong dependence of accretional growth upon cloud temperature appears to reflect the changing efficiency of the diffusional ice growth process as suggested by the theory above. Figure 5 will be discussed in greater detail later in the testing of the physical model. For now, it can be said that accretional growth of ice crystals in the Climax cloud may be safely neglected at least for the colder cloud systems.

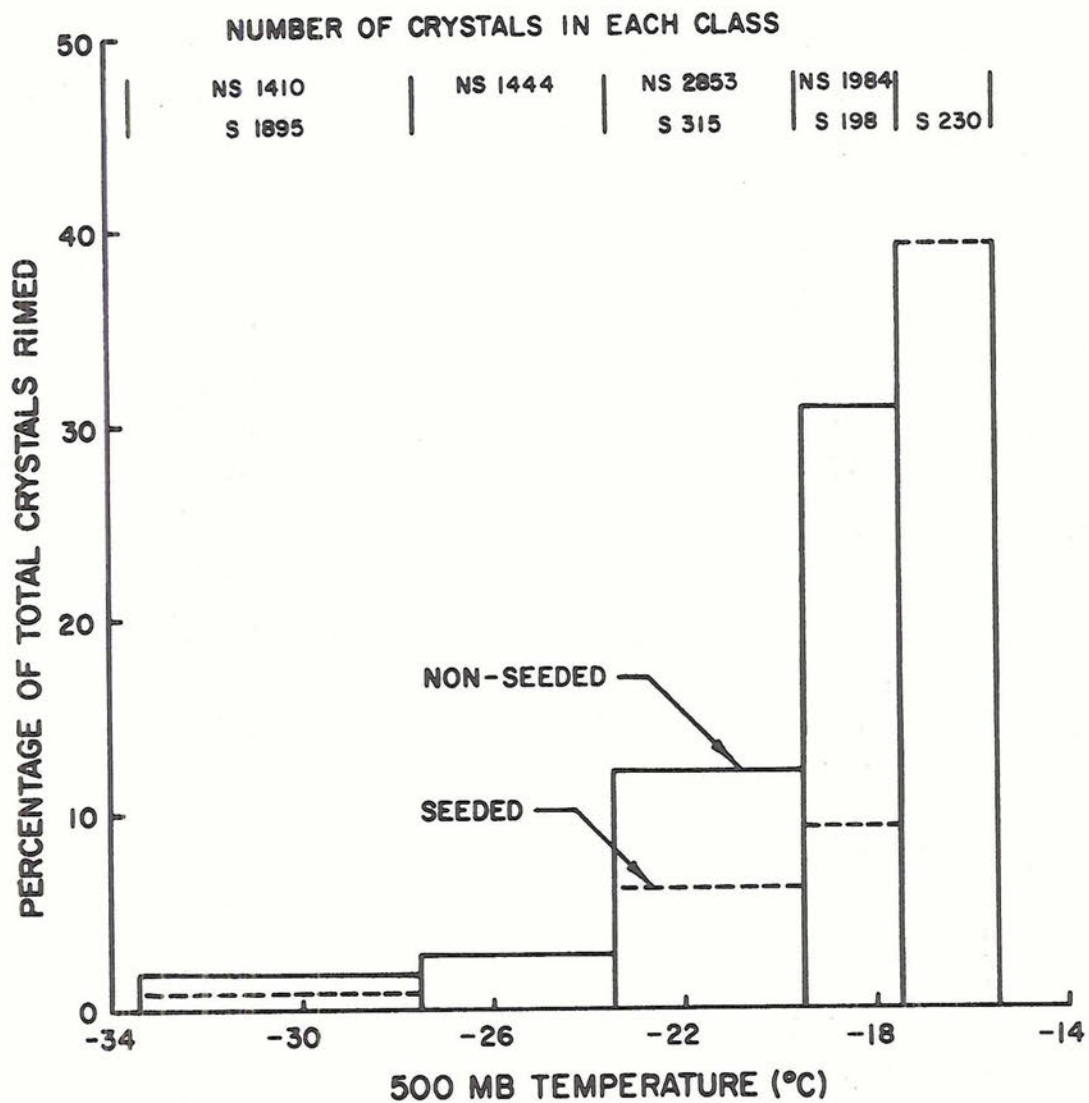


Figure 5. The onset of significant accretional growth in the Climax cloud system (measured by the percentage of total crystals rimed) as a function of 500 mb temperature.

## f. The Acceleration of Accretional Growth

A final point to be made is that accretional growth of ice crystals is a "runaway" process. This can be seen by differentiating (27) with respect to time to give

$$\frac{d}{dt} \left( \frac{dm}{dt} \right)_a = r^2 V_c E Q_w \left( \frac{1}{E} \frac{dE}{dt} + \frac{2}{r} \frac{dr}{dt} + \frac{1}{V_c} \frac{dV_c}{dt} + \frac{1}{Q_w} \frac{dQ_w}{dt} \right) \quad (29)$$

If it is assumed that all liquid water lying in the path of a falling crystal will be collected and that the liquid water is distributed homogeneously through the cloud system, (29) may be written

$$\frac{d}{dt} \left( \frac{dm}{dt} \right)_a = \left( \frac{dm}{dt} \right)_a \left[ 2 \frac{d}{dt} (\ln r) + \frac{d}{dt} (\ln V_c) \right] \quad (30)$$

It is seen that under these conditions, the acceleration of accretional growth is directly proportional to the rate of accretional growth. Thus, when a crystal begins to rime, its fall velocity increases causing a larger volume of cloud droplets to be swept out per unit time. This increases the growth rate of the crystal mass (and radius), which in turn increases the acceleration of crystal growth. This phenomenon could have the very important effect of creating large crystal growth rates in the very lower portion of a cloud system. Braham (1968) estimates that under such conditions, 50 percent of the total crystal growth might occur in the bottom 20 percent of the cloud system.

It has been shown in this chapter that the onset of significant accretional growth in the cold orographic cloud is highly dependent upon diffusional growth rates present in the cloud system. In turn, the diffusional growth rate in the cloud system is mainly controlled by ice crystal concentrations. The microphysical processes which control the

number of ice crystals growing in the cold orographic cloud system are considered in the next section.

#### 4. Ice Crystal Sources in Cold Orographic Clouds

##### a. Primary Ice Nuclei

Bergeron (1933) suggested that ice crystals growing in supercooled clouds at the expense of evaporating cloud droplets might explain the genesis of most raindrops. He postulated that there are present ice nuclei, or sublimation nuclei in the atmosphere that are thermodynamically activated and then grow by vapor deposition into ice crystals. It is generally agreed that most of these primary ice nuclei are silicate minerals, principally of earth origin, and ranging in size from 0.1 to 3 microns in diameter (Schaefer, 1950; Isono, 1955; Kumai, 1961; Byers, 1965).

Measurements of the number of these primary ice nuclei indicate there are significant spatial and temporal variations in their concentrations. Moreover, the number of ice nuclei activating in the atmosphere is strongly dependent upon temperature. In general, most observations have indicated crudely an exponential rise in ice nuclei counts with decreasing temperature (Kline, 1963). Fletcher (1962) suggested a mean activation spectrum could be expressed by the equation  $N = (10^{-5}) \exp(-0.6T)$ , where T is in degrees Centigrade and N is the effective primary ice nuclei per liter. This mean activation spectrum is shown in Figure 6 along with an observed activation spectrum from the Elk Mountain area of southern Wyoming (Veal, et al., 1969).

Reinking (1970) analyzed ice nuclei data at Climax for both seeded and non-seeded experimental days. A least squares exponential curve fit to the non-seeded data performed by the author is also shown in

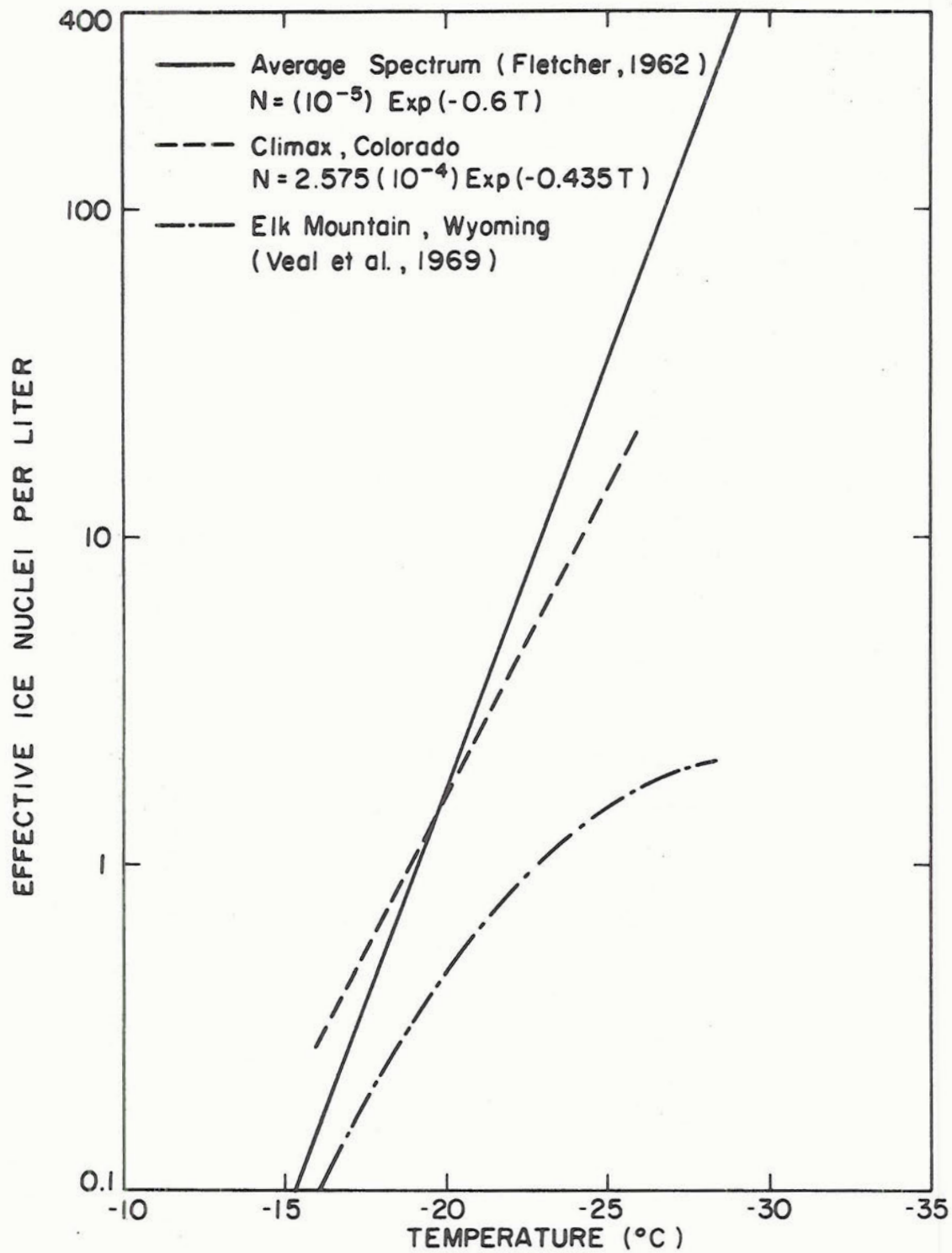


Figure 6. Concentrations of effective primary ice nuclei as a function of environmental temperature.

Figure 6. It was found that the average primary ice nuclei activating as a function of temperature on the non-seeded days at Climax can be expressed by the equation  $N = 2.575(10^{-4})\exp(-0.435T)$ , where T and N are as defined above. It is seen in Figure 6 that the slope of the Climax spectrum is less than the spectrum given by Fletcher. A tenfold increase in ice nuclei is observed at Climax for a 5.3C decrease in temperature compared to a 4C decrease in temperature for Fletcher's curve.

A knowledge of the temperature activation spectrum allows an estimation of the concentration of ice crystals that will originate in the cloud system from the activation of primary ice nuclei. However, there are other ways in which the ice phase may be introduced into a supercooled cloud. These secondary ice crystal sources are considered in the next section.

#### b. Secondary Ice Crystal Sources

Several researchers (Tazawa and Magono, 1966; Mossop et al., 1967; Mossop, 1968; Koenig, 1963, 1968; Braham, 1964; Mossop and Ono, 1969; Veal et al., 1969; Hobbs, 1969; Grant, 1968; Weinstein and Takeuchi, 1970) have shown that concentrations of ice crystals in clouds may exceed concentrations of primary ice nuclei measured in clear air below clouds. Many of these observations are shown in Figure 7. Several possible reasons have been suggested to account for this discrepancy, which apparently can attain two to three orders of magnitude in certain cloud systems within the temperature range between -5C to -15C. These include 1) transport from higher clouds, 2) accumulation of ice nuclei or crystals at a given cloud level, 3) nucleation processes active only in natural clouds, and 4) multiplication of crystals originally formed on primary ice nuclei by processes peculiar to natural clouds.

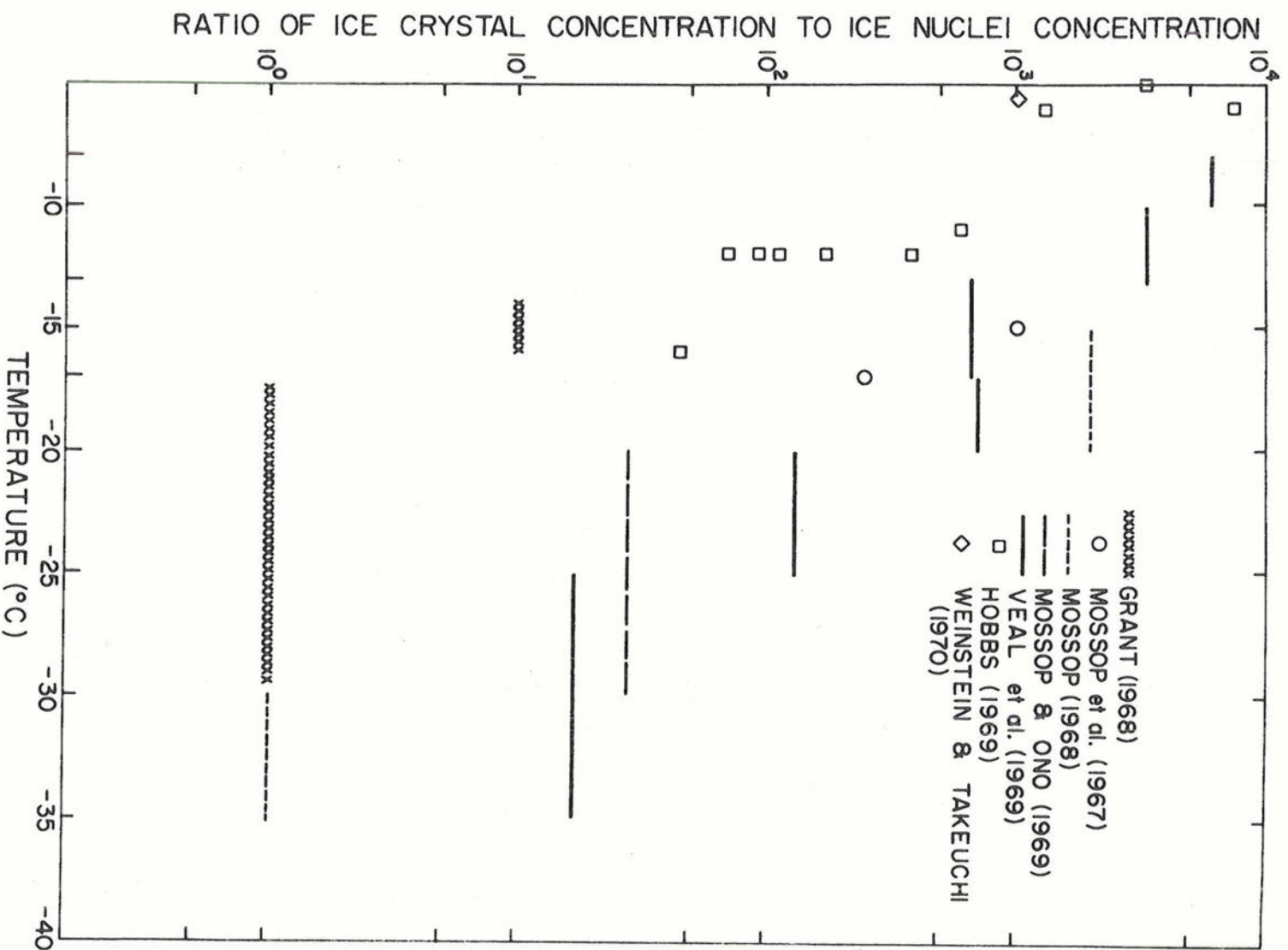


Figure 7. The ratio of ice crystal concentration to corresponding ice nuclei concentration as a function of cloud top temperature.

### 1) Cirrus Seeding, Accumulation Mechanisms and Counter Considerations

The possibility exists that Cirrus clouds might provide a seeding mechanism for middle level cloud types such as Altostratus, Altocumulus, or underlying orographic clouds. This possibility was enhanced by the findings of Braham (1967) and Braham and Spyers-Duran (1967), who found that certain types of cirrus clouds produce crystals that can survive up to 20,000 feet of descent in clear air. However, the effect of cirrus seeding on Colorado orographic snowfall is thought to be quite minor since many visual observations substantiate the absence of these particular cirrus type clouds during most of these episodes.

Mossop et al. (1968) considered possible accumulative mechanisms and concluded these probably can only enhance ice crystal concentrations by a factor of ten at most. This would not explain the larger discrepancies observed.

Measurements of primary ice nuclei in ice nuclei counters are not taken under conditions identical to natural cloud conditions. In particular, nucleation processes are time dependent and the possibility that many more ice nuclei would activate in supercooled clouds than in chamber clouds cannot be discounted. However, this effect is estimated to be considerably less than a factor of 10 (Warner and Newnham, 1958) and again cannot explain the larger discrepancies observed.

Roberts and Hallet (1968) found that certain mineral particles retain sufficient adsorbed ice after evaporation that they will grow crystals again when moisture is supplied at higher temperatures. This effect serves to shift the ice nuclei spectrum toward warmer temperatures. This preactivation of ice nuclei could conceivably be important in orographic clouds where snow cover is quite near or generally within

the cloud system. This pre-activation capability would not be realized in ice nuclei counters where air is preheated above freezing before entering the chamber.

## 2) Ice Crystal Multiplication

Koenig (1968) and Mossop (1970) noted that the observations providing substantial support for the existence of ice multiplication mechanisms were mainly confined to clouds forming in maritime air masses or of the cumulus type. Koenig suggested the occurrence of ice multiplication is related to the coarseness of the cloud droplet spectrum and also noted that ice multiplication is frequently accompanied by large drops or graupel. It therefore seems possible, that the occurrence of ice multiplication may be related to those cloud conditions which give rise to the growth of large supercooled droplets, and that the supercooled droplets may participate directly, or indirectly in the multiplication process.

While field observations suggest the riming process may contribute in some way to ice crystal multiplication, Mossop (1970) points to the lack of laboratory confirmation.

The possibility that the splintering of a freezing drop might provide for the genesis of ice crystals within a cloud system has received considerable attention. Schaefer (1952), Mason (1956), Langham and Mason (1958), Mason and Maybank (1960) found that a freezing drop could produce several small ice fragments under certain conditions. However, Dye and Hobbs (1968) and Brownscombe and Hallet (1967) have shown that many of these early laboratory results cannot be transferred to the actual atmosphere, and that water droplets fragment during freezing only under rather special circumstances.

While these later findings have made splintering a less attractive theory, Hobbs and Alkezweeny (1968) have shown that some 50 to 100 micron diameter droplets do fragment and shed ice splinters under conditions similar to natural clouds.

Another mechanism that might be important in mixed phase clouds is the mechanical breakup of delicate ice crystals through the thermal shock received when colliding with and nucleating supercooled droplets. In laboratory experiments Dye and Hobbs (1968) found that fragile ice crystals often fractured into 5 to 10 pieces after coming into contact with a supercooled drop. If ice crystal multiplication does occur by this method, the number of secondary ice particles produced would probably depend upon drop size distribution and crystal habit in the cloud as pointed out by Hobbs (1969). In addition, it should be most effective at cloud temperatures and supersaturations in which fragile crystals are formed. Figure 8 shows the dependency of crystal habit on temperature and cloud supersaturation according to Kobayashi (1961) and Mason et al., (1963).

It is seen that fragile dendritic growth is favored at temperatures from  $-12^{\circ}\text{C}$  to  $-18^{\circ}\text{C}$  and at cloud supersaturations in excess of water saturation. The effectiveness of this multiplication process in extracting cloud water would also be enhanced when temperatures and supersaturations associated with fragile dendritic growth were present near cloud top. In this case initial dendritic crystal growth would be quite rapid since the thermodynamic function in the diffusional growth equation is largest in this temperature range (and also for these low pressures). Thus, the probability of the crystal riming and fracturing during its longer descent through the cloud system is increased. Should fracture

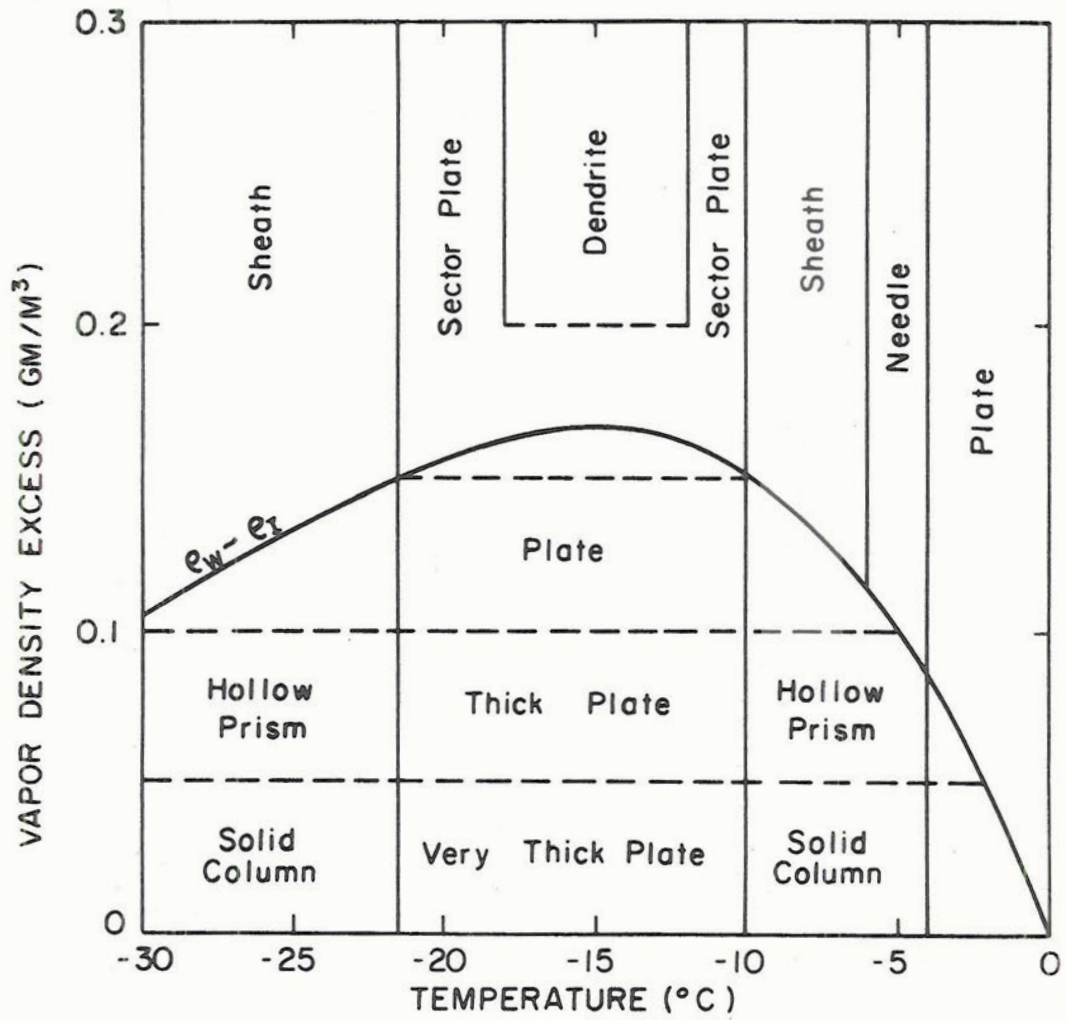


Figure 8. Ice crystal habit regions as a function of temperature and vapor saturation.

occur early in the upper portion of the cloud system, it is conceivable that the process might be repeated again.

Koenig (1968) believes an ice multiplication process involving dendritic crystals and larger supercooled droplets may occur slightly differently. He suggests the collision of a large supercooled drop upon a dendritic surface would give rise to a local area of high supersaturation. In this area fragile whisker-type growth could occur for a short time until warming of the ice and cooling of the freezing drop reduces the local supersaturation. He points out that the process would be inoperative if the crystal surface becomes completely wetted, and that additional growth by deposition after equilibrium is restored would probably destroy the fragile forms. Thus, a timely collision with other hydrometeors (preferably solid) may be required for prolific ice multiplication with this process.

Ice is not a particularly weak substance but crystal habits are relatively fragile and delicate in the temperature range from  $-20^{\circ}\text{C}$  to  $-10^{\circ}\text{C}$  (stellars and dendrites). It is conceivable that in this temperature range where fragile crystal growth occurs, collisions may occur involving these delicate crystals, breaking them into several pieces. This process would be especially favored in clouds where a portion of the crystals are rimed, since this would lead to large relative velocities between rimed and unrimed crystals and increase the probability of collisions. Evidence of the breakup of fragile crystals in the Climax cloud system was reported by Grant (1968) and Brown and Bertolin (1969).

In colder orographic cloud systems, these multiplication processes probably do not exist. This is due not only to the appearance of stronger crystal habits, but also to the greater number of effective

primary ice nuclei growing by vapor diffusion in the cloud system. This leads to lower cloud supersaturation with smaller cloud water content and droplet sizes. The result is an increasing probability that cloud droplets will not attain sufficient size to be collected by crystals, and therefore, that riming will not participate directly or indirectly in the multiplication of existing crystals.

In summary, it appears that seeding from overlying cirrus clouds is not an important process in the Climax orographic cloud system due to the low frequency of occurrence of the particular type of Cirrus clouds capable of acting as secondary sources of crystals. Continental type cloud nuclei, combined with restricted droplet growth times available in orographic clouds of limited geometric extent, make the droplet freezing and splintering mechanism even more unlikely to be important in the Climax cloud system. Pre-activation of ice nuclei would also seem to be generally unimportant in the Climax cloud system since cloud bases usually are above most of the mountainous terrain. During extremely high wind conditions however, this phenomenon could conceivably take on some importance.

It does appear that fracturing due directly or indirectly to accretion of supercooled droplets (thermal shock, whisker growth possibly aided by subsequent hydrometeor collision, collisions of fragile unrimed crystals, probably with higher speed rimed ice particles) are important in the Climax cloud system under certain limited conditions of temperature and supersaturation. The net result would be a natural precipitation process considerably more efficient than one in which only primary ice nuclei were growing by vapor diffusion.

## 5. A Model of Weather Modification Potential

In the development of the conservation and rate equations, the ice crystal growth process was not specified. It has been demonstrated, however, that significant accretional growth of crystals and crystal multiplication in the Climax cloud is probably limited to some of the warmer cloud systems. Even with these warmer cloud systems, crystal replication indicates that accretional growth rarely exceeds the diffusional growth of the crystal and ice crystal multiplication is generally a factor of ten or less. On this basis, a model of the Climax cloud system is developed in this section which incorporates diffusional growth of ice crystals that originate from activation of primary ice nuclei.

### a. Diffusional Rate of Ice Growth Averaged over Cloud System

In (16) and (17) the growth rate of ice averaged over the cloud segment was expressed as  $\overline{N_c (dm/dt)}$ . Assuming only diffusional ice growth in the cloud system and using (25), this may be expressed as

$$\overline{N_c \frac{dm}{dt}} = \overline{8N_c r F_T F_1} \quad (31)$$

Expanding (31) into volume means and deviations from these means it takes the form

$$\begin{aligned} \overline{N_c \frac{dm}{dt}} &= \overline{8N_c r F_T F_1} \\ &+ 8(\overline{N_c r F_T F_1'} + \overline{r F_T F_1' N_c'} + \overline{F_T F_1' N_c' r'} + \\ &+ \overline{F_1' N_c' r' F_T'} + \overline{N_c' F_T' r' F_1'} + \overline{r F_1' N_c' F_T'}) + \\ &+ 8(\overline{N_c r' F_T' F_1'} + \overline{r N_c' F_T' F_1'} + \overline{F_T' N_c' r' F_1'} + \overline{F_1' N_c' r' F_T'}) \\ &+ 8\overline{N_c' r' F_T' F_1'} \quad (32) \end{aligned}$$

It is shown in Appendix A that the combined contribution of all the deviation terms is probably never more than 25 percent of the mean term, and frequently may be less than 10 percent. Thus, the error involved in computing the average diffusional growth rate of ice using only the mean term, is no greater than the inherent uncertainty present in using the theoretical growth equation itself. Therefore, (32) may be written to a first approximation as

$$\overline{N_c \frac{dm}{dt}} = 8 \overline{N_c r F_T F_l} \quad (33)$$

b. Rate of Condensation Averaged over the Cloud System

The term describing the rate of condensation averaged over the cloud system in (16) and (17) can be written

$$\overline{-\omega \rho \frac{\partial r_s}{\partial p}} = \overline{-\omega \rho \frac{\partial r_s}{\partial p}} - \overline{\rho \omega' \frac{\partial r'_s}{\partial p}} \quad (34)$$

if the small deviation quantities of density are neglected.

This is a reasonable simplification since cold orographic clouds generally have limited vertical extent in the Climax area.

The deviation term in (34) is also neglected through the following argument. The assumption that horizontal temperature gradients are small and may be neglected, also implies that horizontal variations of  $\partial r_s / \partial p$  are negligibly small. Vertical variations of  $\partial r_s / \partial p$  are also rather small and moreover, maximum upward speeds tend to be present nearly midway in the cloud system, so that positive and negative correlations of these deviation quantities tend to cancel in a vertical summation.

The rate of condensation averaged over the cold orographic cloud system may therefore be written to a first approximation as

$$\overline{\frac{\partial r}{\partial p}}_s = -\overline{\omega \rho} \frac{\partial \overline{r}}{\partial p} \quad (35)$$

Equation 35 states that the rate of condensation averaged over the cloud segment may be estimated by considering a parcel of unit volume moving with the mean vertical motion of the cloud system and conserving the mean equivalent potential temperature of the cloud system.

c. Relation of Ice Crystals to Precipitation Efficiency

As pointed out previously, a reasonable goal in seeding cold orographic clouds, considering present technology, is to bring about an ice growth rate equal to the condensation rate when averaged over the cloud segment. This desired condition is expressed by equating (33) and (35) to give

$$8\overline{N}_c \overline{r} \overline{F}_T \overline{F}_1 = -\overline{\omega \rho} \frac{\partial \overline{r}}{\partial p}$$

Solving for the average ice crystal concentration yields

$$\overline{N}_{co} = -\frac{\overline{\rho}}{8\overline{F}_1 \overline{F}_T} \left( \frac{\partial \overline{r}}{\partial p} \right) \left( \frac{\overline{\omega}}{\overline{r}} \right) \quad (36)$$

where  $\overline{N}_{co}$  is the optimum number of ice crystals per unit volume needed to bring about the above equivalency.

d. Estimation of Actual Ice Crystal Concentrations

Equation 36 provides estimates of optimum ice crystal concentrations needed to provide for a sufficient rate of cloud water extraction through diffusional growth of crystals. Then, if natural concentrations of ice crystals in the cloud system can be estimated, the two concentrations can be compared to determine if a sufficient natural supply is present.

It has already been demonstrated that the number of primary ice nuclei activating in the cloud system is an exponential function of temperature. This relationship is powerful in that a decrease of about 5.3 degrees C of temperature will cause the number of primary ice nuclei that activate to increase tenfold. Therefore, ice crystal concentrations in the cloud system, in the absence of multiplication processes, is determined largely by the colder cloud regions where condensation occurs (near cloud top).

Through a knowledge of the temperature activation spectrum of primary ice nuclei, an estimate of the vertical distribution of ice crystal generation within the cloud system can be obtained. It is assumed that ice crystals settle through the cloud system from their points of origin, being joined by other crystals generated lower down, so that ice crystal concentrations increase slightly from cloud top to cloud base. For an orographic cloud system with a decrease of about 16 degrees C from cloud base to cloud top (representative of Climax cloud), about 90 percent of all ice crystal generation is in the upper third of the cloud, 9 percent in the middle third and 1 percent in the lower third. It follows that a vertical averaging of ice crystal concentrations from cloud base to cloud top gives a mean ice crystal concentration for the cloud equal to about 0.96 times the primary ice nuclei concentration that activates at the temperature of the cloud top.

A general equation for the mean ice crystal concentration in the cloud segment for non-seeded conditions can therefore be expressed as

$$\overline{(N_c)}_{ns} = [0.96 \overline{R_c} A \exp(BT_{ct})]_{ns} \quad (37)$$

where  $T_{ct}$  is cloud top temperature,  $\overline{R_c}$  the mean ratio of ice crystal concentration to ice nuclei concentration for the cloud segment, and

A and B are coefficients generated by curve fitting the temperature activation spectrum of primary ice nuclei with an exponential function. All quantities are evaluated for non-seeded conditions.

An expression similar to (37) can be derived for seeded conditions or

$$\overline{N_c}_s = [0.96 \overline{R_c} A \exp(BT_{ct})]_s \quad (38)$$

where coefficients now describe the temperature activation spectrum of ice nuclei under seeded conditions, and  $\overline{R_c}$  may be different in this case due to the effect of seeding upon ice crystal multiplication. Cloud top temperature during seeded conditions may also be different than for non-seeded conditions due to affecting changes in buoyancy and latent heat release.

#### e. Estimation of Ice Crystal Deficiency

If (36) is subtracted from (37) the excess or deficit of ice crystals in the cloud system, about the number required to maximize cloud water utilization may be determined by

$$\Delta N_{co} = [(0.96)\overline{R_c} A \exp(BT_{ct})]_{ns} + \frac{\overline{\rho}}{8\overline{F}_1\overline{F}_T} \left( \frac{\partial \overline{r}_s}{\partial p} \right) \left( \frac{\overline{\omega}}{\overline{r}} \right) \quad (39)$$

#### f. Precipitation Equations

It is seen from (16) that the average precipitation rate of the orographic cloud segment is given by the average vapor supply rate minus the average evaporation rates of liquid water and ice particles in the cloud segment. While the loss due to evaporation of liquid water may be eliminated by cloud seeding, generally, there will probably be some loss due to evaporation of ice crystals below cloud base or in the cloud exit region. In this event, the complete conversion of total vapor supplied in the cloud segment to snowfall on the mountain is not likely to be

realized even with proper seeding. Therefore, it is possible to define an "available" rate of vapor supply for the cloud segment, which is equal to the "total" rate of vapor supply minus the evaporative rate of ice crystals.

For simplification, it is now assumed that loss due to evaporation of ice crystals is small compared to the total vapor supplied and can be neglected as a first approximation. From (16) the average non-seeded precipitation intensity of the orographic cloud segment is given by

$$\overline{(P_s)}_{ns} = \begin{cases} \left( -\overline{\omega} \overline{\rho} \frac{\partial \overline{r}}{\partial p} \right)_s \Delta z)_{ns} & \text{if } (8\overline{N}_c \overline{r} \overline{F}_T \overline{F}_1)_{ns} \geq \left( -\overline{\omega} \overline{\rho} \frac{\partial \overline{r}}{\partial p} \right)_s \\ (8\overline{N}_c \overline{r} \overline{F}_T \overline{F}_1 \Delta z)_{ns} & \text{if } (8\overline{N}_c \overline{r} \overline{F}_T \overline{F}_1)_{ns} < \left( -\overline{\omega} \overline{\rho} \frac{\partial \overline{r}}{\partial p} \right)_s \end{cases} \quad (40)$$

where  $\Delta z$  is cloud thickness and all quantities are evaluated for non-seeded conditions. The multiplication by cloud thickness serves to express precipitation in more familiar units (cm H<sub>2</sub>O/sec).

Equation 40 allows the precipitation rate to equal the vapor supply rate when the ice growth rate is efficient. However, the precipitation rate becomes equal to the ice growth rate if the diffusional ice process becomes inefficient.

A similar precipitation equation for seeded conditions can be written

$$\overline{(P_s)}_s = \begin{cases} \left( -\overline{\omega} \overline{\rho} \frac{\partial \overline{r}}{\partial p} \right)_s \Delta z)_{ns} & \text{if } (8\overline{N}_c \overline{r} \overline{F}_T \overline{F}_1)_s \geq \left( -\overline{\omega} \overline{\rho} \frac{\partial \overline{r}}{\partial p} \right)_s \\ (8\overline{N}_c \overline{r} \overline{F}_T \overline{F}_1 \Delta z)_s & \text{if } (8\overline{N}_c \overline{r} \overline{F}_T \overline{F}_1)_s < \left( -\overline{\omega} \overline{\rho} \frac{\partial \overline{r}}{\partial p} \right)_s \end{cases} \quad (41)$$

where all quantities are evaluated for seeded conditions. This equation is general in that possible changes due to seeding in the mean vertical

motion, mean cloud density, cloud top temperature, mean crystal size and mean ventilation factor are included.

#### g. Potential for Modification

The static modification potential (S.M.P.) can be defined as the difference in the natural vapor supply rate and the natural precipitation rate. This can be expressed by subtracting (40) from (35) or

$$\text{S.M.P.} = \left( -\bar{\omega} \frac{\partial \bar{r}}{\partial p} \bar{s} \Delta z \right)_{\text{ns}} - \left( 8 \bar{N}_c \bar{r} \bar{F}_T \bar{F}_1 \Delta z \right)_{\text{ns}} \quad (42)$$

where all quantities are evaluated for natural conditions.

The dynamic modification potential (D.M.P.) may be defined as the difference in the seeded and natural vapor supply rates, or

$$\text{D.M.P.} = \left( -\bar{\omega} \frac{\partial \bar{r}}{\partial p} \bar{s} \Delta z \right)_{\text{s}} - \left( -\bar{\omega} \frac{\partial \bar{r}}{\partial p} \bar{s} \Delta z \right)_{\text{ns}} \quad (43)$$

where the quantities are evaluated for natural and seeded conditions.

The total weather modification potential (T.W.M.P.) is the sum of the static and dynamic modification potentials or

$$\text{T.W.M.P.} = \left( -\bar{\omega} \frac{\partial \bar{r}}{\partial p} \bar{s} \Delta z \right)_{\text{s}} - \left( 8 \bar{N}_c \bar{r} \bar{F}_T \bar{F}_1 \Delta z \right)_{\text{ns}} \quad (44)$$

#### h. Overseeding and Validity of Model Equations

It is important to understand, the model equations are derived solely by considering the efficiency of the cold cloud ice process. It has been tacitly assumed, for the most part, that if cloud efficiency is improved by seeding, it will be reflected in improved precipitation efficiency. This is not necessarily the case. It is conceivable that precipitation efficiency may be impaired by seeding, while simultaneously cloud efficiency is unchanged or even improved. This could occur by lowering cloud supersaturation, which in turn, brings about adverse changes in crystal trajectories that result in ice crystals not reaching

the mountain surface. In general, the rate of ice growth in the cloud segment cannot be increased by seeding without lowering cloud supersaturation to a new steady state value (28). Thus, crystal sizes and possibly crystal fall speeds may be reduced. If the crystals continue to reach the mountain, cloud and precipitation efficiencies are both increased. If the crystals now have trajectories over the mountain barrier, precipitation efficiency is reduced. Under the latter condition (overseeding), the model precipitation and potential equations have no physical meaning and are consequently, physically invalid. Also, under this condition of overseeding, loss due to evaporation of ice crystals is no longer small compared to the total vapor supplied, and the assumption underlying the model precipitation and potential equations no longer holds.

- i. Optimum Ice Crystal Concentration

It follows then, the optimum ice crystal concentration associated with the maximum utilization of cloud water is not single-valued, since crystal radius cannot be considered constant. For a specified updraft speed, crystal size will adapt to changing cloud supersaturation as concentrations of growing crystals vary in the cloud system.

There are boundary conditions that confine desired adjustments between crystal size and concentration within the cold orographic cloud. These boundary conditions are mainly a function of cloud temperature and the speed of the air flow through the cloud system. The effect of cloud temperature may be considered by assuming that the speed of the air flow is small, so that cloud residence times for crystals are quite large. In this case, overseeding would be limited to the very coldest cloud systems and be associated with very small crystal sizes. Under this

condition of very cold cloud temperatures and large crystal concentrations, a point is eventually reached where reduction of crystal size and settling speed through seeding can make the difference between crystals reaching the mountain as precipitation, or being carried into the subsiding airstream to the lee of the mountain. Thus, seeding might be expected to reduce precipitation at these coldest cloud temperatures, nearly irrespective of the speed of the wind flow through the cloud.

On the other hand, it is conceivable that when high wind speeds coexist with the limited geometry of some orographic clouds, overseeding may occur at warmer cloud temperatures. This could happen if the small residence times under these conditions produced small crystals, whose settling speeds were barely placing them on the mountain. In this event, seeding could increase crystal concentrations and therefore, the average rate of ice growth by vapor diffusion in the cloud system. This would lead to lower cloud supersaturation and could cause a reduction of individual crystal sizes and fall speeds below those required to place the crystals on the mountain. This latter case is one in which, it is possible to improve the efficiency of the cloud system, but not have this improved cloud efficiency realized at the surface in the form of increased precipitation. Under these conditions, (36) has no physical interpretation in terms of precipitation efficiency.

In the absence of extremely high wind speeds, however, there is probably a range of optimum ice crystal concentrations that efficiently convert the vapor supplied to ice growth in the cloud, and in a form so that it is realized as precipitation on the mountain. Within this range of optimum ice crystal concentrations, there is a possibility of targeting snowfall on the mountain through seeding, while maintaining

precipitation efficiency. Theoretically, this would be possible by producing variations in crystal size through controlling cloud supersaturation. Other possibilities of targeting snowfall by seeding include changing the amount of crystal riming through control of cloud supersaturation, and controlling agglomeration. These concepts have been discussed in relation to other type cloud systems by Juisto (1968) and Weickmann (1970).

It is apparent from (36), if cloud system geometry is specified (base and top), solutions can be computed for various upward speeds and crystal radii as a function of cloud system temperature. If it is assumed that the convective stability of the cloud layer is nearly neutral with respect to moist convection, these solutions can be expressed as a function of temperature at any level of the cloud system. The particular level chosen here is the 500 mb surface.

Figure 9 shows solutions to (36) for upward speeds of 12 cm/sec and 36 cm/sec, and crystal radii of 125 microns and 375 microns. The cloud base and top were assumed to be 650 mb and 460 mb, respectively. Values of 1.30 and 1.64 were assigned the ventilation factor for crystal radii of 125 microns and 375 microns, respectively.

Figure 9 indicates that at colder cloud temperatures the required concentrations of ice crystals nearly stabilize for a given crystal size and upward speed. This stabilization reflects the region where the amount of moisture supplied decreases with temperature at nearly the same rate as the capacity of the crystal to grow. The optimum concentration of ice crystals becomes increasingly larger for a

given crystal size and upward speed as cloud temperatures become warmer. This is due to increasing cloud water supply rates at these warmer temperatures coupled with slower crystal growth rates, which results in an increasing need for more ice crystals to utilize the cloud water.

The difference in actual and optimum ice crystal concentrations may also be computed as a function of cloud system temperature for various upward speeds and crystal radii if cloud geometry is specified. Specific solutions to (39) are shown in Figure 10. These curves were generated assuming a one to one correspondence between ice crystal concentration and ice nuclei concentration ( $\overline{R}_c = 1$ ), and by inserting the time-averaged temperature activation spectrum of primary ice nuclei observed for non-seeded experimental days at Climax.

It is seen from Figure 10, for a mean upward speed of 12 cm/sec and a mean crystal radius of 125 microns, the conversion of cloud water to ice is efficient up to a 500 mb temperature of about  $-20^{\circ}\text{C}$  (where the specified curve crosses the zero deficiency axis). For 500 mb temperatures warmer than  $-20^{\circ}\text{C}$ , ice crystal concentrations are below the number needed to ensure an efficient cold cloud precipitation process. The deficit reaches about 35 crystals per liter at a 500 mb temperature of  $-10^{\circ}\text{C}$ .

It is also noted that tripling the mean upward speed in the cloud system shifts the warmest temperature, for which the diffusional ice growth process is efficient, about 2 degrees C toward colder temperatures. Thus, cloud top temperature dominates over the mean upward speed of the cloud system in controlling the availability of S.M.P. However, the

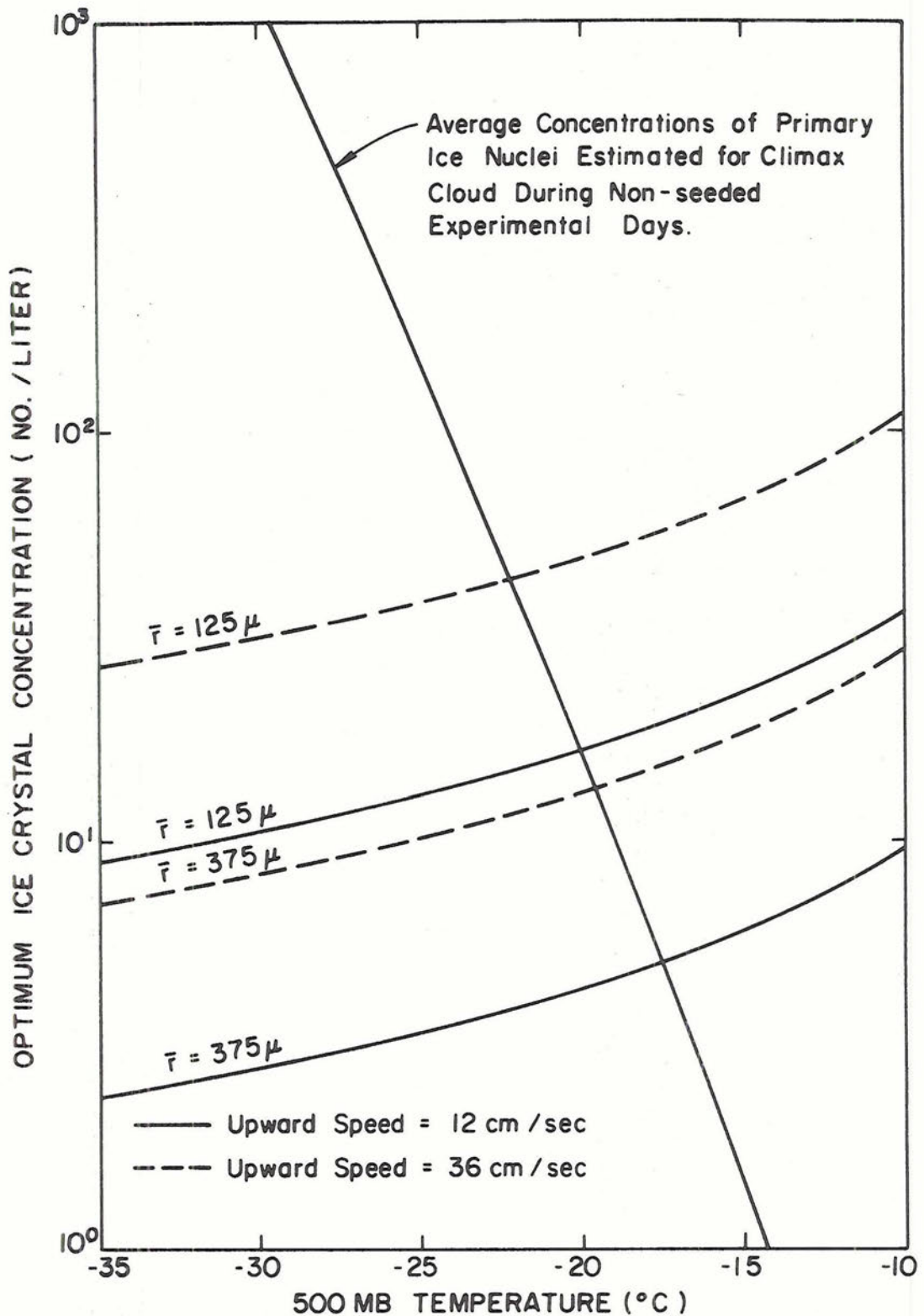


Figure 9. Relationship of ice crystal concentration, ice crystal size, vertical motion and 500 mb temperature which optimizes the efficiency of cloud water utilization. Cloud base and top are assumed to be 650 mb and 460 mb respectively.

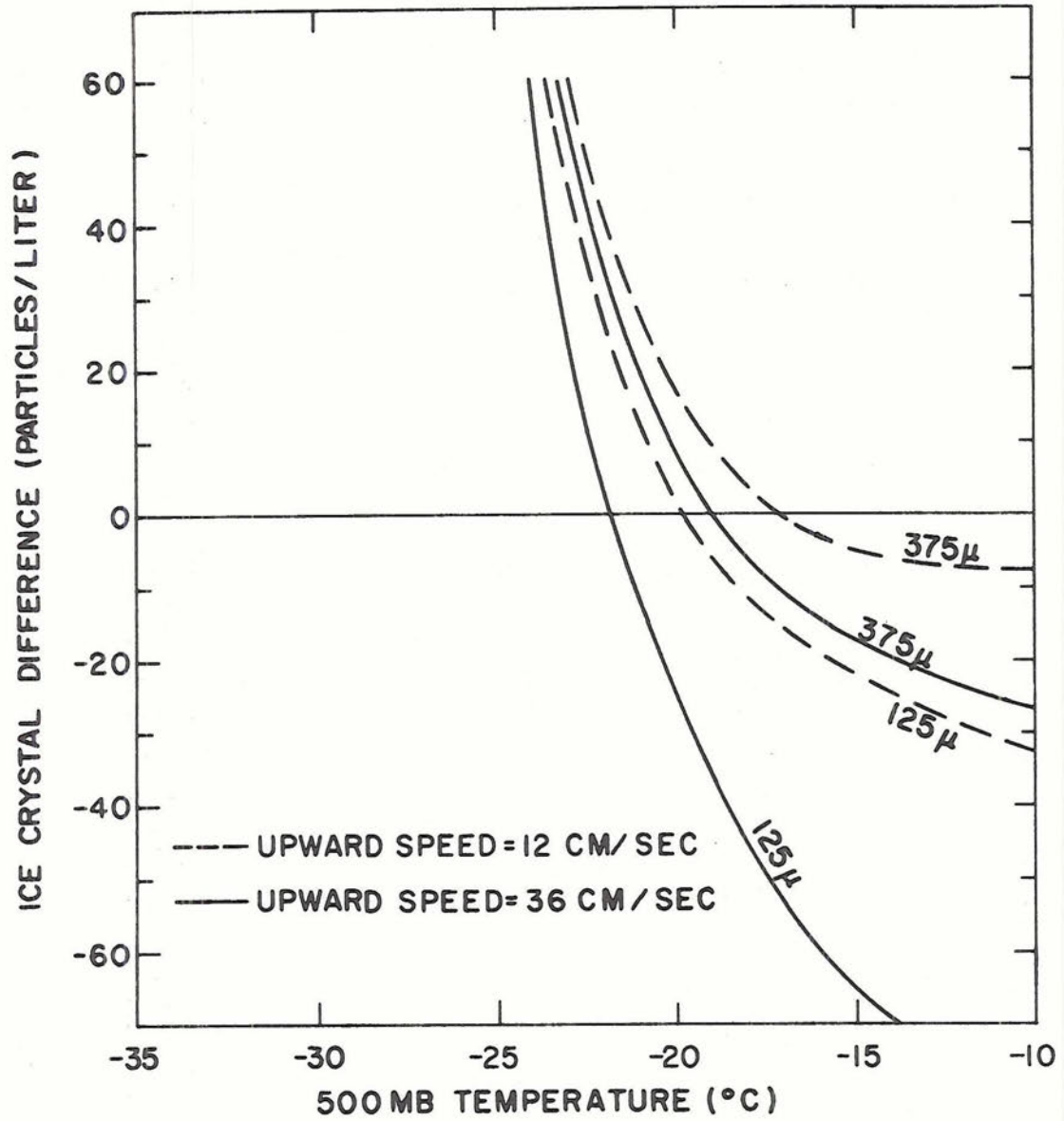


Figure 10. The difference between natural and optimum ice crystal concentrations for various crystal sizes and upward speeds as a function of 500 mb temperature. Cloud base and top are assumed to be 650 mb and 460 mb, respectively.

mean upward speed of the cloud segment becomes quite important in defining the magnitude of S.M.P., once it has been determined to exist at all.

j. Description of Weather Modification Potential Model

A system of equations has been developed which gives expressions for the following quantities:

- (1) Average vapor supply rate
- (2) Average diffusional growth rate of ice
- (3) Average natural ice crystal concentration
- (4) Optimum ice crystal concentration
- (5) Ice crystal concentration required by the cloud to bring the diffusional ice process to full efficiency
- (6) Average natural precipitation rate
- (7) Average seeded precipitation rate
- (8) Static modification potential
- (9) Dynamic modification potential
- (10) Total weather modification potential

This system of equations describes a very simple type of orographic cloud system, i.e., one in which the ice process is paramount in overcoming the microstability of the cloud, and the diffusional growth of ice crystals is the predominate cloud process producing precipitation. A simple cloud geometry was imposed for the model development, consisting of a horizontal cloud base and cloud top. A steady state condition was also imposed, and local and horizontal advective temperature changes within the cloud system were neglected. The less rigorous requirement, that basic equations be satisfied when averaged over the cloud system,

led to the realization that mean cloud quantities would probably describe satisfactorily the overall cloud processes.

In this model the vapor supply rate is determined by the mean vertical motion, mean temperature and mean equivalent potential temperature of the cloud segment. This vapor supply rate is divided by the growth rate of a single ice crystal to determine the optimum ice crystal concentration needed for maximum conversion of cloud water to ice form. The natural ice crystal concentration is estimated from the activation of primary ice nuclei, the latter being a function of cloud top temperature. The optimum ice crystal concentration is subtracted from the natural ice crystal concentration, the difference being the deficit of crystal concentration below that needed to efficiently extract the liquid water forming in the cloud segment and convert it into ice growth.

Natural and seeded precipitation rates in this model are given by the available vapor supply rate, or the rate of ice growth by vapor diffusion, whichever is smallest. The S.M.P. is derived by subtracting the natural rate of ice growth from the available natural vapor supply rate, the difference being an increment of potential precipitation rate. The D.M.P. is derived by subtracting the available vapor supply rate for the natural cloud from that of the seeded cloud, the difference again being an increment of potential precipitation rate. The sum of these two potential precipitation rates gives the T.W.M.P. for the cloud segment.

It was noted in the model development that the basic equations were averaged over the cloud segment. However, with the cloud geometry imposed in the model development, it follows that all quantities in the basic equations have only vertical variations except for the vertical

motion. Thus, the model allows for horizontal variations in precipitation due to differences in the upward speed in various portions of the cloud system.

k. Quantities Representative of Climax Cloud System

Representative estimates of some of the quantities appearing in the system of equations can be accomplished for the Climax cloud system. Crystal replication gives the information needed to estimate mean crystal sizes in the Climax cloud system. The replicated data, however, gives final crystal size and not the mean of the cloud system. A further complication is the fact that considerable crystal growth occurs before appreciable fall velocities develop in the upper portions of the cloud. Considering these factors, the mean crystal radius is estimated to be 125 microns from Figure 3, and a slight dependency upon cloud temperature is neglected. With a value for the mean crystal size, the mean ventilation factor can be computed from (23) and is taken to be 1.3 for the Climax cloud.

The coefficients in the expressions for seeded and non-seeded mean ice crystal concentrations are evaluated from ice nuclei data observed at the High Altitude Observatory (HAO) of the University of Colorado, located at approximately 11,300 ft. msl within the primary target area. This elevation is generally about 1000 ft below cloud base during precipitation occurrence in the area. The exact relationship between primary ice nuclei observations taken at HAO, and those existing within the cloud system is not known. However, it is seen in (45) and (46) that the temperature activation spectra are significantly different on non-seeded and seeded days. It is believed these observations provide for a reasonable estimate of the activation of primary ice nuclei in the

cloud system. The mean ice crystal concentrations for non-seeded conditions are given by

$$(\bar{N}_c)_{ns} = [\bar{R}_c (2.472 \times 10^{-4}) \exp(-0.435T_{ct})]_{ns} \quad (45)$$

and for seeded conditions

$$(\bar{N}_c)_s = [\bar{R}_c (0.254) \exp(-0.217T_{ct})]_s \quad (46)$$

The mean density and mean vertical gradient of saturation mixing ratio are easily determined as a function of cloud temperature when cloud geometry is specified. The mean temperature function,  $F_T$  is evaluated by choosing the function corresponding to a mean pressure of 600 mb and integrating with respect to temperature from cloud top to cloud base. This integration is performed, since in the model about 90 percent of all crystals are generated in the upper third of the cloud system and consequently, their growth rate dependency upon temperature should be integrated downward through the cloud system. This integration over the vertical range of cloud temperature yields a mean thermodynamic function, whose values fluctuate with changing cloud system temperatures, less than the thermodynamic function varies with individual temperatures. The mean thermodynamic function therefore, is not overly sensitive to individual values of the function at specific temperatures.

It should be pointed out that the dual function,  $N_c (dm/dt)_d$  in the model is controlled mainly by the ice crystal concentration term, and is not very sensitive to the growth rate of an individual crystal. The decision to use the theoretical growth equation and to neglect the deviation terms in (32) is therefore not crucial to the final workings of the model. This can be illustrated in Figure 11. If it is assumed that the diffusional growth rate of an individual crystal is

underestimated by a factor of two at all temperatures, the overall effect is to shift the ice growth rate curve toward warmer temperatures by an increment of only 1.5 degrees C. This same effect could be produced through the ice crystal concentration term, by raising the cloud top height by about 13 mb.

On this basis a third degree polynomial fit to the thermodynamic function was determined to facilitate computations. This expression was found to be

$$F_T(600 \text{ mb}) = .0301010 - .6269965T - .0247026T^2 - .0002388T^3 \quad (47)$$

This completes the development of model equations. Before testing the model with results of the Climax and Wolf Creek Pass cloud seeding experiments, the next chapter is devoted to a brief summary of these experiments and the data samples obtained.

## CHAPTER III

### EXPERIMENTAL DATA AND PROCEDURES

#### 1. The Climax Experiment

A study of the precipitation processes that accompany central Colorado mountain snowfall was begun in 1959 at Colorado State University. A systems approach was used which provided observations necessary for a physical evaluation of the experiment. The experimental area was along the Continental Divide in central Colorado in the vicinity of Climax, Colorado. An important part of this investigation included a study of the possibilities of beneficially modifying the natural precipitation process.

The Climax experiment has been discussed by Grant (1960), Grant and Schleusener (1961), and Grant and Mielke (1967). A detailed review of the Climax experiment is given in Appendix C. The experiment was randomized with a 24-hour sampling unit. Eight standard Weather Bureau stations located southwest through northwest to north of the experimental site are used as control stations. The criteria of an experimental day was that at least .01 inches of precipitation be forecasted during a 24-hour sampling unit at Leadville, Colorado, accompanied by a 500 mb wind direction between 210 degrees and 360 degrees, inclusive. This forecast was prepared by the United States Weather Bureau in Denver. Six Colorado State University modified Skyfire, needle-type ground generators were used for seeding using a seeding rate of about 20 grams of silver iodide per hour. Precipitation data from 65 snowfall observation sites were read daily and are available for analysis. A thorough review of the

experimental design, operation procedures, and topography and climatology of the experimental area is presented in Appendix C.

During the period 1960-65, there were 283 experimental days defined for the Climax experiment. Preliminary results of this entire sample were previously discussed (Grant and Mielke, 1967). Chappell (1967) in a further analysis of the 1960-65 Climax data found that several of the experimental events had wind directions that could not bring seeding material toward the primary target area. If only those experimental events with 500 mb wind directions between 210 degrees and 360 degrees inclusive, are considered (as originally defined for the experiment), a sample containing 251 events remains. This sample of 251 cases (Climax I sample) is used here, since it is most appropriate for a physical study of this nature. Use of the sample containing 283 events would only serve to dilute the effects being sought.

During the period 1965-70, there were 384 experimental days defined for the Climax experiment. Twelve of these events were also found to have 500 mb wind directions outside the prescribed direction interval. When those cases are eliminated, a sample containing 372 events (Climax II sample) remains.

The possibility arose, due to upwind seeding activities carried out by Colorado State University in the Berthoud Pass area in 1966, and by Bollay and Associates in the Park Range area during 1965-69, that the Climax target area could have been affected by spurious seeding. In order to compile a sample free of possible upwind seeding effects, cases when this upwind seeding might have affected the primary target area were removed from the Climax II sample.

Criteria used for eliminating these cases were chosen prior to analysis. Effects in the Climax target area from seeding activities conducted at Berthoud Pass were considered possible, when the 700 mb or 500 mb wind direction at Climax was observed from 330 to 030 degrees during the experimental day. Effects in the Climax target area from seeding activities conducted at the Park Range experiment were considered possible, when 700 mb or 500 mb wind directions at Climax were observed to be 290 degrees, or greater, during the experimental day.

When these criteria were applied to the Climax II (372) sample, it was found that 76 days were eliminated, producing a Climax II sample of 296 days. If the Climax II (296) sample is combined with the Climax I (251) sample, a Total Climax sample of 547 days is assembled that is free of possible upwind seeding effects. It should be noted that events, eliminated in order to assemble the Climax II (296) and Total Climax (547) samples, were heavily biased toward northwest flow and larger precipitation episodes. Thus, these data samples are biased toward smaller precipitation events. The unfortunate dilemma arose therefore, whether to analyze the Climax II (372) sample with the possibility of contamination on non-seeded experimental days and a different seeding treatment on seeded experimental days, or eliminate these possible effects, and analyze a data sample strongly biased toward smaller precipitation events. It was decided to work mainly with the Climax I (251), Climax II (372) and Total Climax (623) data samples. However some results of the Climax II (296) and Total Climax (547) data samples are included and identified as such. Otherwise, the designators, "Climax II sample" and "Total Climax sample" refer to the Climax II (372) and Climax Total (623) data samples respectively.

## 2. The Wolf Creek Pass Experiment

The Wolf Creek Pass experiment was inherently an operational program whose basic objective was to augment snowfall over an area of the San Juan Mountain Massif centered at the summit of Wolf Creek Pass. In order to secure useful data from this operational program, three recording precipitation gages were installed near the summit and on the west and east sides of the pass. The basic features incorporated in the Wolf Creek Pass design are given in some detail in Appendix C. A yearly randomization was employed with a 24-hour experimental time unit. Seven standard Weather Bureau stations serve as control stations. The criteria of an experimental day is that at least .01 inches of precipitation occurred during a 24-hour sampling unit at one or more of the recording precipitation gages, or at the control station.

There were 441 days that met the prescribed criteria for an experimental event at Wolf Creek Pass during the five winter seasons from 1964-69. It should be mentioned that in this total sample there were 73 designated seeded cases where no seeding was actually conducted. This represents about 31 percent of the seeded days defined for the experiment. These particular days were biased toward smaller precipitation events, however, since only 25 percent of the total seeded precipitation was not actually seeded. These days were not removed from the seeded sample since there was no satisfactory way to remove their counterpart from the non-seeded sample. Therefore, these 73 days were retained in the seeded sample with the knowledge that their presence might contribute to the dilution of seeding effects and make them conservative.

### 3. Meteorological and Statistical Procedures

#### a. Meteorological Procedures

The hourly distribution of precipitation was investigated for every experimental day. From this information the time of meteorological observations was related to the time of precipitation occurrence. The meteorological data assigned to the precipitation was that nearest the time of precipitation occurrence, or nearest the greatest precipitation amount. The computation of various meteorological parameters used in the analyses is outlined in Appendix D.

#### b. Statistical Procedures

Three statistical procedures are employed in evaluating seeding effectiveness. These include the two-sample Wilcoxon test and the two-sample sum of squared ranks test, both non-parametric procedures. Some of the precipitation changes are expressed by averaging seeded and non-seeded events within given meteorological stratifications and forming seeded to non-seeded precipitation ratios, or computing percentage changes relative to the non-seeded precipitation values.

Additional insight is gained by statistically evaluating the experimental data by two nonparametric methods. The two sample Wilcoxon test gives equal emphasis to all observations while the sum of squared ranks test places greater emphasis on the larger precipitation amounts. Thus, one is able to get an indication of possible variations in seeded effectiveness among precipitation events of differing magnitude.

For more information on the two nonparametric methods employed in this paper, the reader is referred to discussions on these procedures by Taha (1964), Duran and Mielke (1968), Mielke (1967), Grant and Mielke (1967) and Mielke et al. (1970).

CHAPTER IV  
TESTING THE MODEL

1. Introductory Remarks

Many concomitant physical measurements were made in conjunction with the Climax experiment. In spite of these numerous measurements, it is impossible to solve the model equations on a daily basis for all events gathered during the ten year experiment. The mean vertical motion of the cloud system is not known for each day, nor is cloud top height. It is possible to test the model in a time-averaged mode, and this is accomplished in three general ways.

In the next section, the model precipitation equations for natural and seeded conditions are fitted to precipitation observed at HAO during the ten year experiment. In fitting the model precipitation equations to observed precipitation, one may then judge 1) whether the model and observed precipitation functions are similar to one another, 2) whether the model parameters associated with this best fit are reasonable values in a time-averaged mode, 3) whether any difference between observed precipitation and the model precipitation equations are readily explained by processes not included in the model and 4) whether differences between observed precipitation for Climax I and Climax II samples are consistent with model equations. Further testing of the model with observed precipitation is possible, by computing a function representing the difference in seeded and non-seeded precipitation, and comparing its behavior with that given by the S.M.P. equation.

In the third section, the model S.M.P. equation is tested against observed seeding effects for three independent data samples. The seeding effectiveness is computed within stratifications of meteorological parameters, which are explicitly or implicitly expressed within the model S.M.P. equation. These stratifications generally contain sufficient experimental events that meaningful statistical testing for the significance of precipitation changes is possible.

In the fourth section, the behavior of crystal growth processes within the cloud system is compared with that given by the model. In particular, the change in crystal growth processes between non-seeded and seeded conditions is considered.

In the last sections variations in the pattern of seeding effectiveness between Climax I (251) and Climax II (372) samples are exhibited and discussed, and possible upwind seeding effects during the Climax II sampling period are considered.

It may be noted that no attempt is made to test the model D.M.P. equation. In order to do this, very detailed observations of cloud geometry, cloud temperatures and vertical motions would be required between non-seeded and seeded conditions. These detailed observations on the cloud scale are not available. One is therefore limited to considering only the S.M.P. equation. There is still the possibility, however, if the influence of D.M.P. is significant, the observed seeded precipitation will depart substantially from that given by the model S.M.P. equation. Thus, a possibility exists of detecting indirectly a significant D.M.P. effect.

## 2. Testing the Model Precipitation Equations

It is seen from (40), there is a singular solution where

$$\overline{(\dot{P}_s)}_{ns} = \left( -\overline{\omega} \rho \frac{\overline{\delta r}_s}{\partial p} \Delta z \right)_{ns} = \left( 8 \overline{N}_c \overline{r} \overline{F}_T \overline{F}_1 \Delta z \right)_{ns} \quad (48)$$

At this singular point the average rate of ice growth intersects the available average vapor supply rate at a value equal to the average precipitation rate. One may use the value of observed precipitation and a knowledge of cloud temperatures at this singular point to compute the time-averaged mean vertical motion and time-averaged cloud top height. This computation is accomplished by iteration and the methodology for performing the computation is outlined in Appendix B. This computation allows the model precipitation equations to be reasonably fitted to observed precipitation.

### a. Non-seeded Precipitation

The results of fitting the model to non-seeded precipitation observed at HAO during the Climax I (251) and Climax II (372) sampling periods are shown in Figures 11 and 12. It is seen that the model precipitation equation fits observed precipitation data reasonably well for both samples. It is noted that observed precipitation is somewhat higher for the warmer cloud systems than given by the diffusional model. This is not surprising however, for it was seen in Figure 5 that accretional growth of snow crystals may become a factor as diffusional ice growth becomes inefficient. This is due to increased droplet growth associated with rising cloud supersaturation. Also, as pointed out by Grant (1968), occasional ice crystal multiplication is observed in this temperature range. The final result is that natural precipitation at these warmer cloud temperatures is somewhat greater than given by the diffusional model.

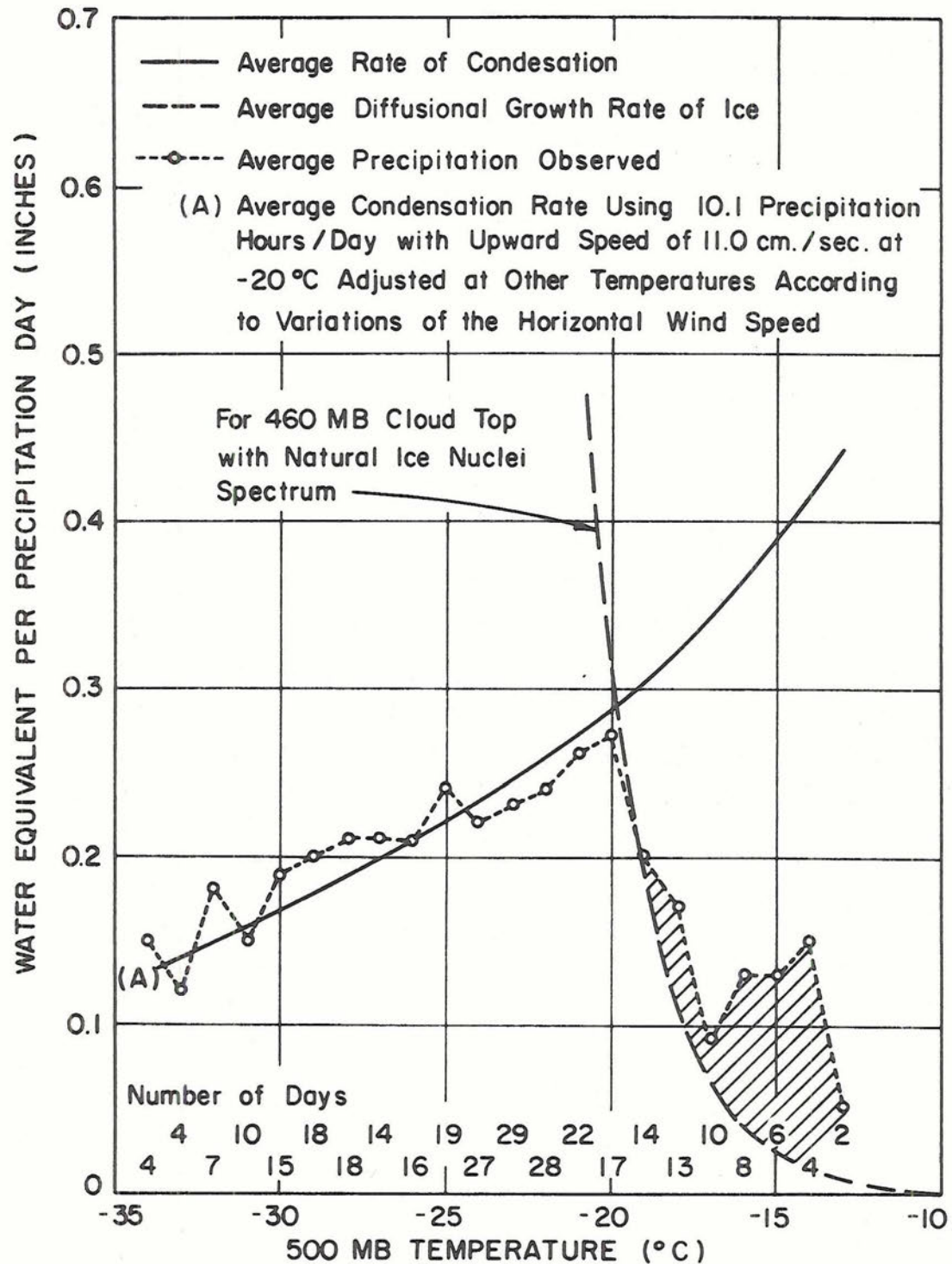


Figure 11. Distribution of non-seeded precipitation at HAO as a function of 500 mb temperature compared to a theoretical distribution computed using the mean diffusional model. Precipitation data are from Climax I sample (251) and values are a running mean over a two-degree temperature interval.

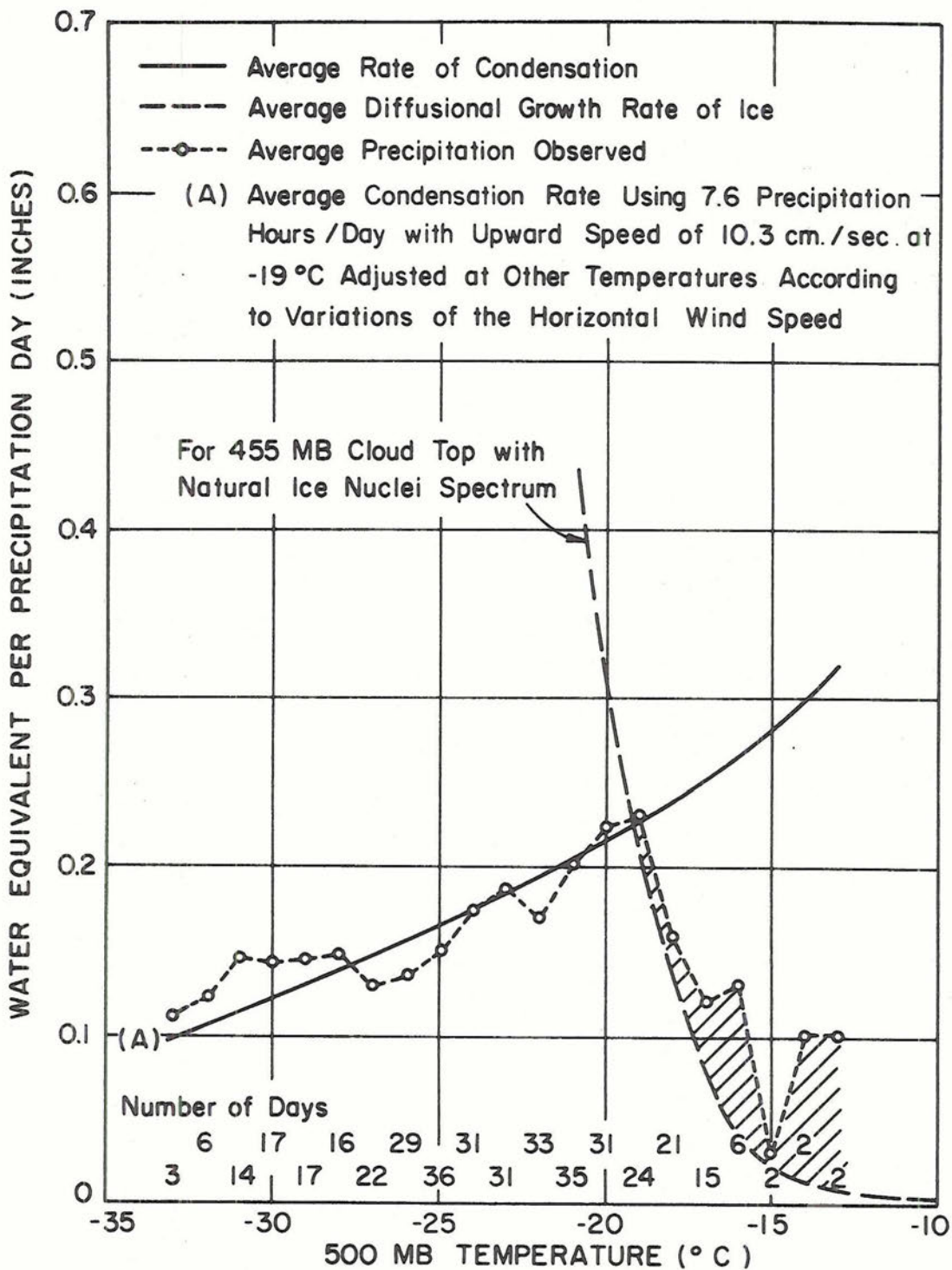


Figure 12. Distribution of non-seeded precipitation at HAO as a function of 500 mb temperature compared to a theoretical distribution computed using the mean diffusional model. Precipitation data are from Climax II sample (372) and values are a running mean over a two-degree temperature interval.

It is of considerable interest that the natural precipitation during the Climax II sampling period does not decrease until a 500 mb temperature of  $-19^{\circ}\text{C}$  is reached. This compares to a temperature of  $-20^{\circ}\text{C}$  for the Climax I sampling period. This maintenance of precipitation efficiency at slightly warmer cloud temperatures during the Climax II sampling period is in agreement with the model, since the available rate of vapor supply was somewhat less during this five year period. The possibility that spurious upwind seeding may have influenced somewhat the 500 mb temperature at which the natural precipitation decreases for the Climax II (372) sampling period is discussed in the last section of this Chapter.

It is seen from Figures 11 and 12, time-averaged cloud tops during precipitation, associated with a reasonable fit, are 460 mb and 455 mb for Climax I (251) and Climax II (372) samples, respectively. These pressure levels are generally near 20,000 feet over the area in the wintertime and this height is in agreement with cloud top radar studies of Furman (1967). The time-averaged mean vertical motion of 11.0 cm/sec at  $-20^{\circ}\text{C}$  for Climax I sampling period, and 10.3 cm/sec at  $-19^{\circ}\text{C}$  for Climax II sampling period, also appear to be reasonable values.

#### b. Seeded Precipitation

The results of fitting the model to seeded precipitation observed during the Climax I (251) and Climax II (372) sampling periods are shown in Figures 13 and 14. The methodology for accomplishing this fit is similar to, but not identical to that used for natural precipitation, and is also set forth in Appendix B. It is seen in the 500 mb temperature range from  $-20^{\circ}\text{C}$  to  $-15^{\circ}\text{C}$ , observed seeded precipitation continues to increase irregularly as given by the model equation. The insertion of the observed seeded ice nuclei spectrum into the model precipitation

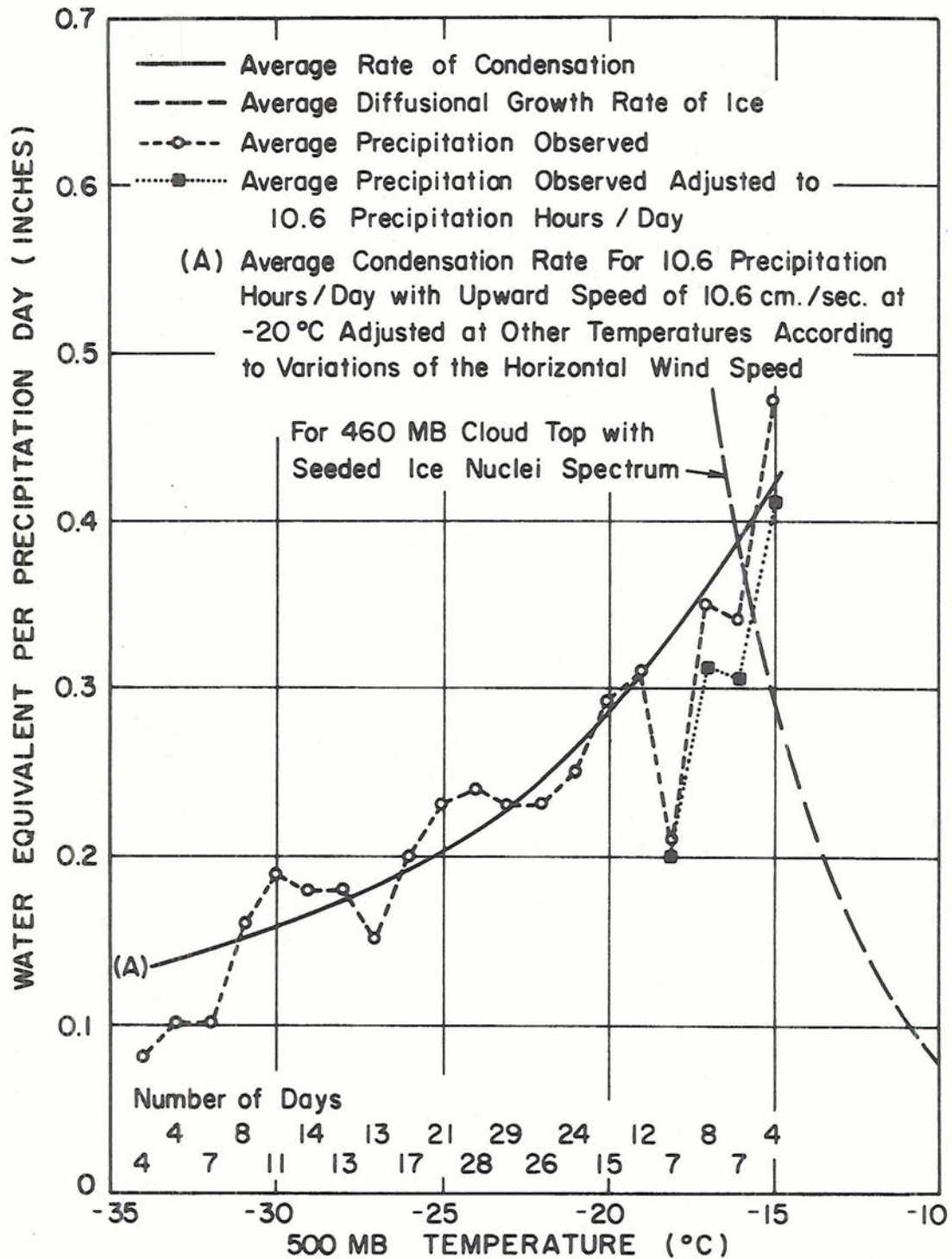


Figure 13. Distribution of seeded precipitation at HAO as a function of 500 mb temperature compared to a theoretical distribution computed using the mean diffusional model. Precipitation data are from Climax I sample (251) and values are a running mean over a two-degree temperature interval.

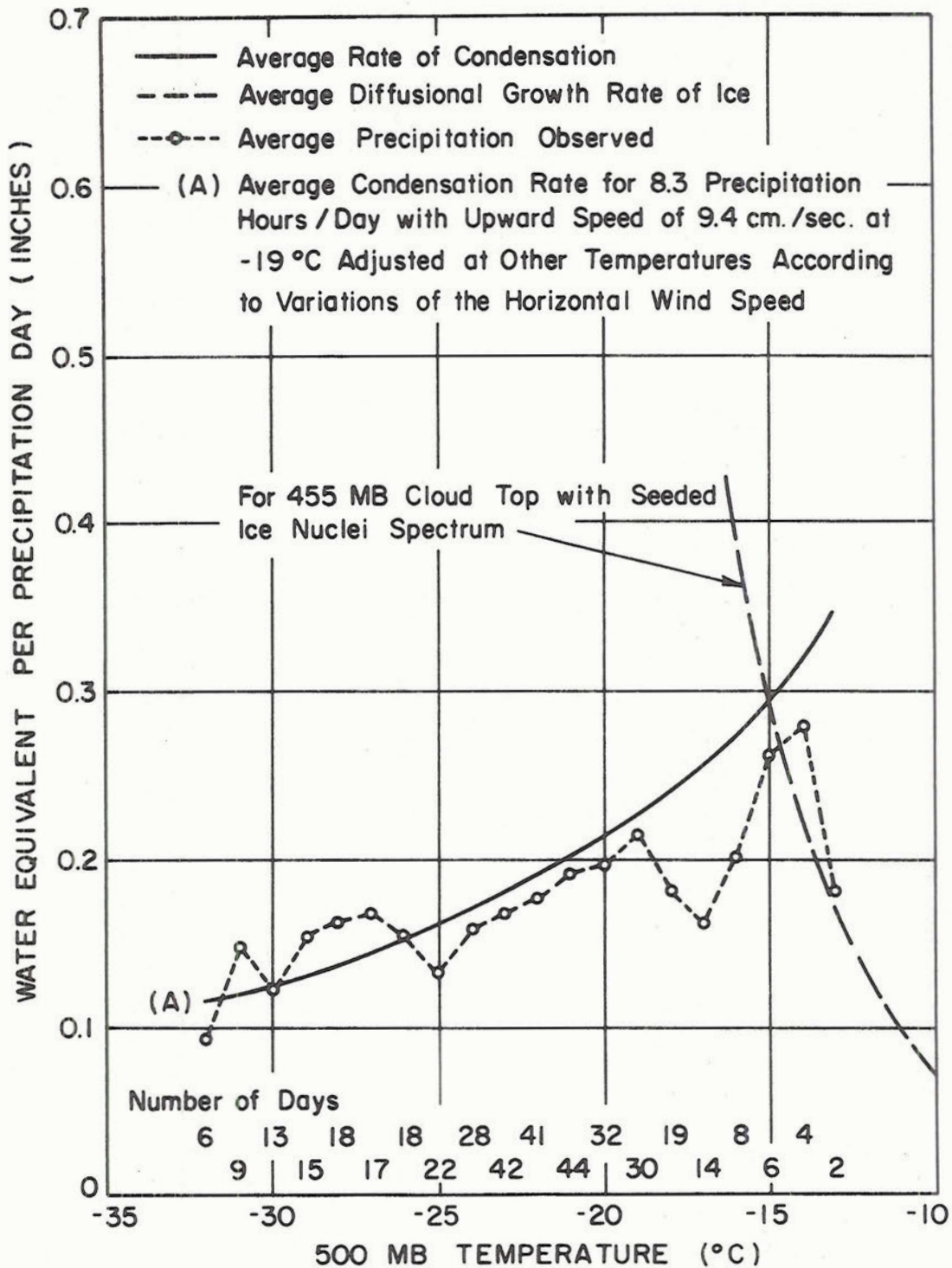


Figure 14. Distribution of seeded precipitation at HAO as a function of 500 mb temperature compared to a theoretical distribution computed using the mean diffusional model. Precipitation data are from Climax II sample (372) and values are a running mean over a two-degree temperature interval.

equation suggests the diffusional ice growth process should be efficient at least up to a 500 mb temperature of about  $-15^{\circ}\text{C}$ , or about 5 degrees C warmer than for the natural precipitation process. The behavior of the observed seeded precipitation is in good agreement with the model in this temperature range.

Unfortunately, there is no way to test the model concerning an expected decrease in seeded precipitation at 500 mb temperatures above about  $-15^{\circ}\text{C}$ . The extremely small number of events that occur in this temperature region do not define the seeded precipitation values with any confidence.

It is seen in Figures 13 and 14, time-averaged mean vertical motions of 10.6 cm/sec and 9.4 cm/sec for Climax I and Climax II sampling periods, respectively, are again reasonable values.

#### c. Seeded Minus Non-seeded Precipitation

If non-seeded precipitation is subtracted from seeded precipitation, a function is generated that describes the change in mean daily precipitation between seeded and non-seeded days as a function of cloud system temperature. This change in precipitation can also be expressed as a percentage change between seeded and non-seeded days.

The behavior of these precipitation change functions, shown in Figure 15, demonstrates three important features in qualitative agreement with the model developed. First, they suggest overseeding may have reduced precipitation on seeded days for the very coldest cloud temperatures. Secondly, they indicate the boundary marking the availability of S.M.P. appears quite abruptly as cloud top temperatures become warmer, and the ensuing precipitation increases realized follow crudely an exponential increase with temperature. Thirdly, they suggest an intermediate

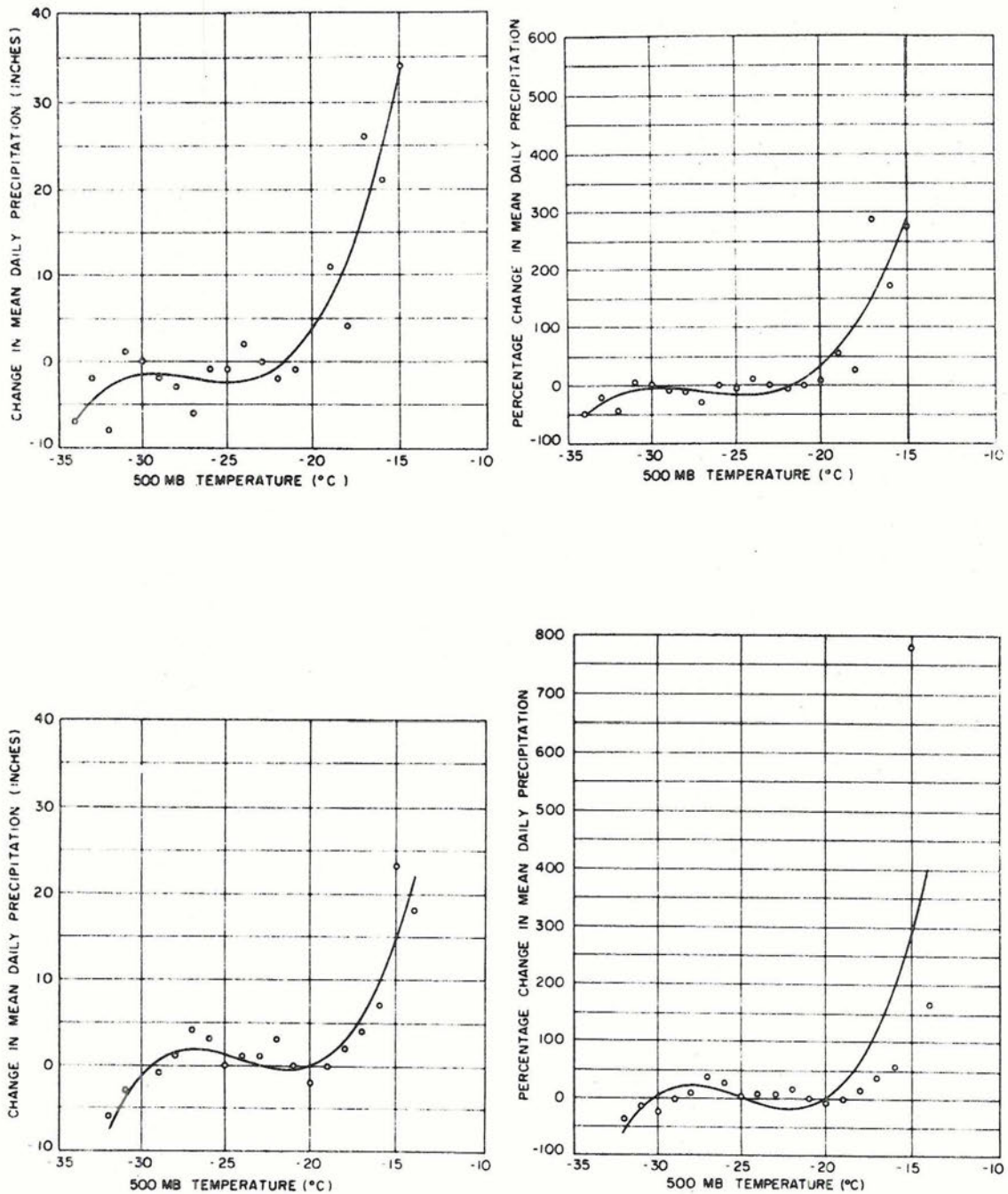


Figure 15. Change and percentage change in mean daily precipitation during seeded days compared with non-seeded days as a function of 500 mb temperature for Climax I (251) (upper) and Climax II (372) (lower) samples. Lines are third degree polynomial curve fits to the plotted values.

range of cloud top temperatures where the precipitation process is efficient, and seeding neither helps nor hinders the precipitation efficiency to any noticeable degree. It is in this range where crystals continue to reach the mountain, even though crystal concentrations may exceed somewhat the optimum concentration required for maximum utilization of cloud water.

### 3. Testing the Model S.M.P. Equation with Observed Seeding Effects

#### a. Introductory Remarks

In this section the model S.M.P. equation is tested with seeding effects computed within stratifications of meteorological parameters expressed explicitly or implicitly within the equation. The model S.M.P. equation, by combining (42) and (45), may be written

$$\text{S.M.P.} = \left( \bar{\omega} \frac{\partial \bar{r}_s}{\partial p} \Delta z \right)_{\text{ns}} - [19.78(10^{-4}) \bar{r} \bar{F}_T \bar{F}_1 \bar{R}_c (\Delta z) \exp(-0.435T_{\text{ct}})]_{\text{ns}} \quad (49)$$

It is seen in (49), in the absence of ice crystal multiplication ( $\bar{R}_c = 1$ ), S.M.P. reduces to a function of cloud system temperatures, cloud top height, and the mean vertical motion and mean crystal size in the cloud system. If cloud base, vertical motion and crystal size are specified, there is a critical cloud top temperature that makes the last term in (49) just equal the first term. This critical cloud top temperature marks the boundary of S.M.P. availability. As cloud top temperatures become warmer than this critical value, S.M.P. increases due to the exponential decrease in the ability of the cloud system to grow ice.

Based on (49) then, a few meteorological parameters are chosen for which to stratify the experimental data. The influence of cloud top temperature upon the natural supply of effective primary ice nuclei

is investigated through the 500 mb temperature. Although it was seen in the last section that cloud tops probably average slightly higher than this pressure level, 500 mb is generally in the vicinity of cloud top, and temperature fluctuations at this level approximate temperature variations at cloud top. The 700 mb equivalent potential temperature is also used for stratification. It is another measure of cloud system temperatures, and in addition, takes into account the available moisture supply. Another parameter employed is the vertical gradient of saturation mixing ratio (potential condensate), which appears directly in (49). Cloud top temperature is also implicit in both these latter parameters. Other parameters chosen relate crudely to vertical motion through orographic influences on the wind flow, convective stability of the cloud layer, and baroclinicity.

Tables 1 through 8 show computed precipitation changes within stratifications of the various meteorological parameters. The tables list total sample size (seeded and non-seeded days), sample size used in the statistical computations (total sample minus any missing data), and estimates of precipitation changes computed with and without control precipitation data. Control precipitation data are not included for the Climax II and Total Climax samples, since statistical tests under the Climax randomization procedure are valid without control. It was also determined during the analysis of the Climax I data sample that inclusion of control precipitation data, having only a mediocre correlation with the target, was probably adding nothing beneficial to the analysis. The two-sample Wilcoxon test is denoted NP1 in the tables, while the two-sample sum of squared ranks test is designated NP2. In order to present some meaningful interpretation of the statistical results, the p-value

(probability that the indicated scale change is exceeded by chance) is also included in the tables.

The results presented in Tables 1 through 8 are for the Climax I (251 days), Climax II (372 days), Climax II (296 days), Total Climax (623 days), Total Climax (547 days) and Wolf Creek (441 days) data samples for identical or similar meteorological stratifications. The Climax II (296) and Total Climax (547) results are shown in parentheses adjacent to the Climax II (372) and Total Climax (623) results, respectively. In the Climax portion of the tables the data presented are based mostly on an average of a precipitation recording gage and a snowboard located adjacent to one another at the High Altitude Observatory (HAO) of the University of Colorado near the center of the designated primary target area. If one of the precipitation observations was missing, the other observation was utilized. In less than one percent of the events, precipitation was estimated from adjacent snowboards (number 9, 11, 12, 13) lying about one mile east of the observatory. This represents the most complete and reliable precipitation data sample gathered within the primary target area. The Wolf Creek Pass portion of the tables is based on recorded hourly precipitation data measured near the summit of the pass.

b. Cloud System Temperatures and Available Moisture

1) 500 mb Temperature (Vicinity of Cloud Top)

The distribution of seeding effects with 500 mb temperature is shown in Table 1. The trend of the seeding effect with temperature is clearly evident and duplicated by all samples. In general, the results indicate that snowfall was unaffected or decreased slightly when very cold cloud systems were seeded. Substantial increases in snowfall are

Table 1. Estimate of scale changes during seeded periods with respect to non-seeded periods as computed by two nonparametric statistical methods. Precipitation data are from the High Altitude Observatory near Climax and near the summit of Wolf Creek Pass. Scale changes are shown within stratifications of the 500 mb temperature. Data for Climax II (296) and Total Climax (547) samples are shown in parentheses.

Stratification (°C)	Total sample size	Sample size used	Method	Without control		With control	
				Scale change (%)	p-value	Scale change (%)	p-value
Climax I (251) Sample							
-39 thru -26	S 32	S 32	NP1	- 31	.0091	- 18	.1093
	NS 34	NS 34	NP2	- 22	.0329	- 8	.3156
-25 thru -21	S 53	S 53	NP1	- 1	.4920	- 1	.4721
	NS 56	NS 56	NP2	- 5	.3897	- 13	.3085
-20 thru -11	S 35	S 35	NP1	+100	.0764	+142	.0409
	NS 41	NS 41	NP2	>+200	.0239	+ 89	.1711
Climax II (372) and (296) Samples							
-39 thru -26	S 39 (27)	S 39 (27)	NP1	0 (+11)	.4766 (.2981)		
	NS 49 (32)	NS 49 (32)	NP2	+ 3 (+17)	.3936 (.2148)		
-25 thru -21	S 70 (58)	S 70 (58)	NP1	+ 41 (+62)	.1020 (.0934)		
	NS 73 (57)	NS 73 (57)	NP2	+ 14 (+47)	.2776 (.1423)		
-20 thru -11	S 73 (62)	S 73 (62)	NP1	+ 37 (+104)	.3156 (.1736)		
	NS 68 (60)	NS 68 (60)	NP2	+ 34 (+124)	.2912 (.1131)		
-18 thru -11	S 36 (31)	S 36 (31)	NP1	>+200(>+200)	.1210 (.1093)		
	NS 47 (44)	NS 47 (44)	NP2	>+200(>+200)	.1314 (.0778)		
Total Climax (623) and (547) Samples							
-39 thru -26	S 71 (59)	S 71 (59)	NP1	- 19 (-20)	.0901 (.0968)		
	NS 83 (66)	NS 83 (66)	NP2	- 12 (-14)	.1867 (.1660)		
-25 thru -21	S123 (111)	S123 (111)	NP1	+ 28 (+24)	.1075 (.1977)		
	NS129 (113)	NS129 (113)	NP2	+ 16 (+18)	.2206 (.2206)		
-20 thru -11	S108 (97)	S108 (97)	NP1	+ 50 (+106)	.1660 (.0901)		
	NS109 (101)	NS109 (101)	NP2	+ 33 (+61)	.2005 (.1056)		
-18 thru -11	S 54 (49)	S 54 (49)	NP1	+170(>+200)	.1038 (.0901)		
	NS 71 (68)	NS 71 (68)	NP2	+ 39 (+107)	.2643 (.1492)		
Wolf Creek Summit (441) Sample							
-39 thru -24	S 82	S 81	NP1	- 2	.4562	0	.4960
	NS 63	NS 63	NP2	- 7	.2981	- 2	.4560
-23 thru -21	S 61	S 56	NP1	+ 4	.4052	+ 33	.0526
	NS 50	NS 49	NP2	+ 8	.3446	+ 41	.1056
-20 thru -11	S106	S 95	NP1	+ 74	.0869	+ 24	.2236
	NS 79	NS 65	NP2	+165	.0129	+171	.0136

indicated for the warmest cloud systems. Some of the statistical tests for the coldest and warmest stratifications show p-values of less than 5 percent for the Climax I and Wolf Creek samples. A difference in seeding effect is noted between the Climax I (251) and Climax II (372) samples for 500 mb temperatures  $-20^{\circ}\text{C}$  and warmer. The Climax I (251) sample shows large increases which are considerably reduced for the Climax II (372) sample. However, if the Climax II (372) sample is evaluated for 500 mb temperatures of  $-18^{\circ}\text{C}$  and warmer, snowfall increases of the same magnitude are found. It is also seen that this difference, in seeding effectiveness for 500 mb temperatures of  $-20^{\circ}\text{C}$  and warmer, is not significant if the Climax I (251) sample is compared with the Climax II (296) sample, which has all spurious upwind seeding events eliminated. This raises the question about the possibility of upwind seeding influencing the results during the Climax II sampling period, especially within the 500 mb temperature range from  $-18^{\circ}\text{C}$  to  $-20^{\circ}\text{C}$ . Whether the slight shift toward warmer cloud temperatures, of the large positive seeding effect for the Climax II (372) sample, is due to spurious upwind seeding effects, or other causes, will be considered further in the last section of this chapter.

Results of the cold orographic cloud seeding experiment conducted at the Park Range in Colorado by Bollay and Associates during 1968-69 (Rhea and Davis, 1970) also indicate large increases (over 100 percent) in precipitation for seeded events when cloud top temperatures were  $-20^{\circ}\text{C}$  and warmer. Little seeding effect or small negative seeding effects were noted for cases with cloud tops colder than  $-20^{\circ}\text{C}$ .

The trend indicated in the seeding effect as a function of the 500 mb temperature is consistent with the model presented. The rather abrupt

appearance of substantial increases in snowfall for the warmest cloud systems indicates that cloud top temperatures have exceeded the critical value that marks the availability of S.M.P.

## 2) Potential Condensate

If a 700 mb parcel of air (generally representative of the subcloud layer in the Colorado Rockies) is lifted dry adiabatically to saturation and moist adiabatically to 500 mb, an estimate may be derived for the value of  $\partial r_s / \partial p$  below 500 mb. This parameter is designated the potential condensate. It is dependent upon cloud system temperatures, but also includes more realistically, variations in the moisture supply of the air mass crossing the mountain barrier.

Table 2 shows the trend of seeding effects with the potential condensate. Seeding effects are generally slightly negative or near zero for the smaller values of potential condensate. Significant positive seeding effects appear for the largest values. Again, some of the statistical tests for the smallest and largest stratifications of potential condensate indicate p-values of less than 5 percent. Both Total Climax samples, Climax II (296) and Wolf Creek samples show p-values less than 1 percent for the largest category. The consistency among all samples, and with the model, is again quite good.

## 3) 700 mb Equivalent Potential Temperature

The equivalent potential temperature evaluated near or just below cloud base is an estimate of the mean pseudo-adiabatic process curve followed by rising cloud parcels. It combines moisture and temperature characteristics of the air mass into a single parameter. Cloud top temperature is also implicit in this parameter. Therefore, the model

Table 2. Estimate of scale changes during seeded periods with respect to non-seeded periods as computed by two nonparametric statistical methods. Precipitation data are from the High Altitude Observatory near Climax and near the summit of Wolf Creek Pass. Scale changes are shown within stratifications of a computed vertical gradient of saturation mixing ratio below the 500 mb level (potential condensate). Data for Climax II (296) and Total Climax (547) samples are shown in parentheses.

Stratification gm/kgm (100 mb)	Total sample size	Sample size used	Method	Without control		With control	
				Scale change (%)	p-value	Scale change (%)	p-value
<b>Climax I (251) Sample</b>							
0 to <0.8	S 30	S 30	NP1	- 40	.0401	- 21	.1635
	NS 35	NS 35	NP2	- 31	.0526	- 15	.2483
0.8 to <1.2	S 48	S 48	NP1	- 12	.2676	- 5	.4129
	NS 50	NS 50	NP2	- 5	.3594	- 35	.1151
1.2 to <2.3	S 42	S 42	NP1	+ 83	.0681	+ 61	.0548
	NS 46	NS 46	NP2	+ 97	.0446	+ 70	.0537
<b>Climax II (372) and (296) Samples</b>							
0 to <0.8	S 49 (34)	S 49 (34)	NP1	- 4 (-6)	.4404 (.4681)		
	NS 44 (29)	NS 44 (29)	NP2	- 13 (-6)	.2578 (.4401)		
0.8 to <1.2	S 56 (44)	S 56 (44)	NP1	- 34 (-24)	.0985 (.2327)		
	NS 75 (58)	NS 75 (58)	NP2	- 12 (-1)	.3228 (.4801)		
1.2 to <2.3	S 77 (69)	S 77 (69)	NP1	+146(>+200)	.0202 (.0023)		
	NS 71 (62)	NS 71 (62)	NP2	+ 93(>+200)	.0217 (.0060)		
<b>Total Climax (623) and (547) Samples</b>							
0 to <0.8	S 79 (64)	S 79 (64)	NP1	- 30 (-42)	.0853 (.0526)		
	NS 79 (64)	NS 79 (64)	NP2	- 32 (-39)	.0392 (.0375)		
0.8 to <1.2	S104 (92)	S104 (92)	NP1	- 3 (-3)	.4286 (.4325)		
	NS125 (108)	NS125 (108)	NP2	- 3 (-2)	.4404 (.4766)		
1.2 to <2.3	S119 (111)	S119 (111)	NP1	+103 (+149)	.0094 (.0064)		
	NS117 (108)	NS117 (108)	NP2	+ 91 (+125)	.0051 (.0036)		
<b>Wolf Creek Summit (441) Sample</b>							
0 to <0.8	S 55	S 53	NP1	+ 6	.4443	+ 6	.4090
	NS 44	NS 41	NP2	+ 9	.3974	+ 3	.4960
0.8 to <1.2	S 97	S 91	NP1	- 18	.2266	+ 3	.4247
	NS 71	NS 70	NP2	- 5	.3336	+ 11	.2946
1.2 to <2.3	S 97	S 88	NP1	+134	.0043	+ 79	.0192
	NS 77	NS 66	NP2	+133	.0107	+146	.0096

equation indicates that the trend of seeding effectiveness with this parameter should be similar to that observed with 500 mb temperature.

Table 3 shows seeding effects within stratifications of the 700 mb equivalent potential temperature. Seeding effects are slightly negative or near zero, when the colder equivalent potential temperatures were seeded. At warmer equivalent potential temperatures the seeding effect reverses, and snowfall increases are substantial when the warmest equivalent potential temperatures were seeded. P-values are again less than 5 percent for some of the statistical tests in the coldest category, and are about 1 percent or less for most Climax and Wolf Creek samples for the warmest stratifications. Again, the agreement among the samples and with the model equation is apparent.

#### c. Vertical Motion

The direction and speed of the air flow relative to the orientation of the mountain barrier have an important bearing on the upward speed imparted to the air crossing the mountain barrier. In this subsection four meteorological parameters related to the nature and magnitude of the upward air motion are stratified and observed seeding effects are discussed relative to the model S.M.P. equation.

##### 1) 700 mb Wind Direction and Speed

The Continental Divide runs west to east across the Climax experimental area, and the better orographic uplifting exists up the Eagle River Valley with northwest wind flow, and up the East Fork of the Arkansas River with southwest wind flow. In a westerly direction, a good orographic fetch toward the Climax area is missing and air is forced over two north-south ranges (Sawatch Range and Chicago Ridge) before reaching the primary target area.

Table 3. Estimate of scale changes during seeded periods with respect to non-seeded periods as computed by two nonparametric statistical methods. Precipitation data are from the High Altitude Observatory near Climax and near the summit of Wolf Creek Pass. Scale changes are shown within stratifications of the 700 mb equivalent potential temperature. Data for Climax II (296) and Total Climax (547) samples are shown in parentheses.

Stratification (°K)	Total sample size	Sample size used	Method	Without control		With control	
				Scale change (%)	p-value	Scale change (%)	p-value
Climax I (251) Sample							
281 to <295	S 23	S 23	NP1	- 38	.0220	- 25	.0890
	NS 21	NS 21	NP2	- 30	.0230	- 13	.1740
295 to <308	S 64	S 64	NP1	- 9	.3020	- 2	.4440
	NS 69	NS 69	NP2	- 5	.3590	- 13	.2150
308 to <326	S 33	S 33	NP1	+112	.0520	+ 80	.0480
	NS 41	NS 41	NP2	+107	.0580	+102	.0570
Climax II (372) and (296) Samples							
281 to <295	S 34 (24)	S 34 (24)	NP1	- 8 (+17)	.4013 (.3121)		
	NS 33 (17)	NS 33 (17)	NP2	- 8 (+42)	.3409 (.2119)		
295 to <308	S 82 (64)	S 82 (64)	NP1	- 25 (-34)	.1635 (.1112)		
	NS 97 (78)	NS 97 (78)	NP2	- 15 (-8)	.2743 (.3897)		
308 to <326	S 66 (59)	S 66 (59)	NP1	>+200(>+200)	.0045 (.0014)		
	NS 60 (54)	NS 60 (54)	NP2	>+200(>+200)	.0073 (.0035)		
Total Climax (623) and (547) Samples							
281 to <295	S 57 (47)	S 57 (47)	NP1	- 30 (-30)	.0606 (.0694)		
	NS 54 (38)	NS 54 (38)	NP2	- 27 (-23)	.0446 (.0901)		
295 to <308	S146 (128)	S146 (128)	NP1	- 6 (-12)	.3632 (.2743)		
	NS166 (147)	NS166 (147)	NP2	- 2 (-9)	.4712 (.3264)		
308 to <326	S 99 (92)	S 99 (92)	NP1	+189(>+200)	.0049 (.0037)		
	NS101 (95)	NS101 (95)	NP2	+133 (+155)	.0066 (.0054)		
Wolf Creek Summit (441) Sample							
285 to <297	S 53	S 53	NP1	- 8	.3336	- 9	.2912
	NS 35	NS 34	NP2	- 5	.3520	- 9	.2236
297 to <303	S 54	S 51	NP1	- 14	.3228	+ 3	.4522
	NS 46	NS 46	NP2	- 8	.3300	+ 4	.4286
303 to <309	S 74	S 68	NP1	+ 16	.2358	+ 24	.0749
	NS 61	NS 59	NP2	+ 23	.2177	+ 51	.0548
309 to <326	S 68	S 60	NP1	>+200	.0136	+125	.0559
	NS 50	NS 38	NP2	>+200	.0102	>+200	.0162

It would be expected from orographic considerations alone, that northwest and southwest flow events would favor positive seeding effects more than westerly flow. This is seen to be the case in Table 4. Figures 16 through 19 show a trend toward warmer 500 mb temperatures and 700 mb equivalent potential temperatures with southwest flow events. These quantities decrease for westerly flow events and are coldest for northwest flow cases. Also, Figures 20 and 21 indicate that the speed of the wind flow generally increases with 500 mb temperature and 700 mb equivalent potential temperature. The combination of these factors probably results in higher condensation rates and warmer cloud systems with southwesterly flow events. The significant increases in snowfall noted with southwest flow events (p-values less than 2 percent for Total Climax samples) therefore, appears consistent with the model equation.

It is also noted in Table 5 that substantial positive seeding effects extended into colder cloud systems for southwest flow events, and this was not observed for other wind directions. Equation 49 indicates that the availability of S.M.P. extends somewhat further into colder cloud systems, when stronger upward motions are present. It is possible then, that extension of positive seeding effects into colder cloud systems with southwest flow may be partially due to the superimposition of synoptic scale upward motion (pre-trough conditions) on the strong orographic effect. For the coldest cloud systems, positive seeding effects also disappear with southwest flow as would be expected from the model equation.

One might question why positive seeding effects are noted for northwest flow conditions, when on the average, they are accompanied by the coldest 500 mb temperatures and 700 mb equivalent potential temperatures.

Table 4. Estimate of scale changes during seeded periods with respect to non-seeded periods as computed by two nonparametric statistical methods. Precipitation data are from the High Altitude Observatory near Climax and near the summit of Wolf Creek Pass. Scale changes are shown within stratifications of the 700 mb wind direction. Data for Climax II (296) and Total Climax (547) samples are shown in parentheses.

Stratification (Degrees)	Total sample size	Sample size used	Method	Without control		With control	
				Scale change (%)	p-value	Scale change (%)	p-value
Climax I (251) Sample							
190 thru 250	S 26	S 26	NP1	>+200	.0721	+ 74	.1314
	NS 25	NS 25	NP2	+183	.0618	+ 58	.1314
260 thru 300	S 56	S 56	NP1	- 38	.0475	- 7	.3409
	NS 67	NS 67	NP2	- 36	.0505	- 7	.3936
310 thru 360	S 26	S 26	NP1	+ 41	.1359	+ 76	.0635
	NS 31	NS 31	NP2	+ 39	.0951	+ 23	.2389
010 thru 180	S 12	S 12	NP1	- 15	.2420	<- 50	.1660
	NS 8	NS 8	NP2	- 17	.1762	<- 50	.1736
Climax II (372) and (296) Samples							
190 thru 250	S 52 (52)	S 52 (52)	NP1	+ 80 (+161)	.1151 (.0446)		
	NS 48 (45)	NS 48 (45)	NP2	+115 (+132)	.0359 (.0301)		
260 thru 300	S 79 (63)	S 79 (63)	NP1	- 6 (-3)	.3745 (.4562)		
	NS 79 (68)	NS 79 (68)	NP2	- 4 (+4)	.3974 (.4013)		
310 thru 360	S 40 (22)	S 40 (22)	NP1	+ 42 (+174)	.1423 (.0618)		
	NS 52 (28)	NS 52 (28)	NP2	+ 18 (+145)	.2611 (.0548)		
010 thru 180	S 11 (10)	S 11 (10)	NP1	- 4 (+8)	.4483 (.4840)		
	NS 11 (8)	NS 11 (8)	NP2	- 36 (+7)	.2514 (.4880)		
Total Climax (623) and (547) Samples							
190 thru 250	S 78 (78)	S 78 (78)	NP1	+157(>+200)	.0188 (.0094)		
	NS 73 (70)	NS 73 (70)	NP2	+172(>+200)	.0057 (.0035)		
260 thru 300	S135 (119)	S135 (119)	NP1	- 20 (-22)	.1335 (.1379)		
	NS146 (135)	NS146 (135)	NP2	- 18 (-20)	.1230 (.1379)		
310 thru 360	S 66 (48)	S 66 (48)	NP1	+ 52 (+106)	.0505 (.0294)		
	NS 83 (59)	NS 83 (59)	NP2	+ 31 (+58)	.0901 (.0606)		
010 thru 180	S 23 (22)	S 23 (22)	NP1	- 31 (-39)	.1949 (.1635)		
	NS 19 (16)	NS 19 (16)	NP2	- 26 (-15)	.1611 (.2451)		
Wolf Creek Summit (441) Sample							
230 thru 250	S 72	S 68	NP1	+ 69	.0351	+ 56	.0446
	NS 39	NS 34	NP2	+ 84	.0073	+101	.0054
260 thru 280	S 56	S 51	NP1	+ 2	.4801	+ 9	.3228
	NS 44	NS 42	NP2	+ 3	.4761	+ 8	.3594
290 thru 360 and 0 thru 90	S 75	S 73	NP1	+104	.0122	+ 81	.0166
	NS 73	NS 69	NP2	+ 73	.0516	+ 63	.0749
100 thru 220	S 46	S 40	NP1	<- 50	.0139	- 18	.1562
	NS 36	NS 32	NP2	<- 50	.0179	- 31	.1292

Table 5. Estimate of scale changes during seeded periods with respect to non-seeded periods as computed by two nonparametric statistical methods. Precipitation data are from the High Altitude Observatory near Climax for the Total Climax (623) and (547) samples. Scale changes are shown within various double stratifications of the meteorological parameters. Data for Total Climax (547) sample are shown in parentheses.

Double stratification (700 mb equivalent potential temperature) (700 mb wind direction)	Total sample size	Sample size used	Method	Without control	
				Scale change (%)	p-value
281K to less than 308K 190 thru 250 degrees	S 37 (37)	S 37 (37)	NP1	+111 (+148)	.0838 (.0694)
	NS 32 (31)	NS 32 (31)	NP2	+193 (+190)	.0294 (.0375)
281K to less than 308K 260 thru 300 degrees	S 92 (80)	S 92 (80)	NP1	- 35 (-40)	.0367 (.0307)
	NS104 (94)	NS104 (94)	NP2	- 32 (-38)	.0307 (.0207)
281K to less than 308K 310 thru 360 degrees	S 55 (40)	S 55 (40)	NP1	- 3 (+19)	.4522 (.2743)
	NS 68 (47)	NS 68 (47)	NP2	- 4 (+6)	.4325 (.3707)
308K to less than 326K 190 thru 250 degrees	S 41 (41)	S 41 (41)	NP1	>+200(>+200)	.0643 (.0537)
	NS 40 (39)	NS 40 (39)	NP2	>+200(>+200)	.0233 (.0197)
308K to less than 326K 260 thru 300 degrees	S 42 (39)	S 42 (39)	NP1	+ 34 (+65)	.2709 (.1492)
	NS 42 (41)	NS 42 (41)	NP2	+ 19 (+47)	.2877 (.1814)
308K to less than 326K 310 thru 360 degrees	S 11 (8)	S 11 (8)	NP1	>+200(>+200)	.0003 (.0017)
	NS 15 (12)	NS 15 (12)	NP2	>+200(>+200)	.0004 (.0036)
281K to less than 298K 190 thru 250 degrees	S 8 (8)	S 8 (8)	NP1	- 2 (-5)	.4801 (.4522)
	NS 8 (7)	NS 8 (7)	NP2	0 (-2)	.4960 (.4562)
298K to less than 308K 190 thru 250 degrees	S 29 (29)	S 29 (29)	NP1	>+200(>+200)	.1292 (.1292)
	NS 24 (24)	NS 29 (24)	NP2	>+200(>+200)	.0571 (.0571)
(500 mb temperature) (700 mb wind direction)					
-39C thru -21C 190 thru 250 degrees	S 41 (41)	S 41 (41)	NP1	+ 41 (+72)	.1867 (.1056)
	NS 33 (30)	NS 33 (30)	NP2	+ 56 (+71)	.1020 (.0778)
-39C thru -21C 260 thru 300 degrees	S 84 (74)	S 84 (74)	NP1	- 13 (-8)	.2327 (.3409)
	NS101 (92)	NS101 (92)	NP2	- 14 (-17)	.2061 (.1894)
-39C thru -21C 310 thru 360 degrees	S 50 (37)	S 50 (37)	NP1	+ 11 (+27)	.2643 (.1711)
	NS 61 (42)	NS 61 (42)	NP2	+ 8 (+16)	.2877 (.2266)
-20C thru -11C 190 thru 250 degrees	S 37 (37)	S 37 (37)	NP1	>+200(>+200)	.0233 (.0233)
	NS 40 (40)	NS 40 (40)	NP2	+119(>+200)	.0918 (.0918)
-20C thru -11C 260 thru 300 degrees	S 51 (45)	S 51 (45)	NP1	- 34 (-30)	.1762 (.2743)
	NS 45 (43)	NS 45 (43)	NP2	- 12 (0)	.3192 (.4081)
-20C thru -11C 310 thru 360 degrees	S 16 (11)	S 16 (11)	NP1	>+200(>+200)	.0778 (.0582)
	NS 22 (17)	NS 22 (17)	NP2	>+200(>+200)	.0764 (.0233)

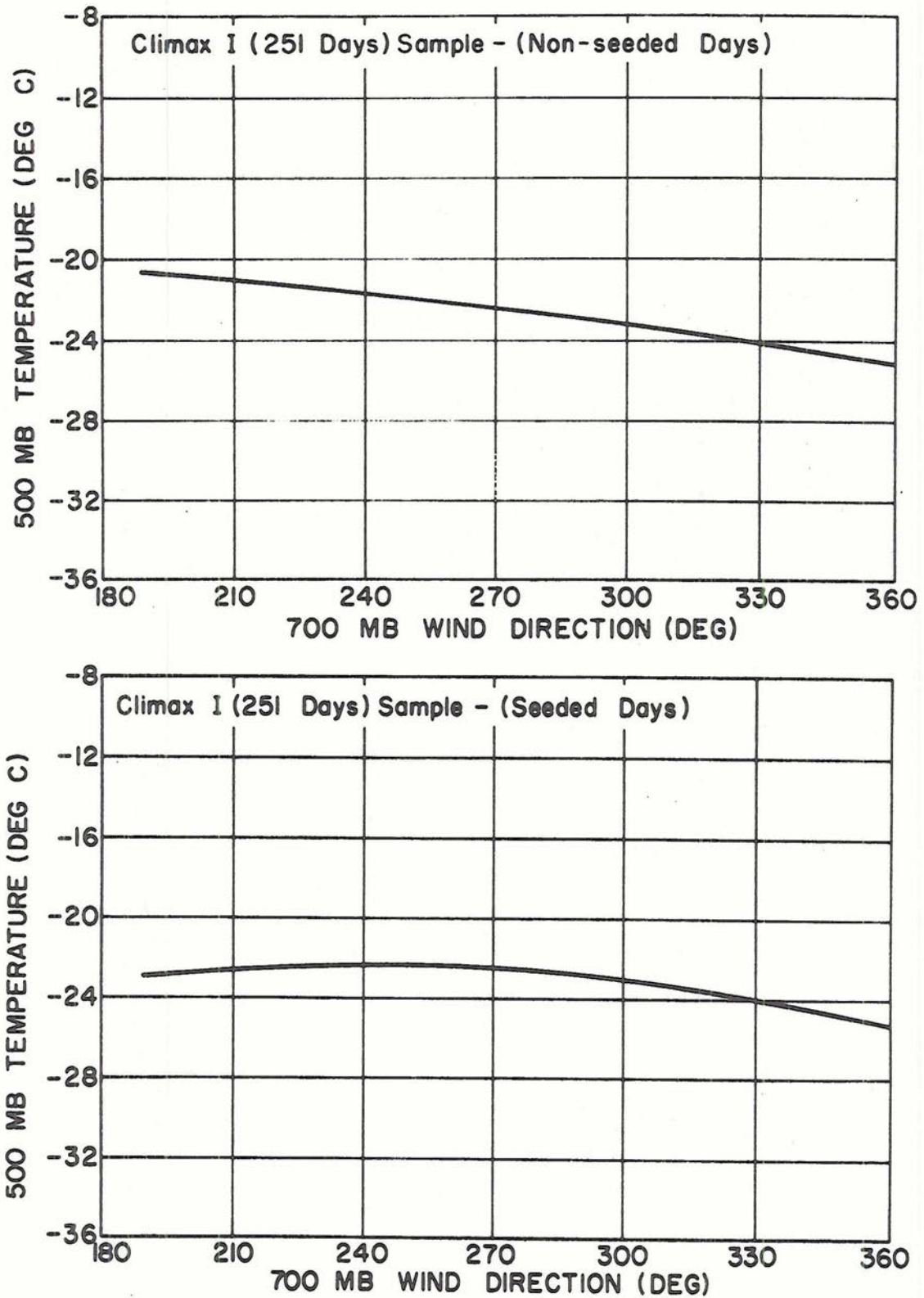


Figure 16. Relationship of 500 mb temperature with 700 mb wind direction for non-seeded days (upper) and seeded days (lower) for Climax I sample (251 days). Curve is a second degree polynomial curve fit to the observed meteorological data.

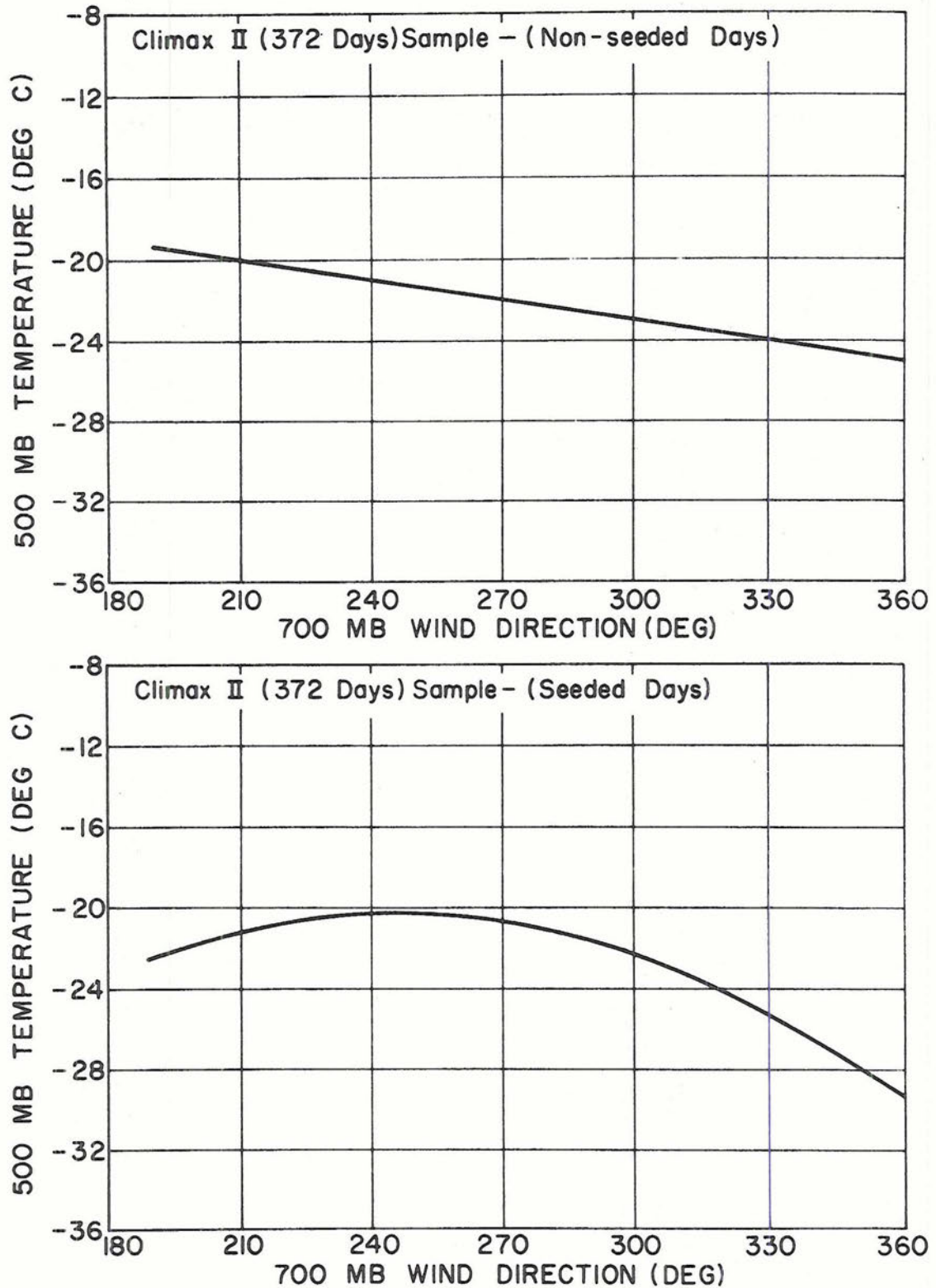


Figure 17. Relationship of 500 mb temperature with 700 mb wind direction for non-seeded days (upper) and seeded days (lower) for Climax II sample (372 days). Curve is a second degree polynomial curve fit to the observed meteorological data.

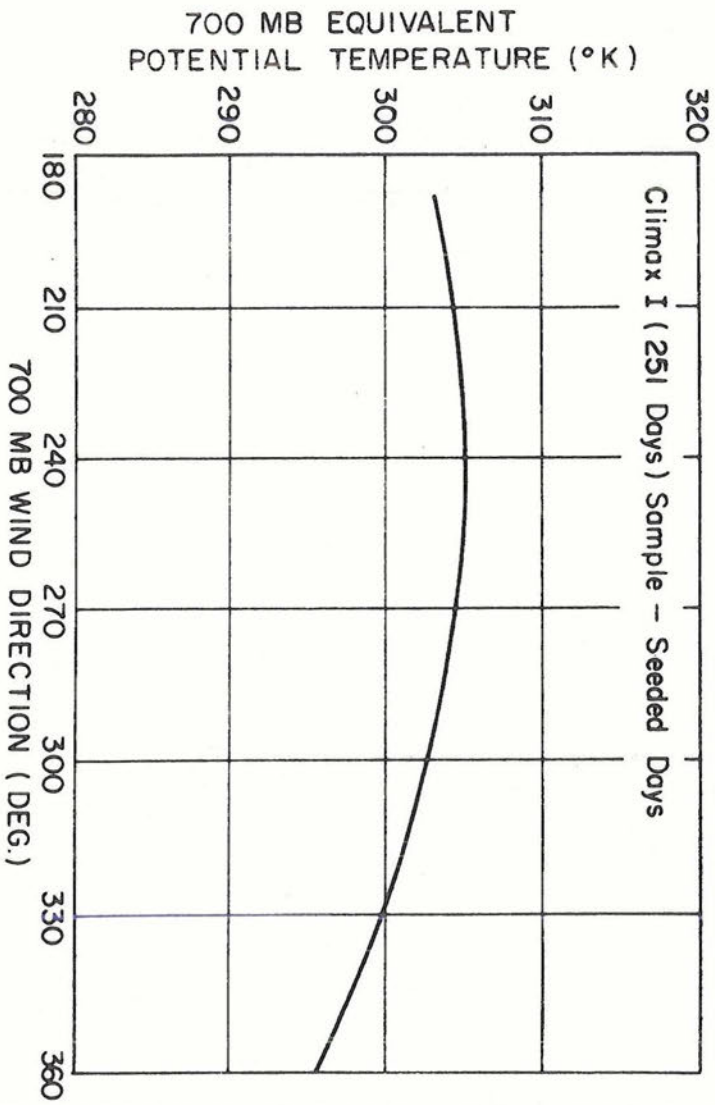
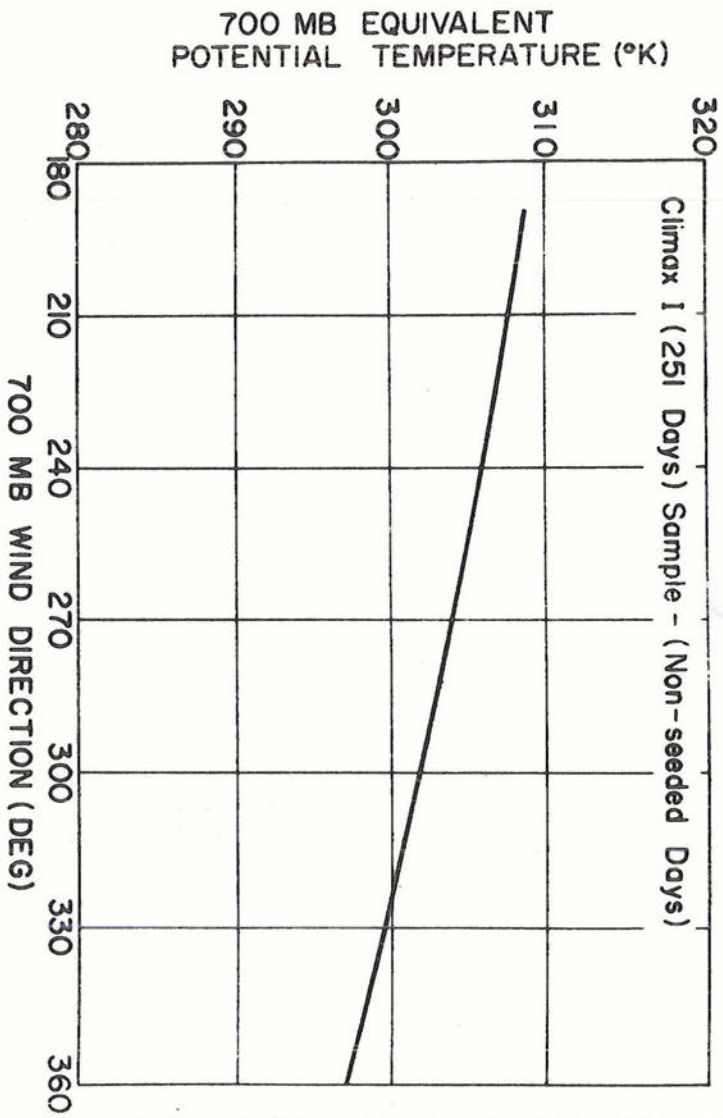


Figure 18. Relationship of 700 mb equivalent potential temperature with 700 mb wind direction for non-seeded days (upper) and seeded days (lower) for Climax I sample (251 days). Curve is a second degree polynomial curve fit to the observed meteorological data.

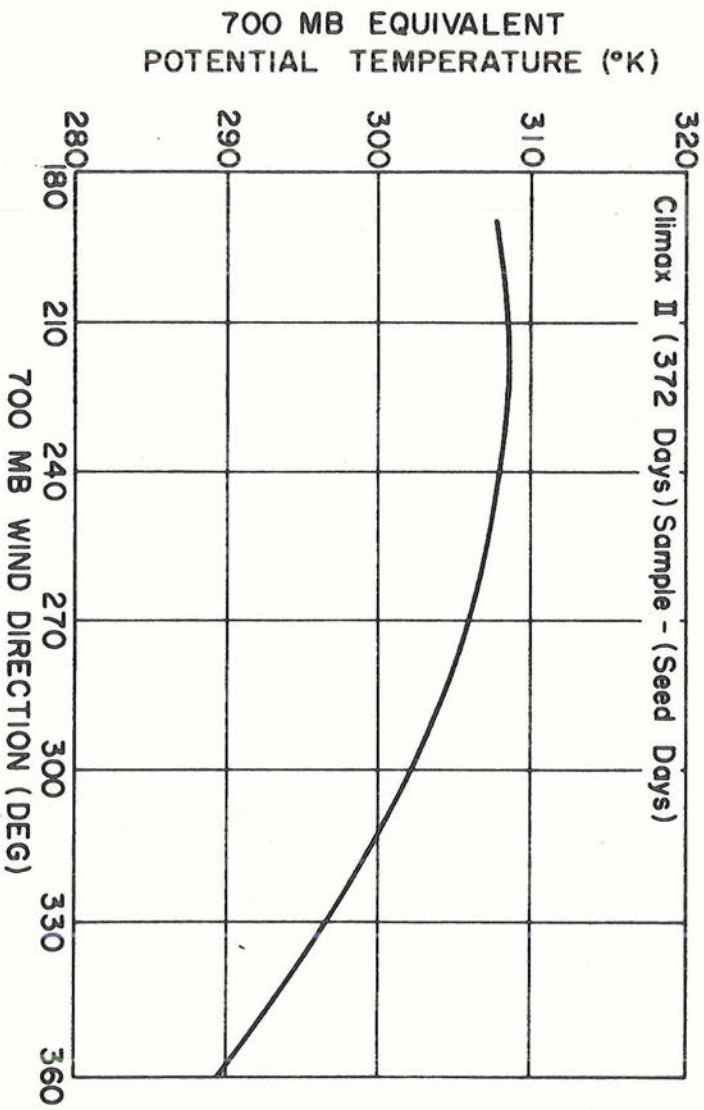
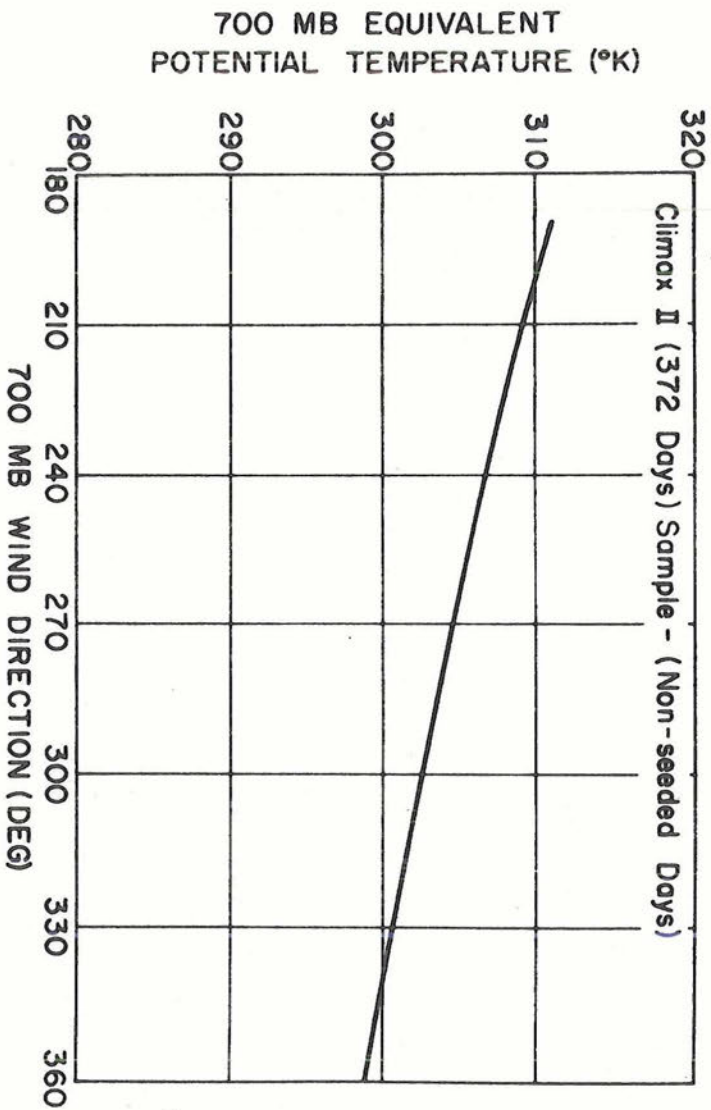


Figure 19. Relationship of 700 mb equivalent potential temperature with 700 mb wind direction for non-seeded days (upper) and seeded days (lower) for Climax II sample (372 days). Curve is a second degree polynomial curve fit to the observed meteorological data.

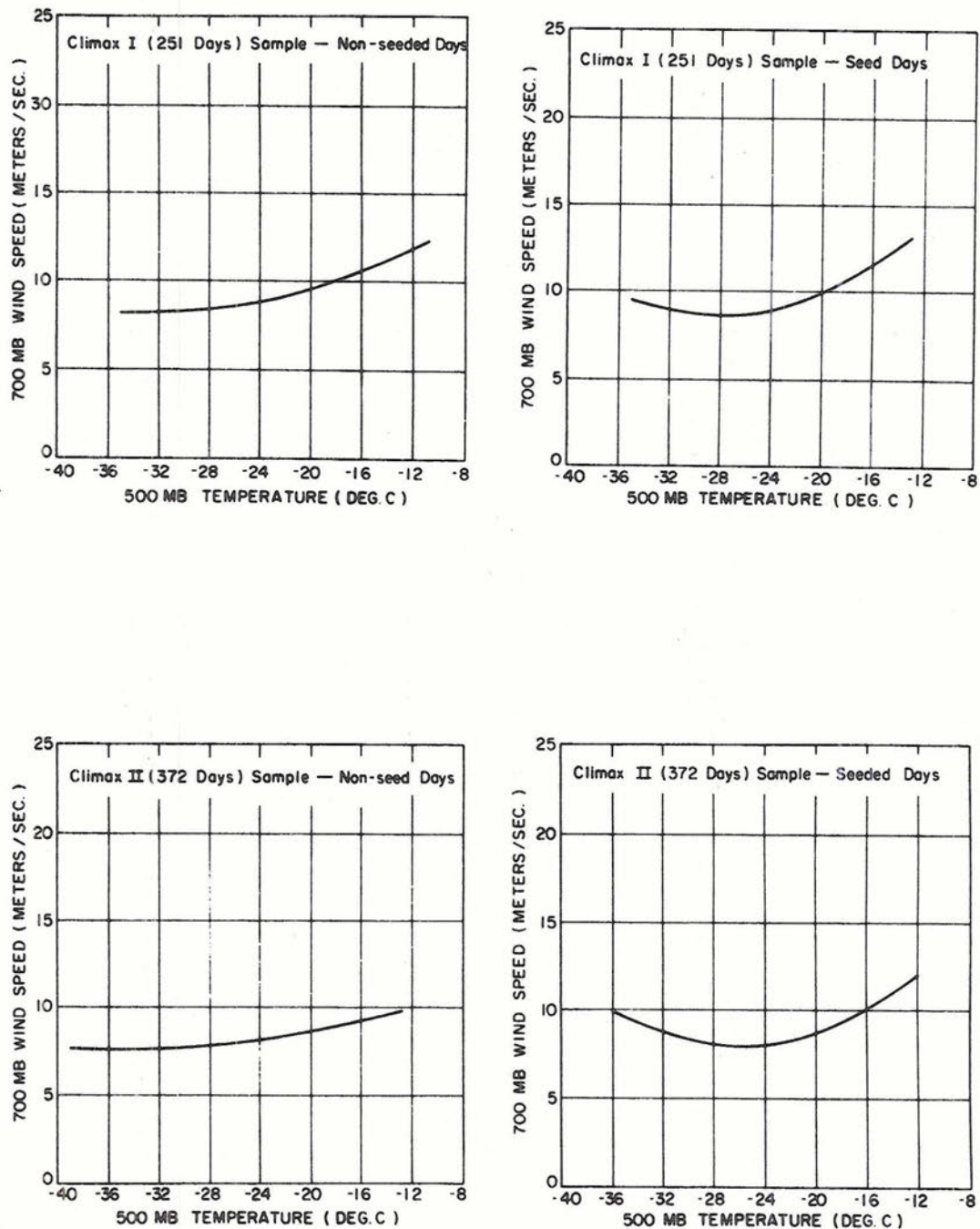


Figure 20. Relationship of 700 mb wind speed with 500 mb temperature for seeded and non-seeded days of the Climax I sample (upper) and Climax II sample (lower). Curve is a second degree polynomial curve fit to the observed meteorological data.

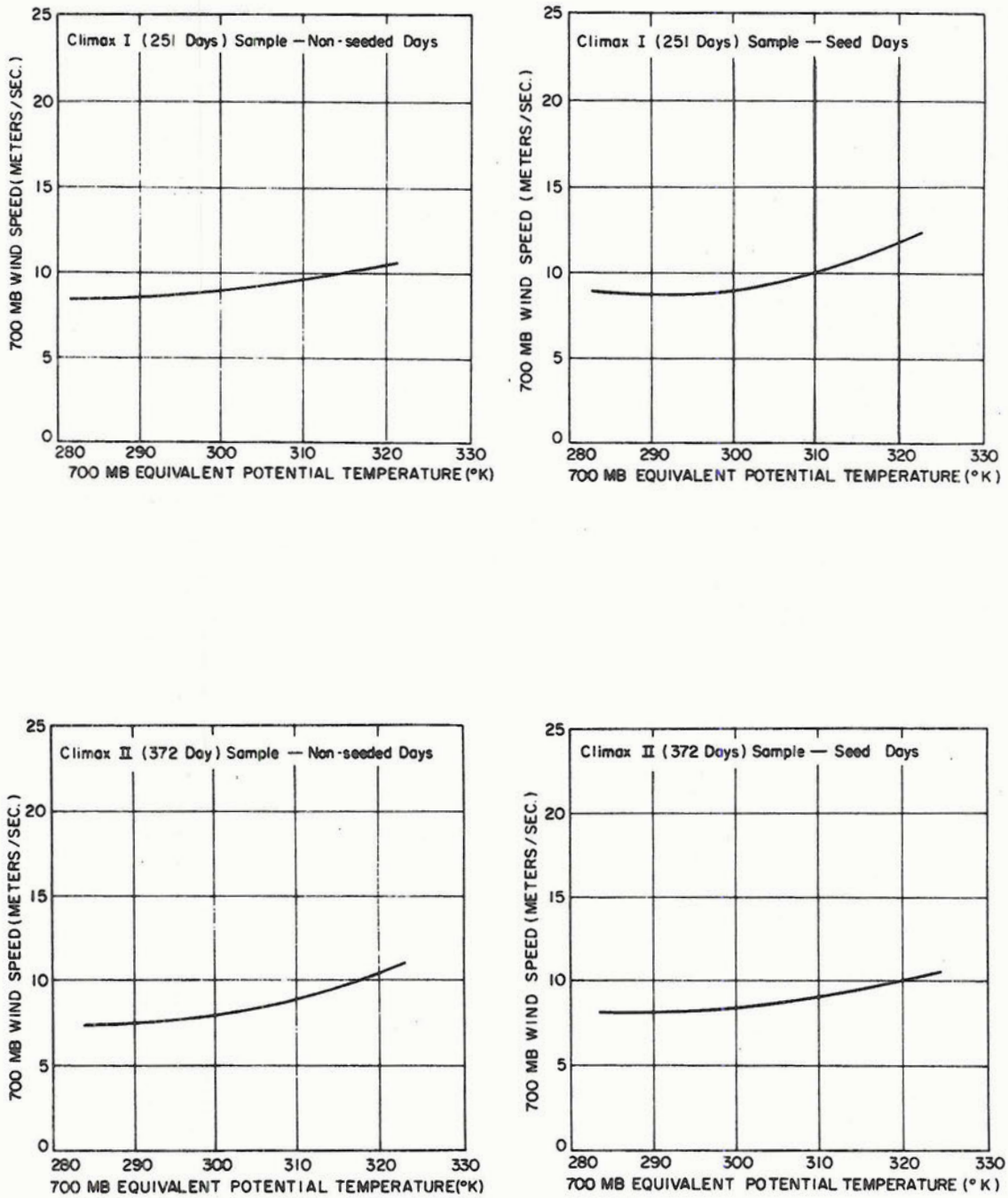


Figure 21. Relationship of 700 mb wind speed with 700 mb equivalent potential temperature for seeded and non-seeded days of the Climax I sample (upper) and Climax II sample (lower). Curve is a second degree polynomial curve fit to the observed meteorological data.

A possible explanation of this is seen in Table 5. First, it is noted that in spite of the colder temperatures on the average, there was a population of warm northwest flow storms which produced significant increases in snowfall (p-values less than 1 percent for Total Climax samples), when they were seeded. These relatively few events apparently more than compensate for little seeding effect or slight negative seeding effects for the colder cloud systems.

The lack of any substantial negative seeding effect with northwest flow, for the coldest 500 mb temperatures and 700 mb equivalent potential temperatures, is probably due to somewhat lower cloud tops on the average for these conditions. Coldest northwest flow events generally occur between upper level trough passage and the cessation of precipitation, which seems to be brought about by increasing subsidence over the area and a gradual thinning and eventual breakup of the orographic cloud. Under these conditions of decreasing cloud top heights, the colder 500 mb temperatures indicated for this stratification may be somewhat misleading.

The reason for the lack of positive seeding effects with westerly winds is not obvious from an inspection of the meteorological data, since these precipitation events generally average within the intermediate range of 500 mb temperatures and 700 mb equivalent potential temperatures. Even if westerly flow cases are subdivided into warm and cold stratifications, only a small positive seeding effect is noted for warmer equivalent potential temperatures and little effect is noted for the warmer 500 mb temperatures. Significant decreases are noted for the

colder westerly flow events (p values less than 4 percent for Total Climax samples.

A contributing factor, to the lack of substantial increases in snowfall for the warmer westerly flow conditions, may be the seeding from the long distance generators at Aspen and Reudi. The possibility exists that seeding from these generators increases snowfall over the Sawatch Range (the major north-south range lying about 15 miles west of Climax) to the detriment of the primary target area, which in this event would lie considerably downwind of the major seeding effect. Another contributing factor may be smaller upward motions stemming from weaker orographic influences present with this type flow.

The Wolf Creek Pass area also shows substantial positive seeding effects when wind flow is oriented more nearly normal to the mountain barrier. Little seeding effect is noted for wind flows nearly parallel to the mountain barrier. Figures 22, 23, 24 and 25 again suggest that southwest wind flow is accompanied by warmest 500 mb temperatures and 700 mb equivalent potential temperatures, and also higher wind speeds. These two factors again combine to produce warmer cloud tops and higher condensation rates with southwest flow, and the most significant increases in snowfall are observed with these conditions (p-values are 4 percent or less).

All other effects being equal, S.M.P. is favored by increasing wind flow over the barrier, since condensation rates are related to the mass flow rate over the barrier. Observed seeding effects in Table 6 show slight negative effects for the lowest wind speeds which change to significant positive effects as wind speeds increase. All statistical

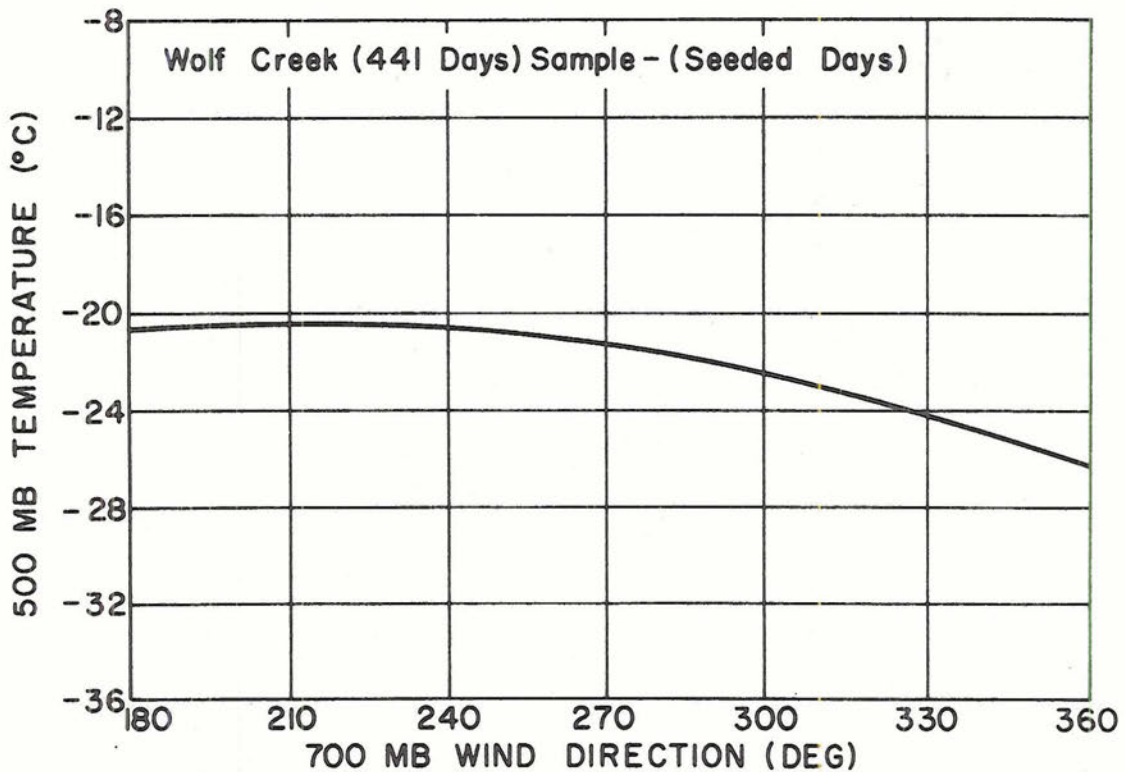
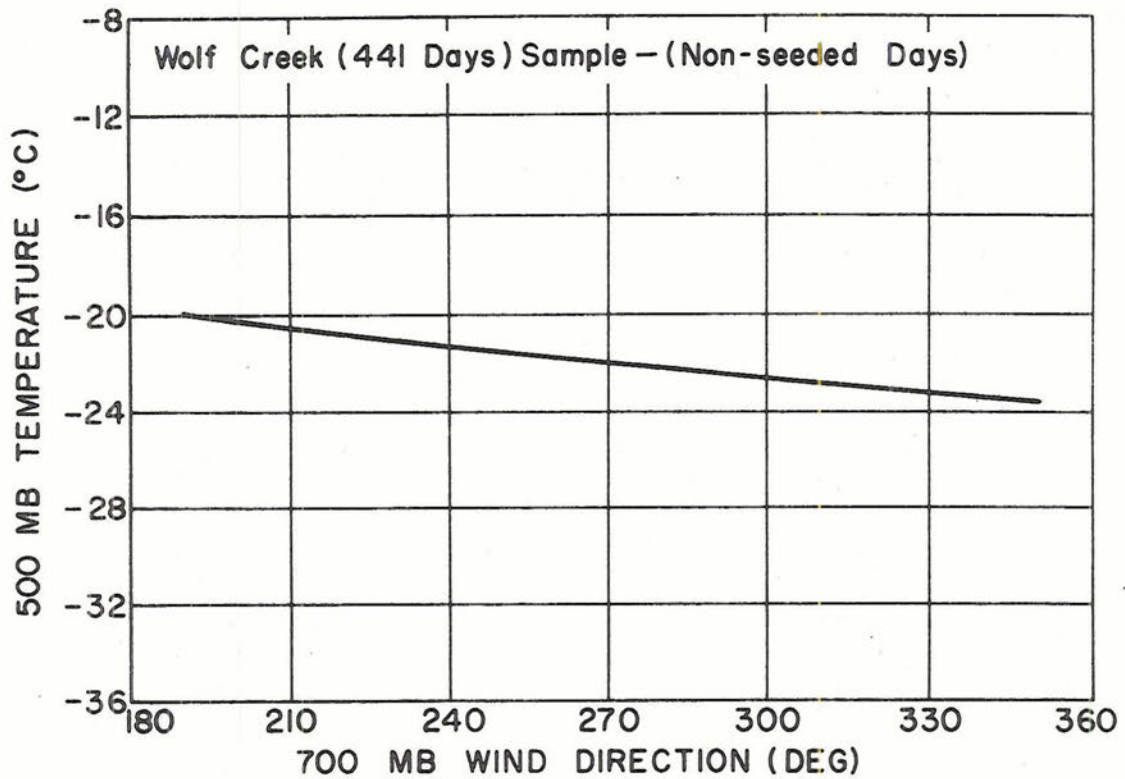


Figure 22. Relationship of 500 mb temperature with 700 mb wind direction for non-seeded days (upper) and seeded days (lower) for Wolf Creek sample (441 days). Curve is a second degree polynomial curve fit to the observed meteorological data.

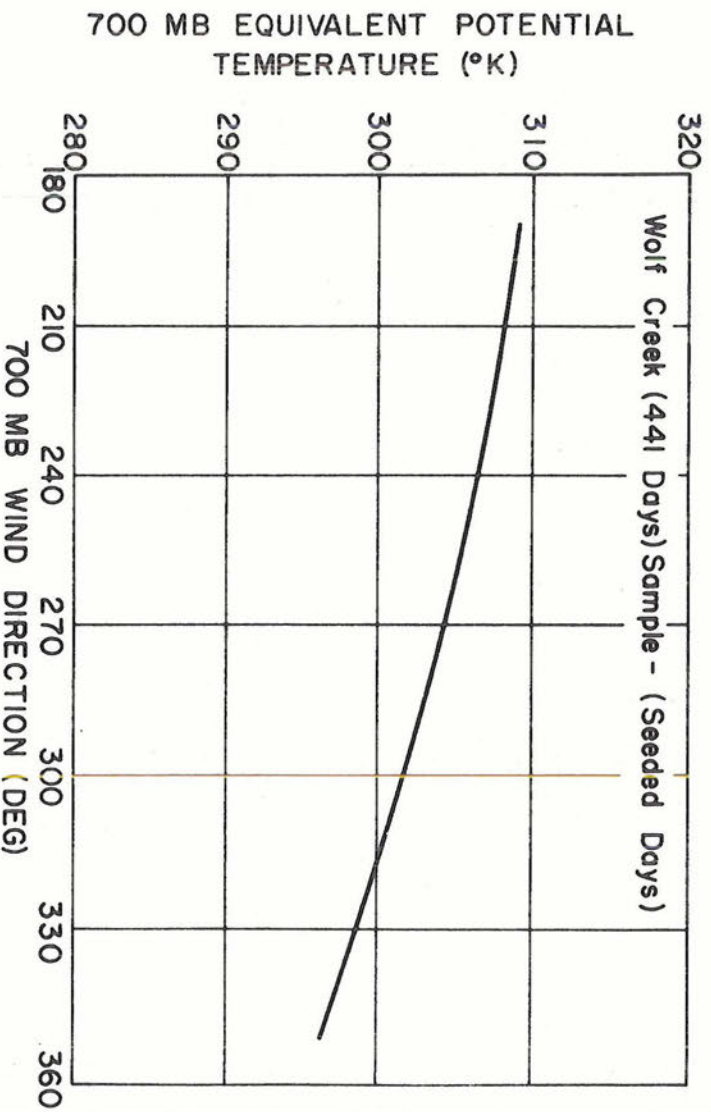
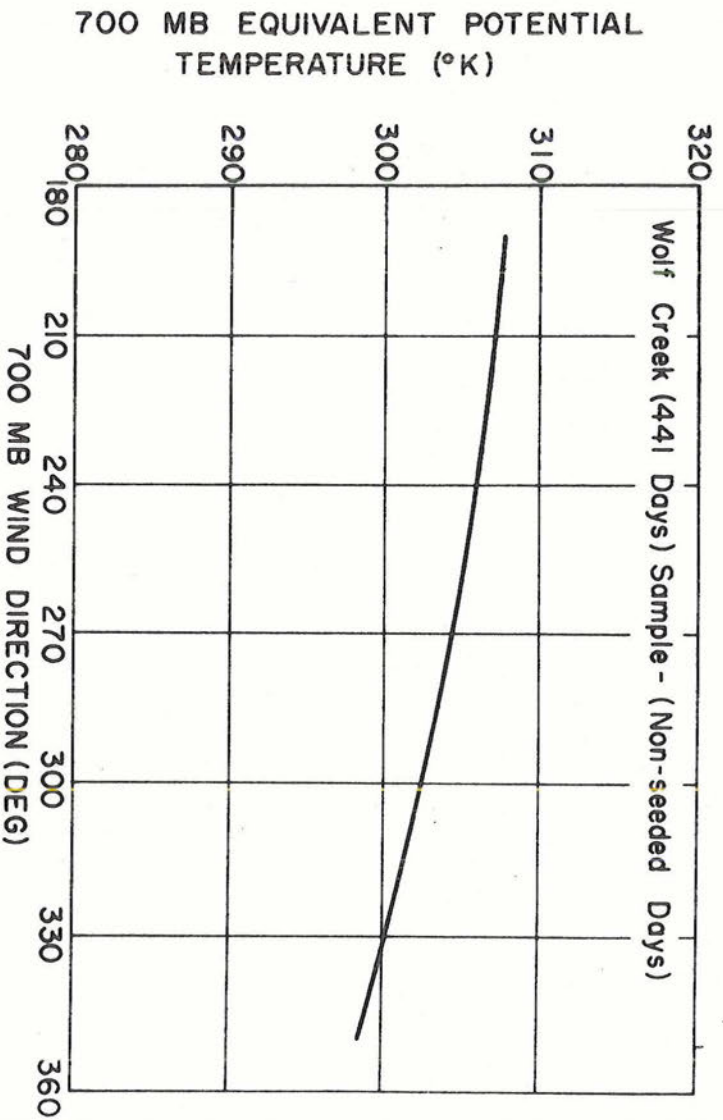


Figure 23. Relationship of 700 mb equivalent potential temperature with 700 mb wind direction for non-seeded days (upper) and seeded days (lower) for Wolf Creek sample (441 days). Curve is a second degree polynomial curve fit to the observed meteorological data.

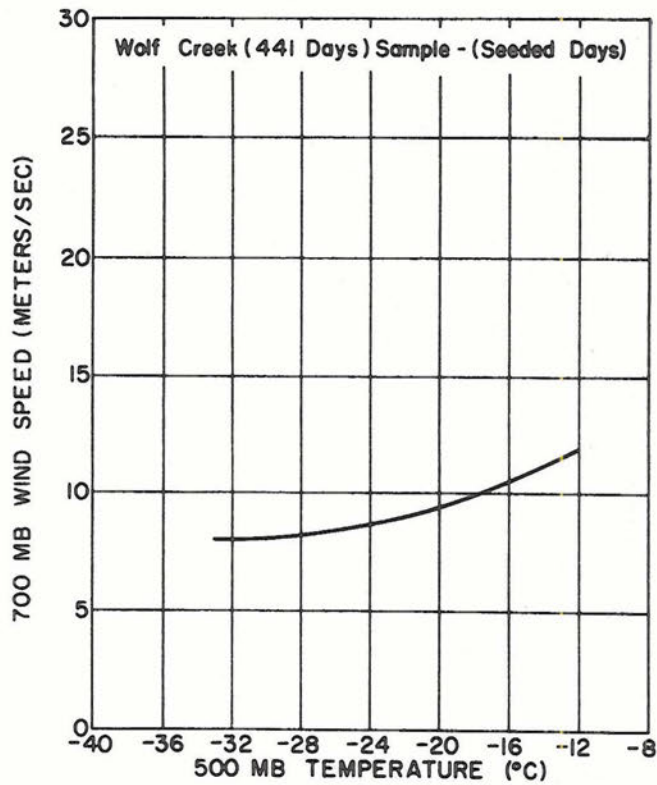
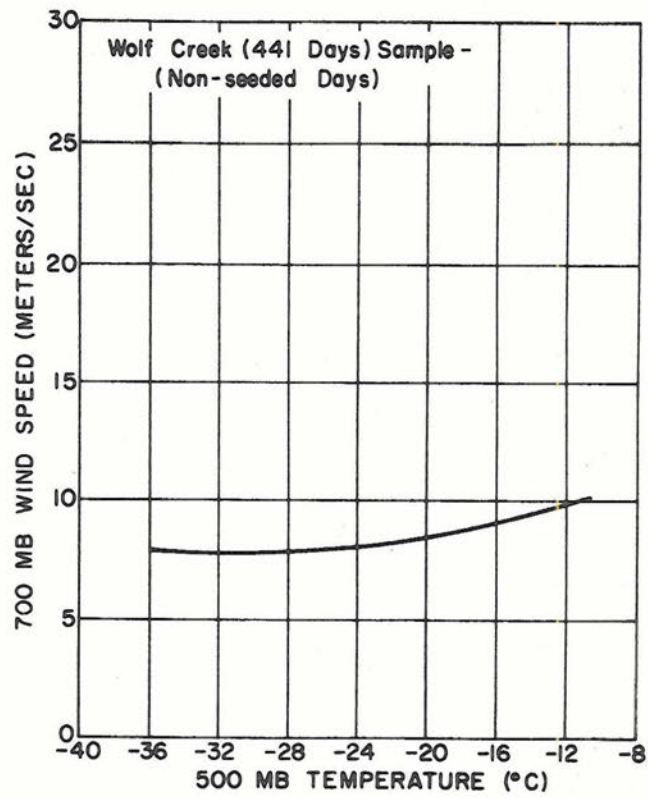


Figure 24. Relationship of 700 mb wind speed with 500 mb temperature for non-seeded days (upper) and seeded days (lower) for Wolf Creek sample (441 days). Curve is a second degree polynomial curve fit to the observed meteorological data.

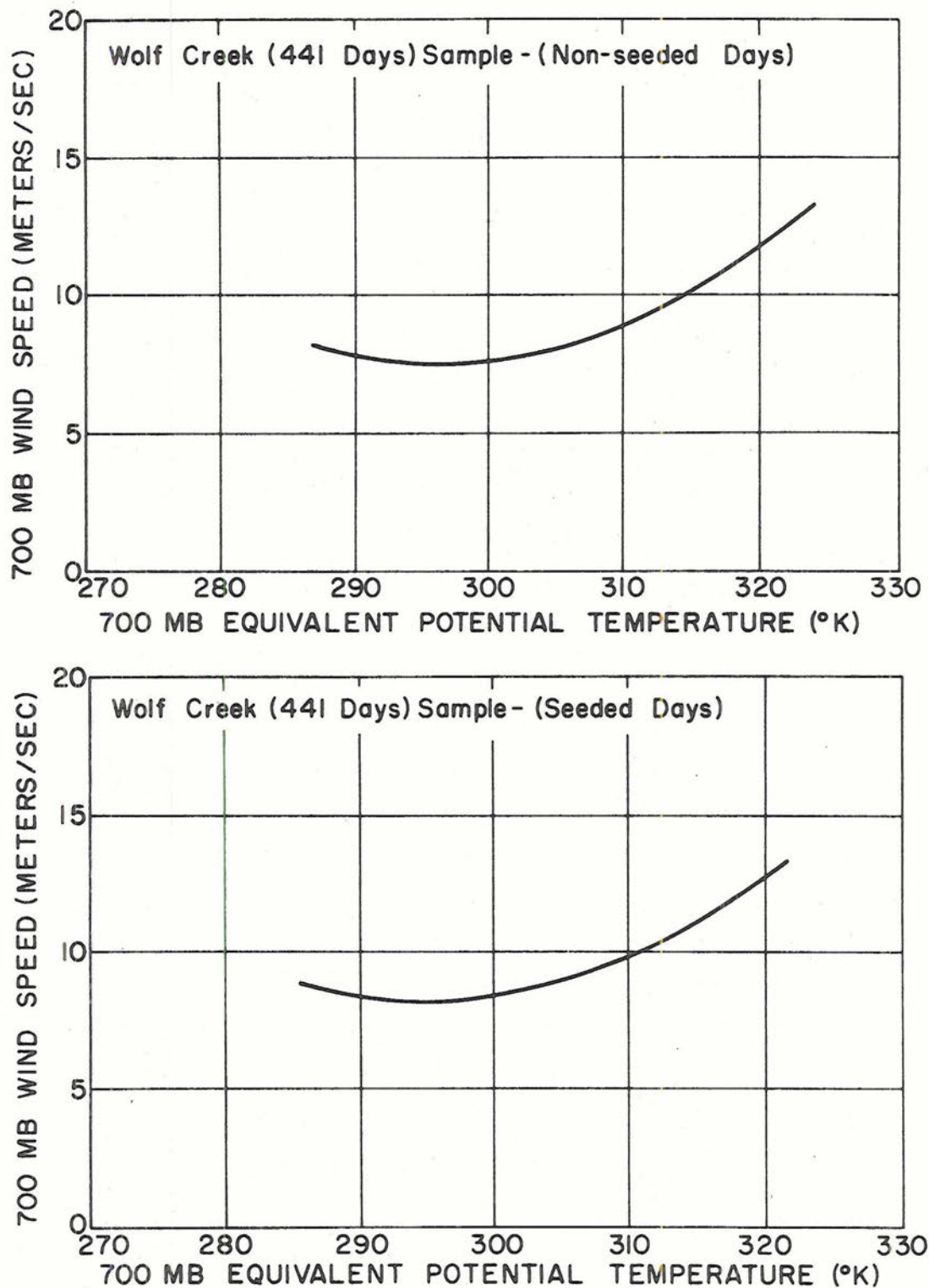


Figure 25. Relationship of 700 mb wind speed with 700 mb equivalent potential temperature for non-seeded days (upper) and seeded days (lower) for Wolf Creek sample (441 days). Curve is a second degree polynomial curve fit to the observed meteorological data.

Table 6. Estimate of scale changes during seeded periods with respect to non-seeded periods as computed by two nonparametric statistical methods. Precipitation data are from the High Altitude Observatory near Climax and near the summit of Wolf Creek Pass. Scale changes are shown within stratifications of the 700 mb wind speed. Data for Climax II (296) and Total Climax (547) samples are shown in parentheses.

Stratification (meters/sec)	Total sample size	Sample size used	Method	Without control		With control	
				Scale change (%)	p-value	Scale change (%)	p-value
<b>Climax I (251) Sample</b>							
0 to < 9	S 52	S 52	NP1	- 14	.2946	- 10	.3015
	NS 65	NS 65	NP2	- 17	.2327	- 2	.4880
9 to <12	S 42	S 42	NP1	+ 7	.4247	+ 36	.1401
	NS 29	NS 29	NP2	+ 28	.2514	+ 20	.3594
12 to <15	S 13	S 13	NP1	>+200	.0197	>+200	.0062
	NS 23	NS 23	NP2	+193	.0495	>+200	.0045
15 to <29	S 13	S 13	NP1	<- 50	.0571	- 41	.0465
	NS 14	NS 14	NP2	- 46	.1093	- 36	.0571
<b>Climax II (372) and (296) Samples</b>							
0 to < 9	S 90 (74)	S 90 (74)	NP1	- 9 (-11)	.3632 (.3669)		
	NS104 (86)	NS104 (86)	NP2	- 4 (0)	.4483 (.4880)		
9 to <12	S 41 (31)	S 41 (31)	NP1	- 3 (+1)	.4364 (.4920)		
	NS 43 (31)	NS 43 (31)	NP2	- 10 (+4)	.3156 (.4247)		
12 to <15	S 34 (29)	S 34 (29)	NP1	>+200(>+200)	.0002 (.0001)		
	NS 30 (23)	NS 30 (23)	NP2	>+200(>+200)	.0014 (.0007)		
15 to <29	S 17 (13)	S 17 (13)	NP1	<- 50 (<-50)	.0516 (.0582)		
	NS 13 (9)	NS 13 (9)	NP2	- 49 (-23)	.1131 (.1841)		
<b>Total Climax (623) and (547) Samples</b>							
0 to < 9	S142 (126)	S142 (126)	NP1	- 14 (-13)	.2514 (.3121)		
	NS169 (151)	NS169 (151)	NP2	- 10 (-10)	.3015 (.3632)		
9 to <12	S 83 (73)	S 83 (73)	NP1	+ 10 (+19)	.3264 (.2643)		
	NS 72 (60)	NS 72 (60)	NP2	+ 10 (+10)	.3300 (.3050)		
12 to <15	S 47 (42)	S 47 (42)	NP1	>+200(>+200)	.0002 (.0002)		
	NS 53 (46)	NS 53 (46)	NP2	>+200(>+200)	.0007 (.0008)		
15 to <29	S 30 (26)	S 30 (26)	NP1	<- 50 (<-50)	.0066 (.0107)		
	NS 27 (23)	NS 27 (23)	NP2	- 38 (-41)	.0307 (.0594)		
<b>Wolf Creek Summit (441) Sample</b>							
0 to < 4	S 23	S 17	NP1	<- 50	.0985	<- 50	.0505
	NS 25	NS 24	NP2	- 18	.3745	- 4	.4562
4 to <11	S139	S131	NP1	- 9	.3409	+ 5	.3483
	NS115	NS108	NP2	- 10	.2546	+ 6	.3859
11 to <15	S 59	S 57	NP1	+ 92	.0188	+ 88	.0166
	NS 41	NS 37	NP2	+114	.0129	+149	.0125
15 to <30	S 28	S 27	NP1	- 2	.1980	+ 1	.4760
	NS 11	NS 8	NP2	- 2	.1131	- 10	.2060

tests for all Climax samples have p-values less than 5 percent for wind speeds of 12 to 15 meters/sec and for 11 to 15 meters/sec for the Wolf Creek sample. At very high wind speeds, positive seeding effects disappear and are replaced by significant negative seeding effects. This variation of seeding effect with wind speed is consistent with the model S.M.P. equation if the existence of overseeding at very high wind speeds can be demonstrated. It was shown previously that model S.M.P. and seeded precipitation equations are physically invalid under these conditions. The possibility of overseeding is considered in greater detail in a later chapter.

## 2) Cloud Layer Convective Stability

The stability of the air mass approaching the mountain barrier influences the S.M.P. in complex ways. If the air mass is convectively unstable precipitation may tend to concentrate in small cells and convective lines. The stronger upward motions in these cells and lines would result in high supply rates of cloud water in localized areas. However, these stronger upward motions would also result in localized higher cloud tops and more effective losses due to convective towers protruding into a relatively dry environment. The higher cloud tops would also be colder and could produce greater numbers of effective ice nuclei for which to seed the underlying orographic cloud.

The stability of the air mass also affects the nature of the laminar flow over the mountain barrier. This is demonstrated in the wave equation for flow over mountain barriers as discussed by Scorer (1949). Numerical solutions to this wave equation indicate for conditions of neutral stability, upwind cloud tops are considerably higher than for

more stable cases. It follows, then, that greater concentrations of natural ice nuclei might be available under the former conditions and the S.M.P. would be reduced.

Elliott (1966) has argued for seeding unstable conditions from an energy approach. He concluded that seeding in the Southern California mountains enhanced the orographic circulation at the expense of the individual convective cell circulations. The result of seeding, according to Elliott, was to stabilize the air mass, reduce between-cells evaporation and increase the mean temperature of the cloud system. This increased the buoyancy on the orographic scale and since this scale is subject to less frictional dissipation and losses due to evaporation, the net condensation rate and precipitation rate of the cloud system was increased.

It is not clear from the model S.M.P. equation what the effect will be of seeding convectively unstable air masses. It is difficult to determine whether the mean vertical motion will be increased or not, since any increased vertical motion in cells is likely to be compensated by a reduction of upward vertical motion between cells. Unless seeding does suppress the local cell circulations and enhances the larger scale orographic motions, as claimed by Elliott, there does not appear to be any reason why these events would be especially favored for seeding.

The results of stratifying the Climax and Wolf Creek samples with a convective stability index (500 mb equivalent potential temperature) do not show any substantial positive seeding effect for the unstable cases. There is some evidence that seeding effectiveness is greatest for the slightly stable cases (+1 to less than +5 degrees C). This is shown by the Climax II (372) and Wolf Creek samples in Table 7.

Table 7. Estimate of scale changes during seeded periods with respect to non-seeded periods as computed by two nonparametric statistical methods. Precipitation data are from the High Altitude Observatory near Climax and near the summit of Wolf Creek Pass. Scale changes are shown within stratifications of a convective stability index expressed as the difference in equivalent potential temperature between the 700 mb and 500 mb levels. Data for Climax II (296) and Total Climax (547) samples are shown in parentheses.

Stratification (°C)	Total sample size	Sample size used	Method	Without control		With control	
				Scale change (%)	p-value	Scale change (%)	p-value
Climax I (251) Sample							
-8 to <+ 1	S 32	S 32	NP1	+ 24	.2451	+ 6	.3446
	NS 40	NS 40	NP2	+ 6	.3446	+ 47	.0668
+1 to <+ 5	S 40	S 40	NP1	- 15	.2776	+ 11	.2912
	NS 41	NS 41	NP2	0	.4840	- 6	.4286
+5 to <+23	S 48	S 48	NP1	- 1	.4880	+ 2	.4522
	NS 50	NS 50	NP2	- 1	.4880	- 8	.3520
Climax II (372) and (296) Samples							
-8 to <+ 1	S 50 (47)	S 50 (47)	NP1	+ 7 (+30)	.3632 (.1867)		
	NS 52 (42)	NS 52 (42)	NP2	+ 7 (+20)	.3121 (.2177)		
+1 to <+ 5	S 60 (43)	S 60 (43)	NP1	+ 48 (+24)	.1335 (.2981)		
	NS 63 (50)	NS 63 (50)	NP2	+ 47 (+39)	.1251 (.1423)		
+5 to <+23	S 72 (57)	S 72 (57)	NP1	+ 5 (+66)	.4522 (.1685)		
	NS 75 (57)	NS 75 (57)	NP2	- 13 (+27)	.3783 (.3085)		
Total Climax (623) and (547) Samples							
-8 to <+ 1	S 82 (79)	S 82 (79)	NP1	+ 7 (+25)	.3409 (.1685)		
	NS 92 (82)	NS 92 (82)	NP2	+ 10 (+22)	.2358 (.1492)		
+1 to <+ 5	S100 (83)	S100 (83)	NP1	+ 18 (+16)	.2546 (.3050)		
	NS104 (91)	NS104 (91)	NP2	+ 9 (+10)	.3192 (.3192)		
+5 to <+23	S120 (105)	S120 (105)	NP1	+ 2 (+4)	.4766 (.4602)		
	NS125 (107)	NS125 (125)	NP2	- 15 (-13)	.2810 (.3372)		
Wolf Creek Summit (441) Sample							
-4 to <+ 1	S 53	S 47	NP1	+ 23	.2810	+ 23	.1515
	NS 40	NS 37	NP2	+ 30	.2119	+ 39	.0869
+1 to <+ 3	S 48	S 43	NP1	>+200	.0012	+189	.0004
	NS 37	NS 36	NP2	+138	.0091	+173	.0037
+3 to <+ 5	S 51	S 50	NP1	+ 54	.1056	+ 12	.2546
	NS 44	NS 40	NP2	+ 40	.1711	+ 23	.1867
+5 to <+ 8	S 52	S 48	NP1	- 14	.3264	+ 2	.4801
	NS 42	NS 39	NP2	+ 4	.5000	+ 14	.3015
+8 to <+20	S 45	S 44	NP1	- 19	.2946	- 20	.2912
	NS 29	NS 25	NP2	+ 21	.4641	+ 21	.4761

P-values are less than 1 percent for the Wolf Creek sample. Little seeding effect is noted for the very stable cases.

Figures 26, 27, 28 and 29 show that unstable and least stable cases tend to occur with warmer cloud systems and southwest flow. Since these factors favor a positive seeding effect from other considerations, they may largely explain the observed precipitation increases for the least stable cases. These factors also dramatize the lack of positive seeding effects with the unstable cases.

### 3) Baroclinicity

It is generally implied from the adiabatic equation for vertical motion that horizontal warm advection in the lower and middle troposphere is frequently associated with ascending air motion. Table 8 shows the distribution of seeding effects with the mean temperature advection in the 700-500 mb layer. The results of the Climax and Wolf Creek samples indicate significant positive seeding effects for mean temperature advectons from +1 to less than +4 degrees C per 12 hours. P-values are less than 5 percent for many of the statistical tests performed on all samples and less than 1 percent for tests of both Total Climax samples. Positive seeding effects with other temperature advectons are not significant.

It appears that the superimposition of synoptic scale upward motion on the orographic component enhances the mean vertical motion of the cloud system and favors the availability and increases the magnitude of S.M.P. This appears consistent with the model S.M.P. equation.

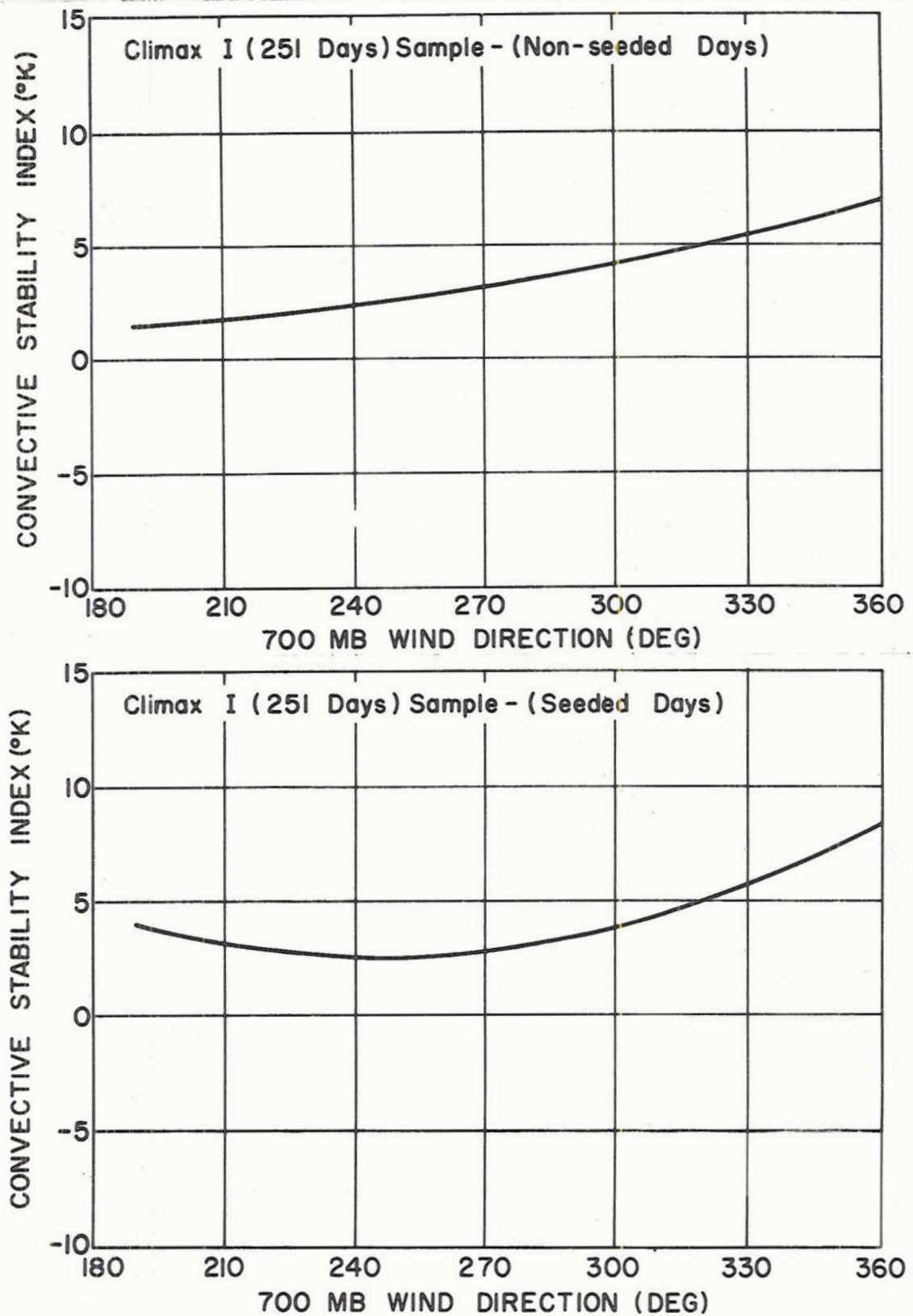


Figure 26. Relationship of the convective stability index with 700 mb wind direction for non-seeded days (upper) and seeded days (lower) for Climax I sample (251 days). Curve is a second degree polynomial curve fit to the observed meteorological data.

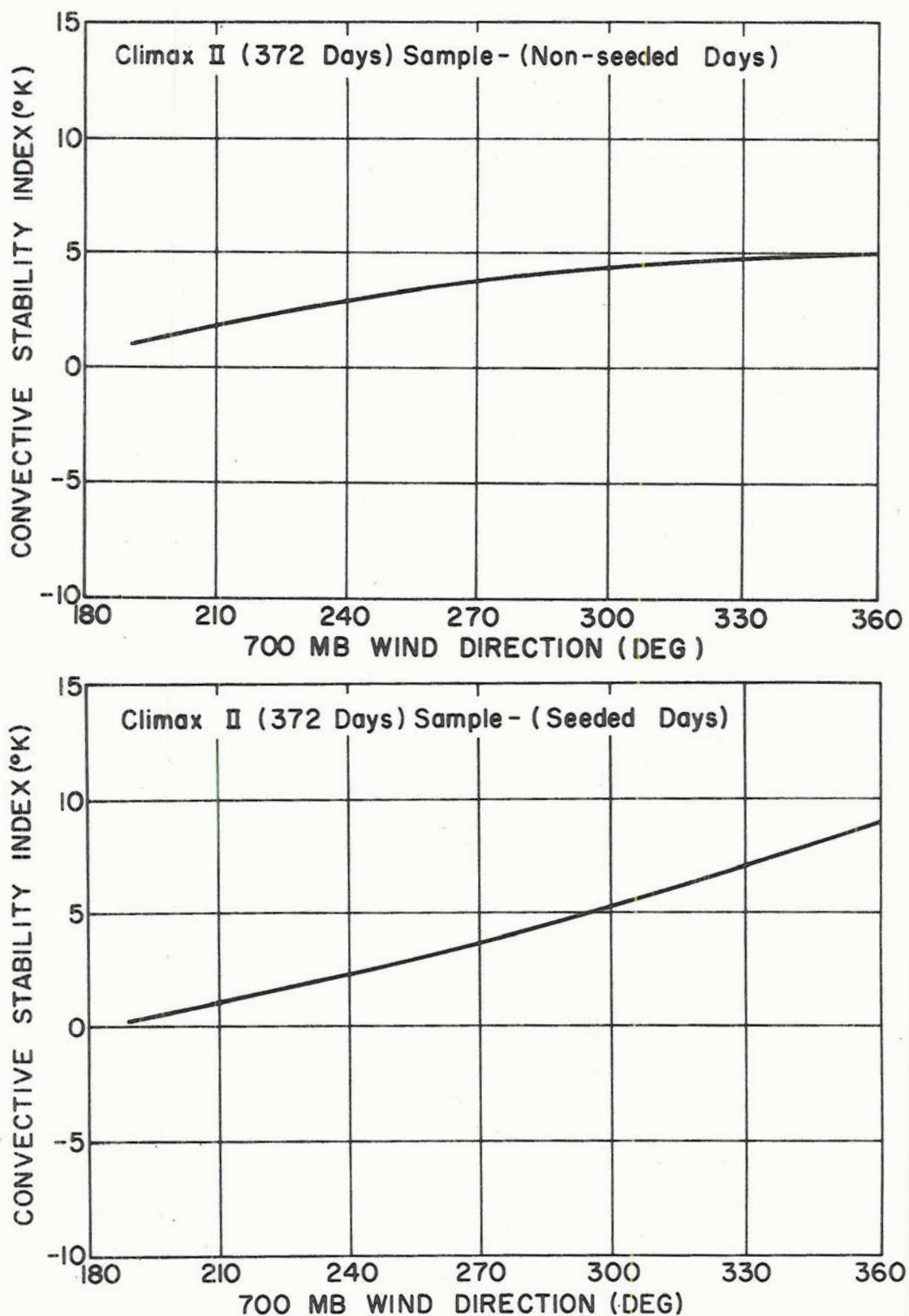


Figure 27. Relationship of the convective stability index with 700 mb wind direction for non-seeded days (upper) and seeded days (lower) for Climax II sample (372 days). Curve is a second degree polynomial curve fit to the observed meteorological data.

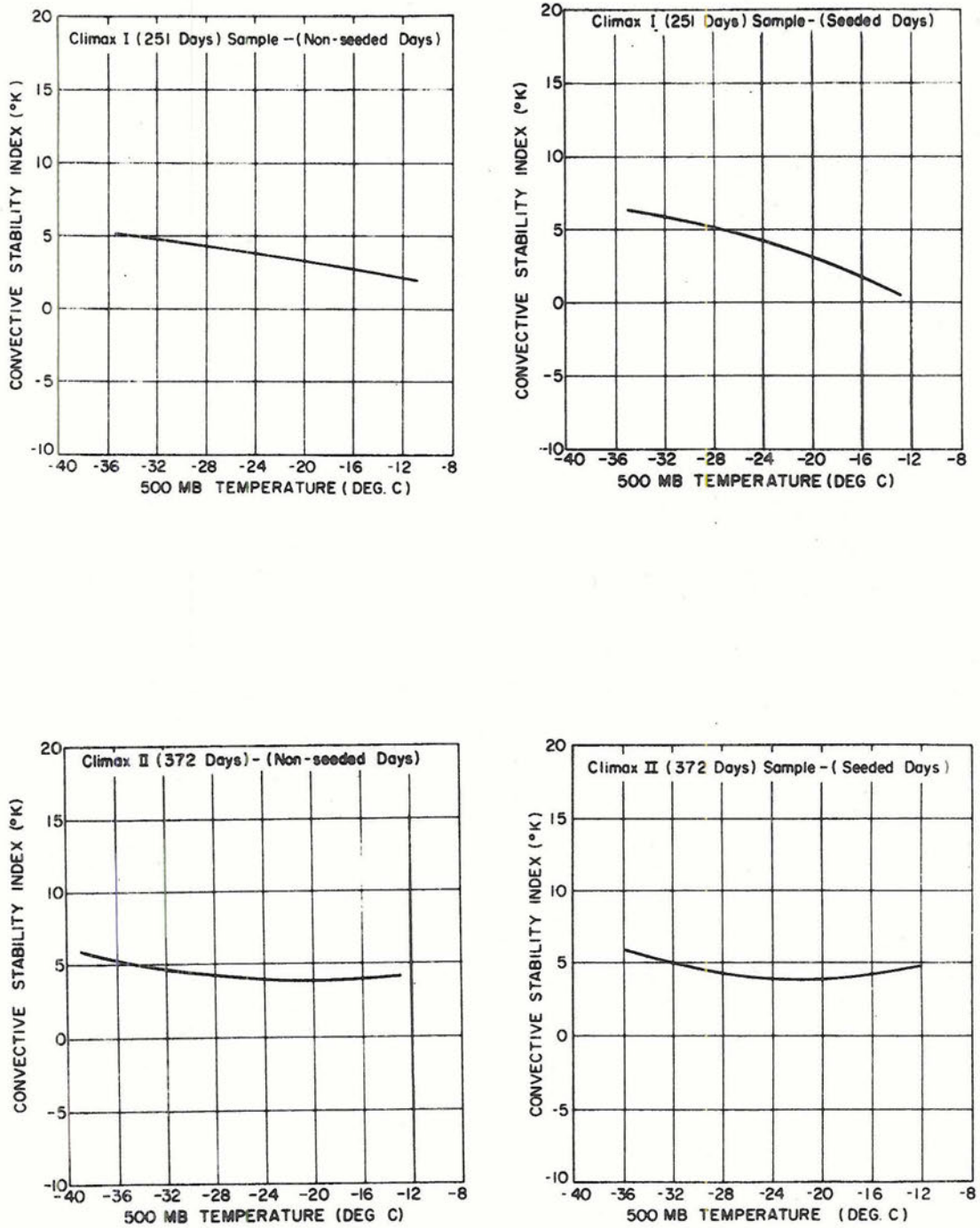


Figure 28. Relationship of the convective stability index with 500 mb temperature for seeded and non-seeded days of the Climax I sample (upper) and Climax II sample (lower). Curve is a second degree polynomial curve fit to the observed meteorological data.

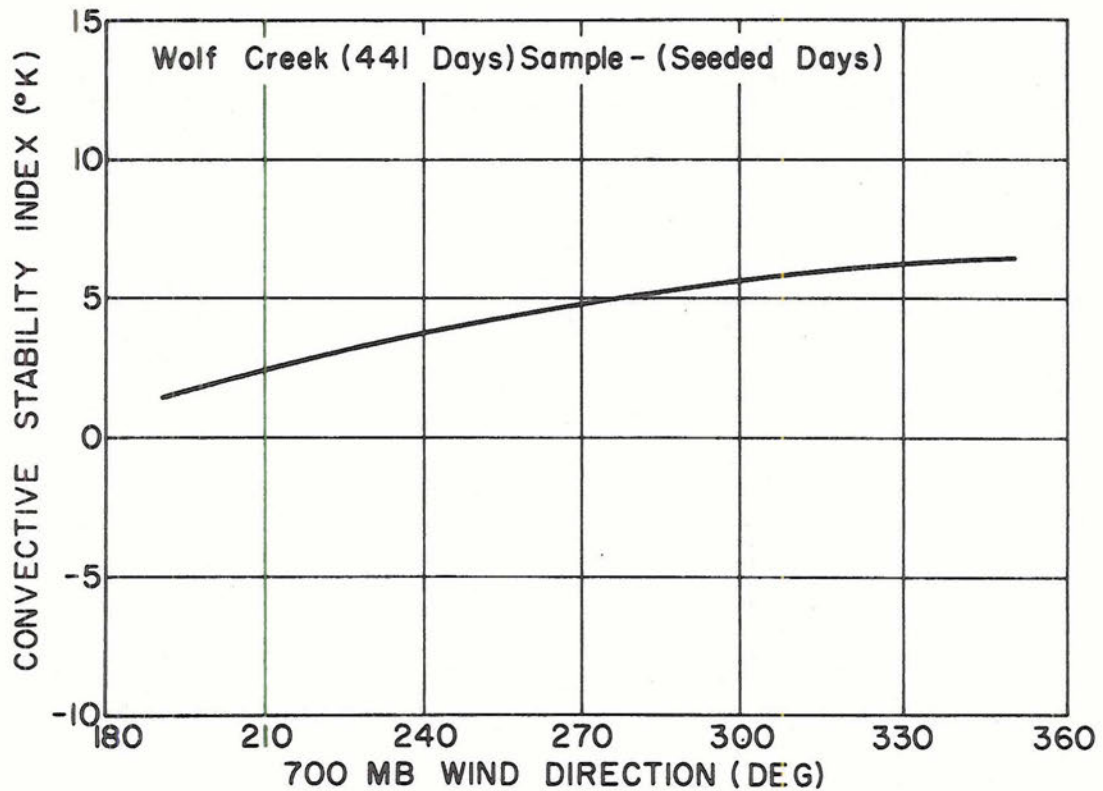
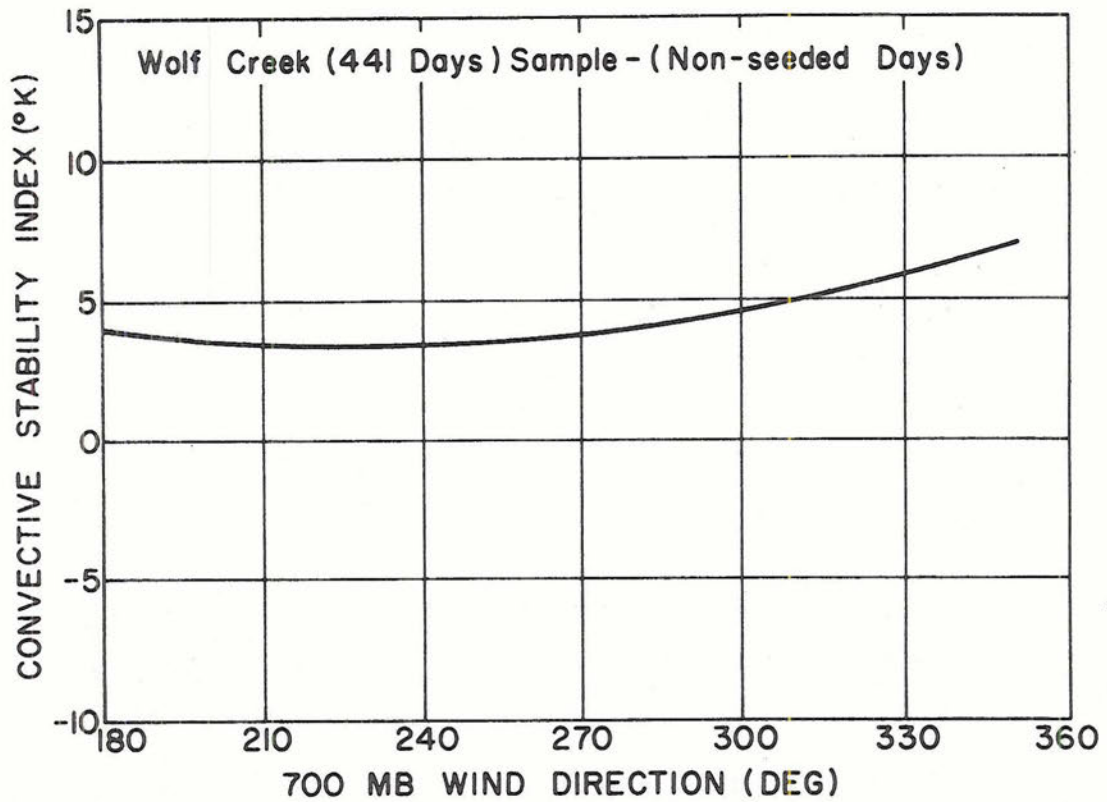


Figure 29. Relationship of the convective stability index with 700 mb wind direction for non-seeded days (upper) and seeded days (lower) for Wolf Creek sample (441 days). Curve is a second degree polynomial curve fit to the observed meteorological data.

Table 8. Estimate of scale changes during seeded periods with respect to non-seeded periods as computed by two nonparametric statistical methods. Precipitation data are from the High Altitude Observatory near Climax and near the summit of Wolf Creek Pass. Scale changes are shown within stratifications of a computed mean temperature advection in the 700-500 mb layer. Data for Climax II (296) and Total Climax (547) samples are shown in parentheses.

Stratification (Degrees C/12 hrs)	Total sample size	Sample size used	Method	Without control		With control	
				Scale change (%)	p-value	Scale change (%)	p-value
Climax I (251) Sample							
+ 1 to <+ 4	S 29	S 29	NP1	>+200	.0113	>+200	.0059
	NS 32	NS 32	NP2	>+200	.0262	+114	.1020
- 1 to <+ 1	S 37	S 37	NP1	- 40	.0436	- 31	.0367
	NS 43	NS 43	NP2	- 26	.1359	- 13	.2177
- 4 to <- 1	S 25	S 25	NP1	+ 42	.2358	+ 64	.0668
	NS 30	NS 30	NP2	+ 4	.3821	+ 36	.2236
+ 4 to <+19 and -12 to <- 4	S 29	S 29	NP1	- 34	.0721	- 19	.1660
	NS 26	NS 26	NP2	- 25	.1020	- 16	.2266
Climax II (372) and (296) Samples							
+ 1 to <+ 4	S 55 (48)	S 55 (48)	NP1	+169(>+200)	.0307 (.0087)		
	NS 49 (42)	NS 49 (42)	NP2	+185(>+200)	.0075 (.0012)		
- 1 to <+ 1	S 56 (48)	S 56 (48)	NP1	+ 31 (+40)	.2912 (.2776)		
	NS 63 (57)	NS 63 (57)	NP2	- 13 (-11)	.3300 (.3859)		
- 4 to <- 1	S 31 (20)	S 31 (20)	NP1	- 7 (-23)	.4207 (.2514)		
	NS 47 (31)	NS 47 (31)	NP2	- 13 (-31)	.2946 (.1587)		
+ 4 to <+19 and -12 to <- 4	S 40 (31)	S 40 (31)	NP1	- 14 (-15)	.3085 (.3228)		
	NS 31 (19)	NS 31 (19)	NP2	- 2 (+9)	.3859 (.4562)		
Total Climax (623) and (547) Samples							
+ 1 to <+ 4	S 84 (77)	S 84 (77)	NP1	>+200(>+200)	.0021 (.0021)		
	NS 81 (74)	NS 81 (74)	NP2	+177(>+200)	.0013 (.0010)		
- 1 to <+ 1	S 93 (85)	S 93 (85)	NP1	- 26 (-30)	.1660 (.1587)		
	NS106 (100)	NS106 (100)	NP2	- 23 (-23)	.1401 (.1515)		
- 4 to <- 1	S 56 (45)	S 56 (45)	NP1	+ 8 (+11)	.3446 (.3372)		
	NS 77 (61)	NS 77 (61)	NP2	+ 2 (-6)	.4286 (.4721)		
+ 4 to <+19 and -12 to <- 4	S 69 (60)	S 69 (60)	NP1	- 28 (-36)	.0808 (.0436)		
	NS 57 (45)	NS 57 (45)	NP2	- 16 (-20)	.1515 (.1190)		
Wolf Creek Summit (441) Sample							
+ 1 to <+ 4	S 45	S 43	NP1	+ 73	.0526	+ 81	.0146
	NS 36	NS 34	NP2	+ 79	.0401	+109	.0359
- 1 to <+ 1	S102	S 95	NP1	+ 25	.1611	+ 19	.2119
	NS 85	NS 83	NP2	+ 30	.1190	+ 29	.1190
- 4 to <- 1	S 73	S 66	NP1	+ 21	.2578	+ 29	.0808
	NS 49	NS 43	NP2	+ 35	.1711	+ 58	.0571
+ 4 to <+14 - 9 to <- 4	S 29	S 24	NP1	- 41	.1151	- 19	.1401
	NS 22	NS 20	NP2	- 14	.1685	- 5	.2676

#### 4. Testing the Model Theory with Changes in Crystal Growth Processes

In the development of the model it was demonstrated from the equation for cloud supersaturation that the onset of accretional growth in the cloud system under steady state conditions is controlled by the interplay between updraft speed and the diffusional growth rate of ice. If the magnitude of the latter exceeds the vapor supply rate, the probability of accretional growth in the cloud system is extremely small. As the magnitude of the diffusional growth rate of ice decreases, relative to the vapor supply rate, accretional growth of ice crystals may become significant in the cloud system. If seeding is effective in the cloud system, it should increase the diffusional growth rate of ice for warmer cloud systems. This, in turn, should displace the onset of significant accretional growth of crystals into warmer cloud systems.

It is seen in Figure 5 the number of crystals exhibiting accretional growth for the colder non-seeded conditions is extremely small until a 500 mb temperature of about  $-21^{\circ}\text{C}$  to  $-22^{\circ}\text{C}$  is attained. The percentage of rimed crystals increases rapidly with temperature above this point. This is in reasonably good agreement with Figures 11 and 12, which suggests the diffusional growth rate of ice exceeds the vapor supply rate in the cloud system for 500 mb temperatures below about  $-20^{\circ}\text{C}$ .

It is also seen in Figure 5 the number of crystals exhibiting riming for seeded conditions is less for all cloud temperatures. Further, the onset of accretional growth for seeded conditions occurs at 500 mb temperatures of about  $-16^{\circ}\text{C}$  to  $-17^{\circ}\text{C}$ . This suggests the diffusional ice growth process during seeded conditions was efficient for an additional 5 degrees C warming of the cloud systems. This is about the same increment of cloud temperature that separates the non-seeded and seeded

average diffusional growth rate curves computed from the model precipitation equations. This can be observed in Figures 39 and 40. Thus, there is a consistent internal verification of the model. The observed ice nuclei spectra on non-seeded and seeded days are significantly different. When placed into the model precipitation equations, these ice nuclei spectra indicate the diffusional ice growth process maintains the precipitation efficiency under seeded conditions for an additional 5 degrees C increase in cloud temperatures. Then, it is seen that the onset of significant accretional growth in the cloud system is also displaced an additional 5 degrees C toward warmer cloud temperatures. There is a nice consistency between the model equations and observed behavior of ice crystal growth processes in the cloud system.

##### 5. Testing the Model with Elevation and Spatial Variations of Seeding Effect

Previously in this chapter the model was tested in several ways using mainly precipitation data at one location within the primary target areas. In this section precipitation data from the entire Climax observing network is utilized to exhibit elevation and spatial variations of seeding effect over the experimental area. These data are introduced in order to 1) show that seeding effects discussed previously in this chapter cover a substantial area and 2) show that differences in observed patterns of seeding effectiveness, between Climax I (251) and Climax II (372) samples, are in qualitative agreement with the response of the model to differences in the potential for precipitation augmentation and suppression on seeded days during these two sampling periods.

The 65 snowboards of the Climax observing network were partitioned into 11 groups as illustrated in Figure C3. If one-half or more of the snowboards within a group had snowfall measurements on a given day, the individual observations were averaged to derive a group average for the day. If less than one half of the snowboards within a group had missing data, the entire group precipitation was considered missing. Results for the 11 snowboard groups, plus the HAO snowboard and recording gage combination (designated SG by Mielke et al., 1970), are shown as percentage changes in average daily precipitation during seeded days compared with non-seeded days.

It is seen in Figures 30 and 31, positive seeding effects for the warmest cloud temperatures cover the experimental area, and the down-wind extent of these effects is not defined. This was demonstrated previously by Mielke et al. (1970). Seeding effectiveness increases sharply, from the 500 mb temperature stratification  $-20^{\circ}\text{C}$  through  $-11^{\circ}\text{C}$  to the one from  $-18^{\circ}\text{C}$  through  $-11^{\circ}\text{C}$ , in agreement with the model.

A difference in the pattern of seeding effectiveness between Climax I (251) and Climax II (372) samples is noted in Figure 32. It is of interest, whether variations in the potential for precipitation augmentation and suppression on seeded days during the two climax sampling periods may explain part of this difference.

In order to investigate this possibility, distributions of seeded experimental events among various stratifications of 700 mb equivalent potential temperature and 700 mb wind directions were computed. These are shown in Table 9.



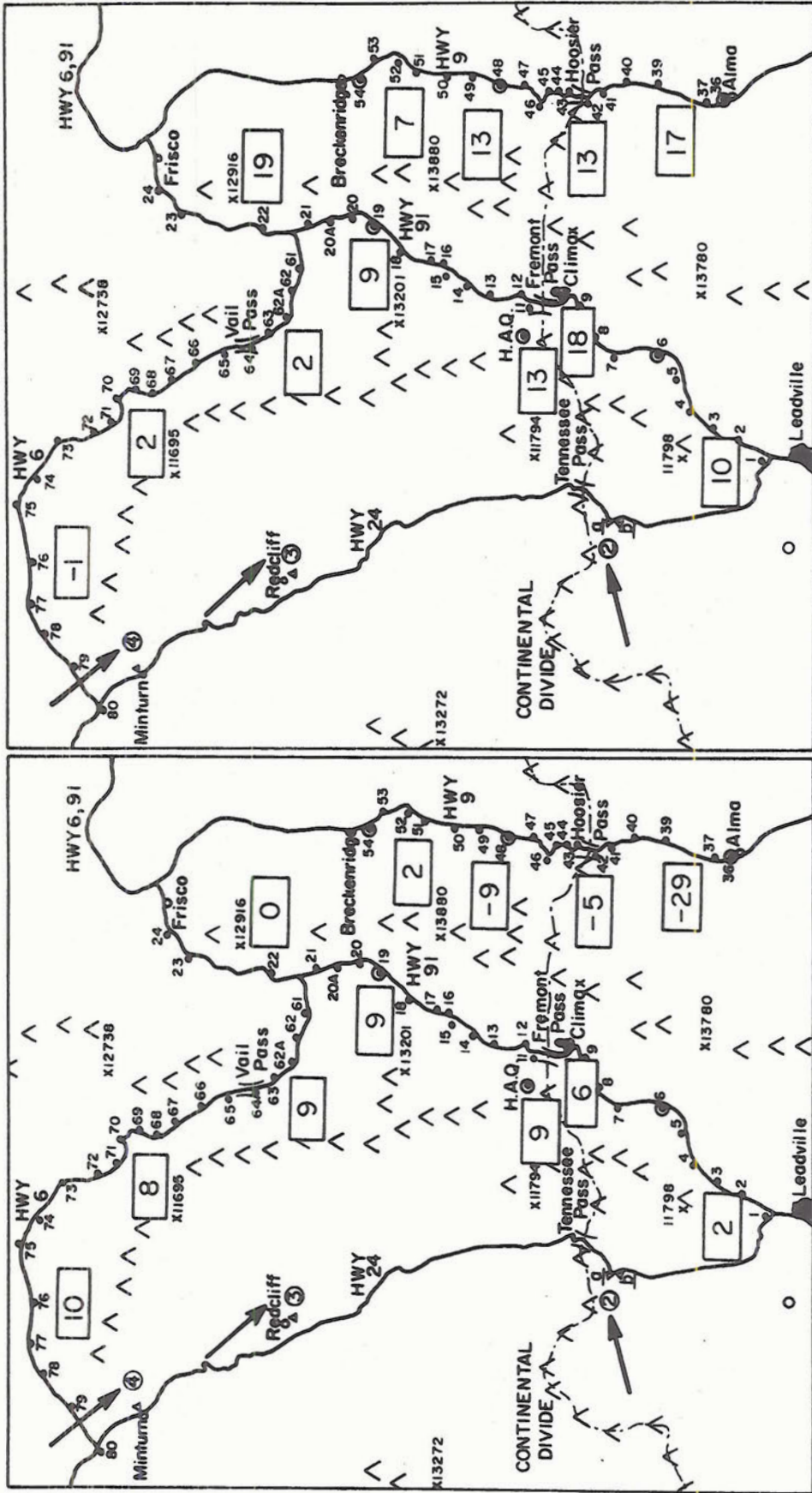


Figure 32. Percentage change in average precipitation during seeded days compared with non-seeded days for Climax I (251) sample (left) and Climax II (372) sample (right).

Table 9. Distribution of seeded experimental events among various stratifications of 700 mb equivalent potential temperature and/or 700 mb wind directions for Climax I (251) and Climax II (372) samples

700 mb Wind direction (degrees)	700 mb Equiv. pot. temp. (degrees K)	Climax I (251) sample (%)	Climax II (372) sample (%)
190-250		24.1	30.6
260-300		51.9	45.9
310-360		24.0	23.5
	281 to <295	16.7	17.7
	295 to <308	52.8	46.5
	308 to <326	30.5	35.8
190-250	281 to <295	2.8	1.8
	295 to <308	12.0	10.6
	308 to <326	9.3	18.2
260-300	281 to <295	9.3	7.1
	295 to <308	26.9	24.1
	308 to <326	15.7	14.7
310-360	281 to <295	4.6	8.8
	295 to <308	13.9	11.8
	308 to <326	5.5	2.9

It is seen in Table 9 that 6.5 percent more of the total experimental events occurred with southwest flow during the Climax II sampling period. Most of this increase in southwest flow cases came from a decrease in westerly flow cases. Also, it is seen that 5.3 percent more of the total experimental events occurred in the warmest cloud temperature category, and little change was observed in the coldest category where a potential for overseeding may exist. With more southwest flow events and warmer cloud conditions, one might expect some increase in the positive seeding effect over the experimental area during the Climax II sampling period. This is seen to be the case in Figure 32.

It is also seen in Table 9, there are some important differences between the two Climax samples in the distributions of seeded experimental events among double stratifications of 700 mb wind direction and 700 mb equivalent potential temperature. The percentage of warmest southwest flow events was nearly doubled, and the percentage of coldest southwest flow events was reduced for the Climax II (372) sample. Also, the percentage of warmest northwest flow cases was almost halved, and the percentage of coldest northwest flow cases was almost doubled for the Climax II (372) sample. The model response to the Climax II distribution of seeded events would suggest a larger positive seeding effect with southwest flow and a smaller positive seeding effect with northwest flow events than was observed for the Climax I distribution. This is seen to be the case in Figures 33 and 34. It appears the larger positive seeding effects on the southern slopes of Fremont and Hoosier Passes during southwest flow, and the reduction of positive seeding effects on the northern slopes of these passes during northwest flow, have resulted in a reversal of the pattern in overall seeding effectiveness observed in Figure 32 between the two Climax samples.

It is of considerable interest that the differing distributions of seeded days among the various classes of meteorological parameters was mainly due to the results of randomization, rather than real differences in existing weather regimes during the two sampling periods.

#### 6. The Problem of Spurious Upwind Seeding

It was mentioned previously that upwind seeding activities were conducted during the 1965-69 Climax experimental period. These were conducted for the most part at the Park Range experiment about 75 miles northwest of Climax, Colorado. While it is outside the scope of this

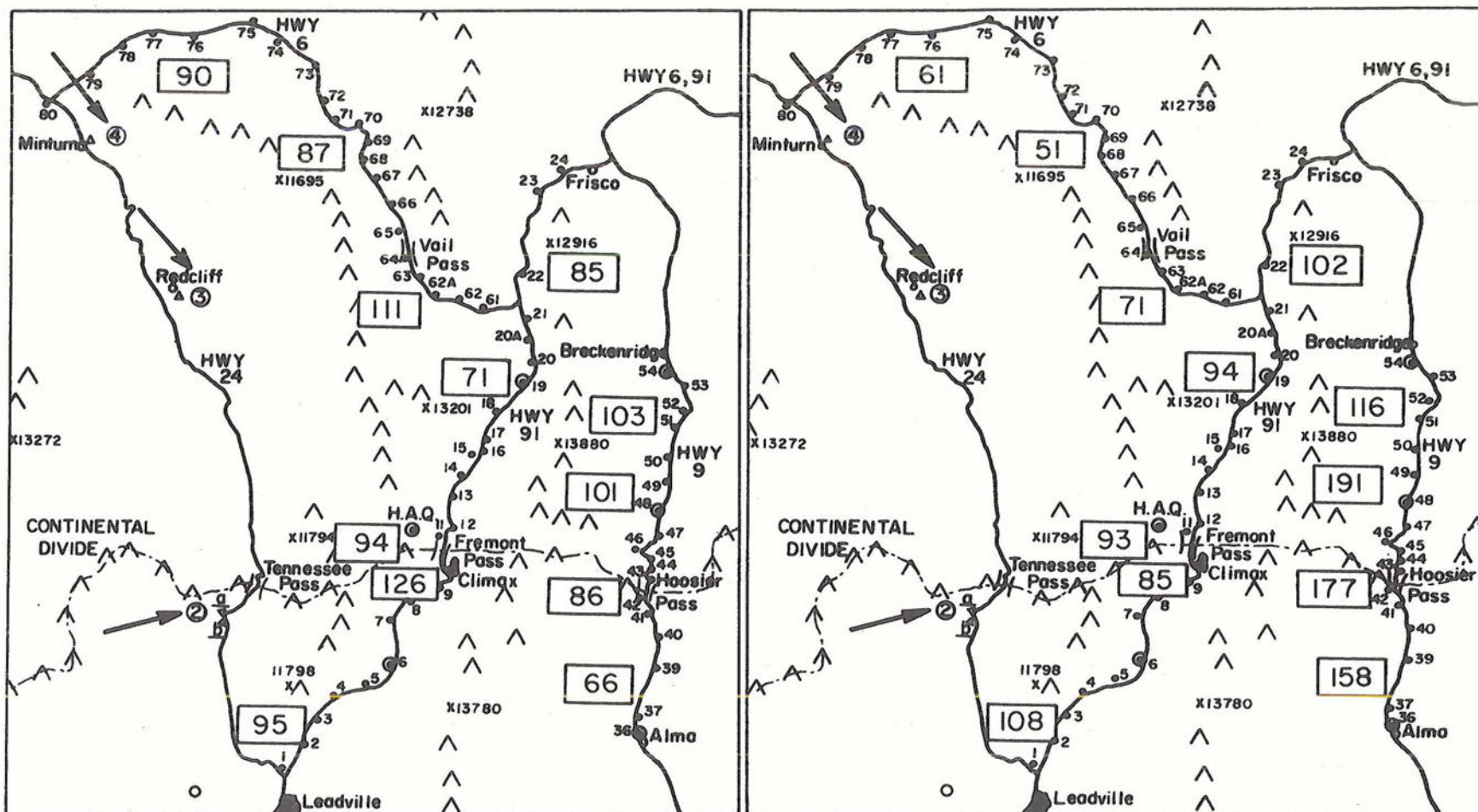


Figure 33. Percentage change in average precipitation during seeded days compared with non-seeded days for 700 mb wind directions 190 through 250 degrees. Results are shown for Climax I (251) sample (left) and Climax II (372) sample (right).

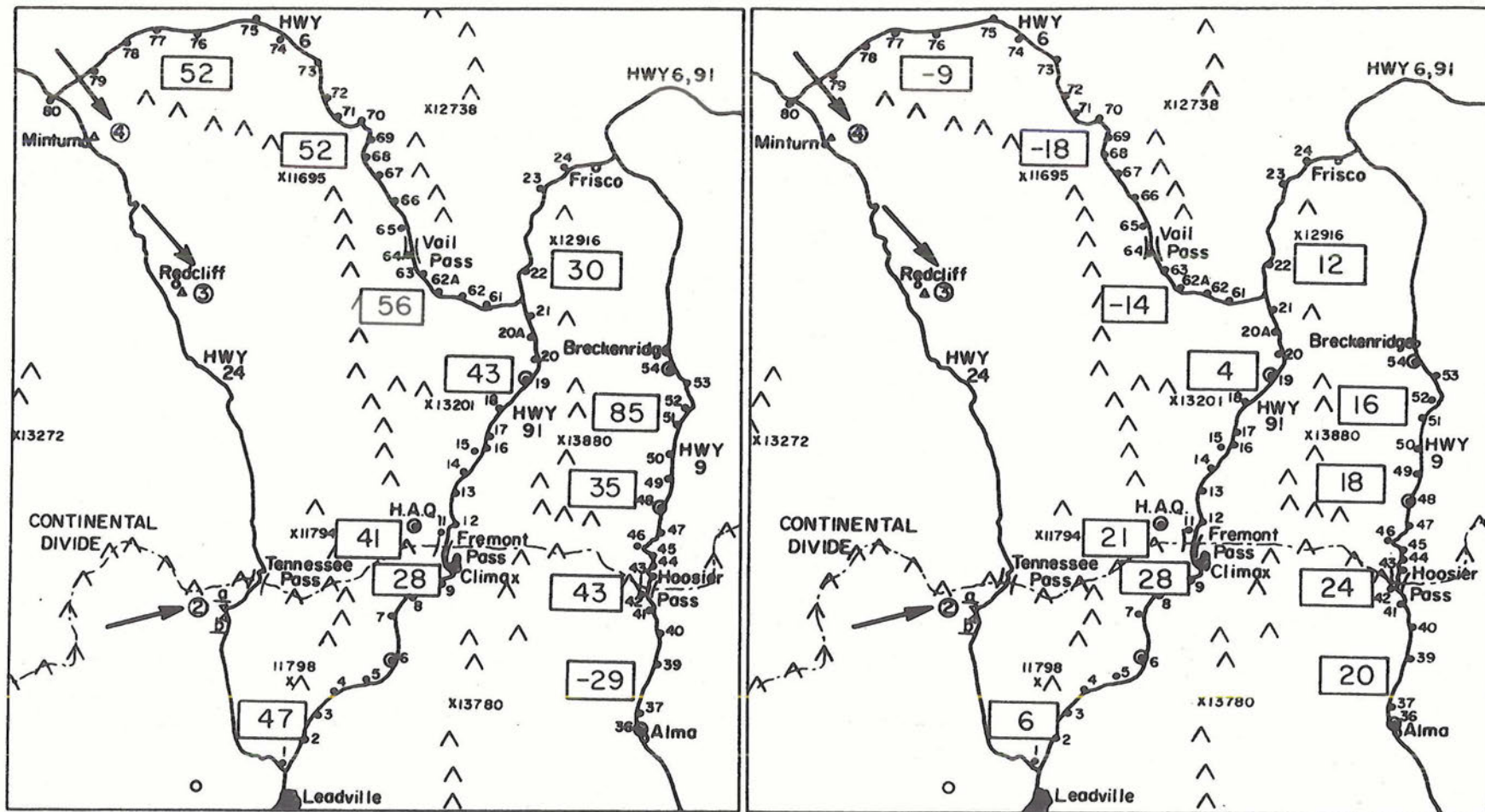


Figure 34. Percentage change in average precipitation during seeded days compared with non-seeded days for 700 mb wind directions 310 through 360 degrees. Results are shown for Climax I (251) sample (left) and Climax II (372) sample (right).

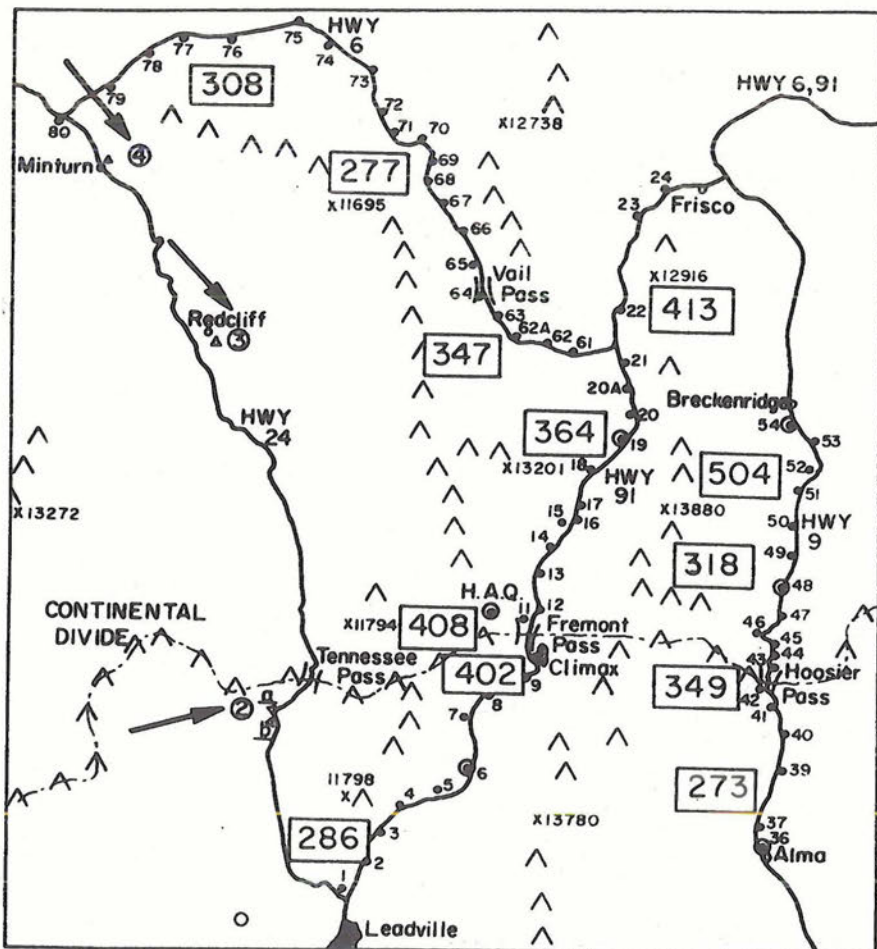


Figure 35. Percentage change in average precipitation during seeded days compared with non-seeded days for equiv. pot. temps. from 308K to less than 326K and 700 mb wind directions from 310 thru 360 degrees for Total Climax sample (623 days).

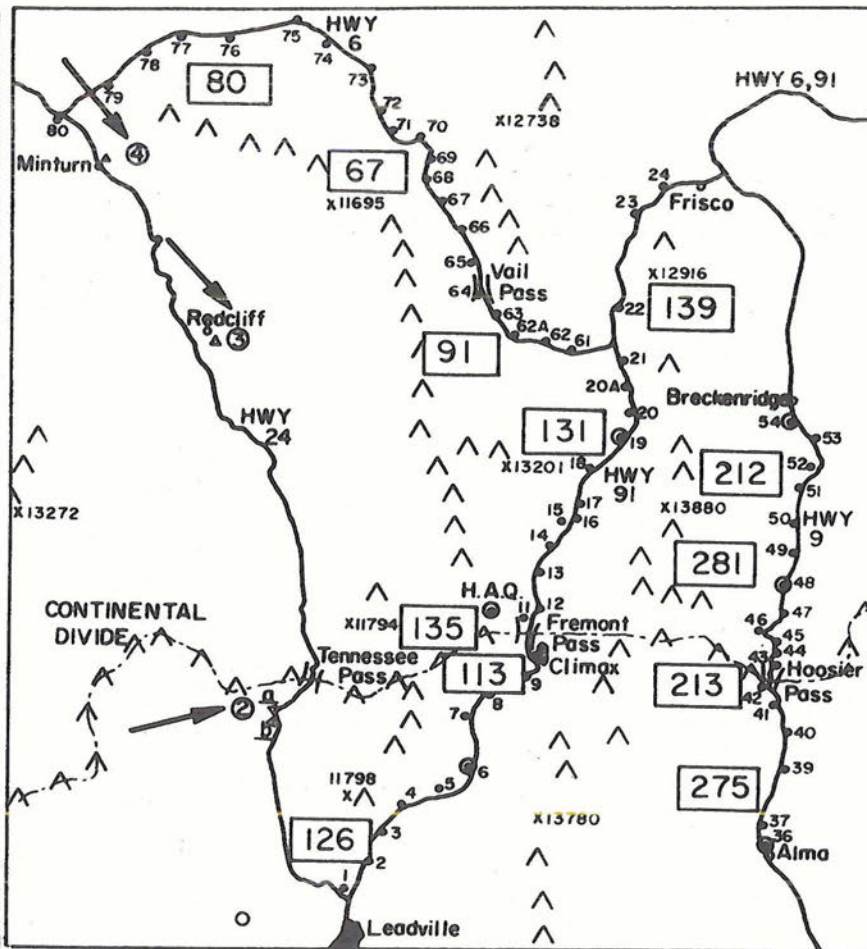


Figure 36. Percentage change in average precipitation during seeded days compared with non-seeded days for equiv. pot. temps. from 308K to less than 326K and 700 mb wind directions from 190 through 250 degrees for Total Climax sample (623 days).

paper to perform a detailed analysis of possible upwind seeding effects, data already presented allows for a preliminary look at the problem.

It appears there was no critical confounding of the Climax experiment during the 1965-70 period from upwind seeding activities. It was seen that results of the Climax II (372) sample were in agreement for the most part with the results of the Climax I sample and with model equations. Further, it was seen that differences in the pattern of seeding effectiveness between these two samples were in qualitative accord with indications of the model. There is a suggestion in Table 1 however, that elimination of possible upwind seeding events has generally increased positive seeding effects for most cloud temperatures, and especially for warmer cloud temperatures. This suggests that elimination of these particular events, which are strongly biased toward heavy precipitation, has left the Climax II (296) sample strongly biased toward smaller precipitation events. It would seem to follow then, that cloud systems associated with these events would also be biased toward either 1) smaller than average upward speeds, 2) smaller than average cloud thickness (which very likely means lower than average cloud tops) or 3) a combination of both. The lower than average cloud tops are a possible explanation for the general increase in positive seeding effects observed over most of the range of cloud temperature.

The main discrepancy between the Climax II (372) and Climax II (296) samples appears in the warmest, or largest categories of Tables 1, 2 and 3. A substantial increase in the positive seeding effect is observed for the Climax (296) sample. It is of considerable interest whether this might be due to the upwind seeding. It has already been shown that the available average condensation rate was somewhat lower

during the five-year period from 1965-70, and consequently, the model suggests that S.M.P. should therefore become available at slightly warmer temperatures. Thus, the smaller positive seeding effects observed for the Climax II (372) sample for 500 mb temperatures of -20C and warmer is in qualitative agreement with the model. On the other hand, if upwind seeding increased the precipitation on Climax II non-seeded days within the -18C to -20C temperature range, this same result in seeding effectiveness would be observed. In investigating this possibility, it was found that three unusually heavy precipitation events (between .50 and .87 inches of water equivalent per day) occurred within this temperature range on Climax II non-seeded days, when seeding was conducted upwind at the Park Range. It was also discovered that the average precipitation for 500 mb temperatures of -18C to -20C is slightly high for the Climax II (372) sample than the Climax I (251) sample, even though precipitation in general, tended lower over the Climax II sampling period. It seems possible, therefore, that some downwind seeding effect was experienced at Climax, especially within the 500 mb temperature range from -18C to -20C. Thus, the exact 500 mb temperature at which the natural precipitation efficiency begins to decrease for the Climax II (372) sample is somewhat in doubt. This region of doubt, however, probably does not exceed 2 degrees C of temperature and does not seriously affect a general verification of the model.

## CHAPTER V

### CLOUD MICROSTABILITY AND THE NATURE OF THE SEEDING EFFECT

#### 1. Introductory Remarks

It is seen in Figures 11 and 12 that the model equation describing the average diffusional growth rate of ice in the cloud system decreases very rapidly as cloud temperatures become warmer, reaching rapidly a very small fraction of the average vapor supply rate. If cold cloud microstability exists, such that a given magnitude of ice growth rate (or nearly equivalently, a given ice crystal concentration) is required to overcome this microstability and initiate a precipitation release, the major effect of seeding might be to increase the duration of precipitation. If this is not true, then the major effect of seeding the warmer cloud systems must be to increase precipitation rates during snowfall hours.

The character of precipitation changes that result from seeding cold orographic clouds have not been defined nor treated statistically. In this chapter the total precipitation change is partitioned into precipitation duration and intensity change components. These components are evaluated for the Climax experimental data and the results subjected to statistical tests. These results are analyzed relative to their relation to precipitation initiation, precipitation suppression (overseeding) and precipitation forecasting.

In order to partition the total precipitation change into meaningful components, the experimental design must satisfy two important

requirements. The experimental sampling unit must be considerably longer than the average natural precipitation episode, and the experimental design must call for seeding irrespective of whether snow is occurring naturally. The Climax experimental design fulfills these criteria quite well, for seeding generators were normally run regardless of current local weather, and the 24-hour sampling unit employed is two and one half times the average daily snowfall duration.

The hourly precipitation data used in this study was from the Climax 2NW recording gage (United States Weather Bureau Station #05-1660). This gage is located at the High Altitude Observatory (HAO) of the University of Colorado and is very near the center of the designated primary target area of the Climax experiment. Results from the Total Climax (623) sample are shown in this chapter.

## 2. Definition of Precipitation Change Components

Precipitation during a 24-hour sampling unit can be expressed as the number of precipitation hours times the hourly intensities averaged over these same hours. Therefore, the change in the 24-hour precipitation that results from seeding can be decomposed into intensity and duration change components.

The total change in precipitation associated with seeding is defined in terms of a ratio of the average precipitation on seeded days compared with non-seeded days within a given meteorological stratification or grouping

$$\bar{T}_s = \frac{\text{total precipitation in seeded group}}{\text{number of days in seeded group}}$$

$$\bar{T}_{ns} = \frac{\text{total precipitation in non-seeded group}}{\text{number of days in non-seeded group}}$$

$$\text{Total precipitation change} = \bar{T}_s / \bar{T}_{ns}$$

The change in the intensity of precipitation is defined in terms of a ratio of the average hourly intensity on seeded days compared with non-seeded days.

$$\bar{I}_s = \frac{\text{total precipitation in seeded group}}{\text{number of seeded precipitation hours in group}}$$

$$\bar{I}_{ns} = \frac{\text{total precipitation in non-seeded group}}{\text{number of non-seeded precipitation hours in group}}$$

$$\text{Precipitation intensity change} = \bar{I}_s / \bar{I}_{ns}$$

The change in the duration of precipitation is defined in terms of a ratio of the average number of precipitation hours on seeded days compared with non-seeded days.

$$\bar{D}_s = \frac{\text{number of seeded precipitation hours in group}}{\text{number of days in seeded group}}$$

$$\bar{D}_{ns} = \frac{\text{number of non-seeded precipitation hours in group}}{\text{number of days in non-seeded group}}$$

$$\text{Precipitation duration change} = \bar{D}_s / \bar{D}_{ns}$$

It can be noted from an inspection of the defined ratios, the intensity change and duration change ratios multiply to give the total precipitation change ratio or

$$\bar{T}_s / \bar{T}_{ns} = (\bar{D}_s / \bar{D}_{ns}) (\bar{I}_s / \bar{I}_{ns})$$

### 3. Precipitation Change Components as a Function of 700 mb Equivalent Potential Temperature

The above ratios were generated as functions of the 700 mb equivalent potential temperature using a running mean over a five degree

interval. Figure 37 shows the three precipitation change ratios plotted as a function of the 700 mb equivalent potential temperature for the Total Climax (623) sample.

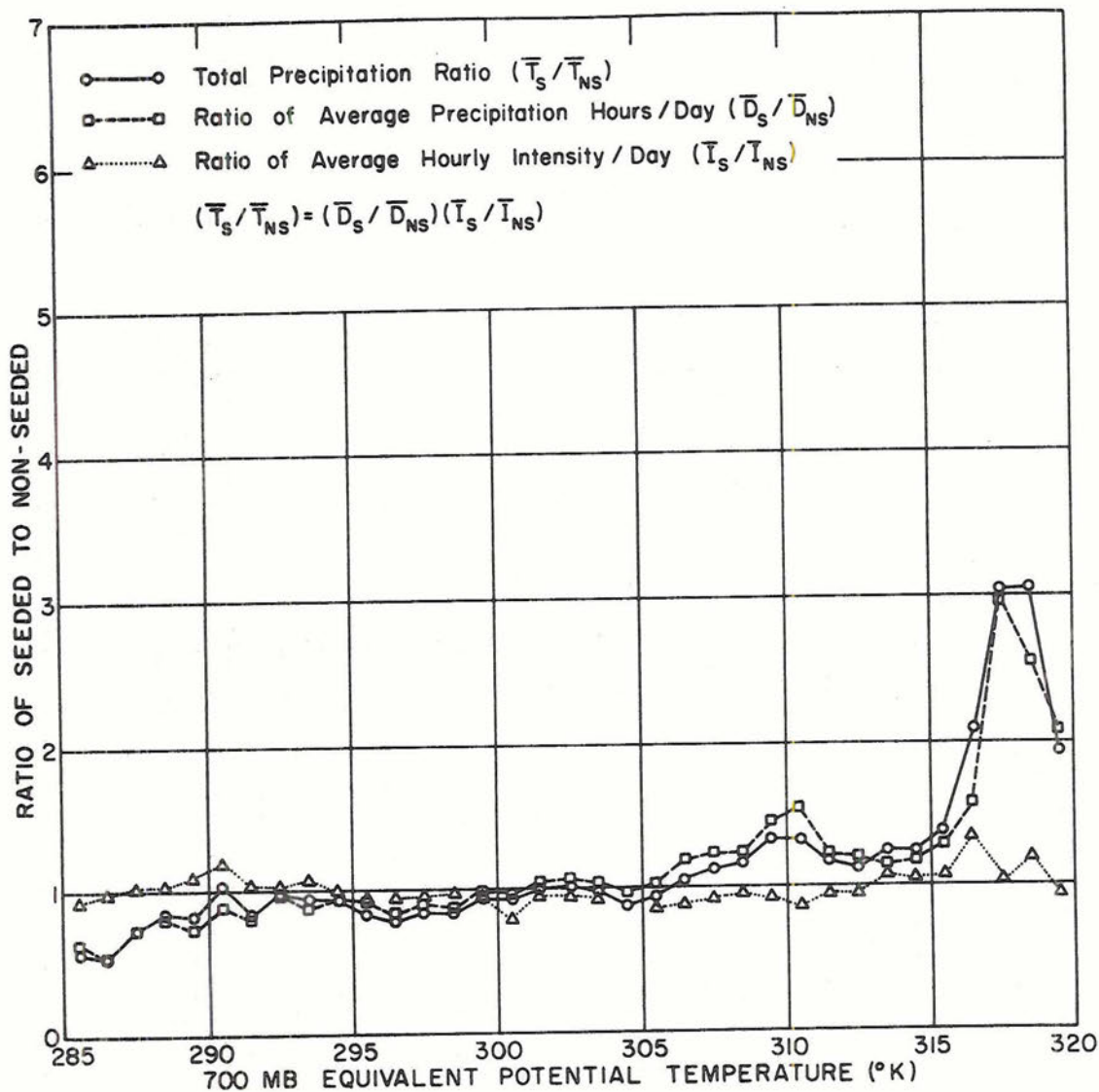


Figure 37. Seeded to non-seeded ratios of total precipitation change, precipitation duration change and precipitation intensity change. Ratios were generated as a function of 700 mb equivalent potential temperature by computing running means over a five degree temperature interval. Precipitation data were measured at HAO during experimental days of the Total Climax (623) sample.

It is seen for temperatures below 306K, all three precipitation change ratios are nearly one until the very coldest temperatures are reached. At an equivalent potential temperature of about 290K, the total precipitation change and duration change ratios decrease and reach values near 0.5 to 0.6 for the very coldest temperatures. Above an equivalent potential temperature of 306K, there is an irregular rise in the total precipitation change ratio. It reaches a minor peak around 310K and attains a major peak of over 3.0 around 317K to 318K.

It is interesting to note that in general, fluctuations in the total precipitation ratio are mainly controlled by the variations of the duration change ratio. The major effects of seeding the Climax cold orographic cloud system appear to be 1) to suppress precipitation during some hours with the coldest cloud systems, when it would have occurred naturally and 2) to affect a precipitation release during many hours with the warmest cloud systems, when it would not have occurred naturally. Only for the warm cloud systems does there appear a relatively small contribution to the total precipitation change from an intensity change.

It should be noted that the intensity change computed here compares the average hourly precipitation intensity for seeded conditions with that for non-seeded conditions. The average hourly precipitation intensity for favorable seeding conditions may include those hours when snow would have occurred naturally, plus additional hours of precipitation arising from the seeding. This analysis therefore, does not measure exactly the intensity change that would result from seeding natural snowfall hours only. However, distributions of hourly precipitation

intensities for natural and seeded conditions suggest that the additional hours of precipitation produced by seeding the warmer cloud systems, are distributed among the hourly intensity classes similarly to the natural precipitation hours. The intensity change computed here therefore, approximates closely the intensity change to be expected for natural snowfall hours.

#### 4. Duration and Intensity Change Components as a Function of Total Precipitation Change

Figure 38 is an attempt to show the duration and intensity change ratios as a function of the total precipitation change ratio. The curves are fitted by eye with the restriction that points on the duration and intensity change curves must multiply to give the total precipitation change ratio. It is seen that the duration change ratio exerts major control over the total precipitation change ratio.

#### 5. Duration Effect and the Number of Precipitation Hours

In order to statistically test the significance of the precipitation duration change, distributions of positive and zero precipitation hours for seeded and non-seeded Climax experimental days were investigated, when 700 mb equivalent potential temperatures were 315K through 320K. The contingency table is shown in Table 10. The null hypothesis for this test is that seeding has no effect on the number of individuals in the zero category. The alternate hypothesis is that seeding reduces the number of zero precipitation hours. The value of chi-square for this test suggests the null hypothesis may be rejected in favor of the alternate hypothesis and there is a very high probability that some positive precipitation hours on seeded days would be zero without seeding.

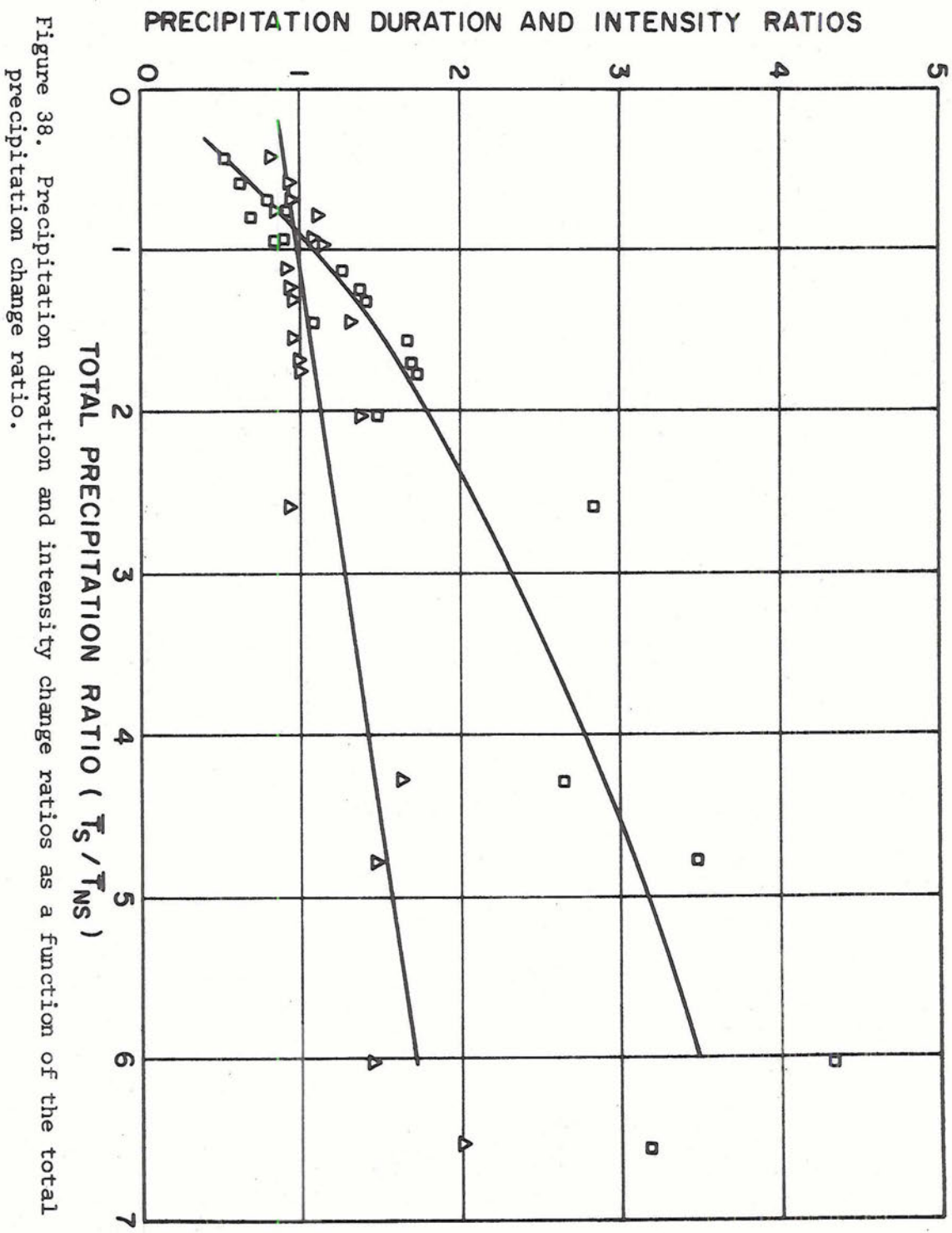


Figure 38. Precipitation duration and intensity change ratios as a function of the total precipitation change ratio.

Table 10. Contingency table showing the number of positive and zero precipitation hours distributed according to seeded and non-seeded conditions for the Total Climax (623) sample, when 700 mb equivalent potential temperatures were 315K through 320K.

---

	Seeded	Non-seeded
positive precipitation hours	106	45
zero precipitation hours	299	465

chi-square = 49.3 with 1 degree of freedom

$$P(\chi^2 \geq 49.3) < .001$$


---

A null hypothesis stating that the average number of precipitation hours on seeded experimental days (6.28 hrs) is equal to that on non-seeded experimental days (2.12 hrs) may be rejected at the 3 percent significance level using Student's t-test. On the basis of these two tests, there seems to be little doubt that seeding had a pronounced influence in affecting a change in the distribution of zero and positive hours of precipitation for these typical warmest cloud systems. It can also be demonstrated that seeding probably produces a decrease in the number of precipitation hours for the cold and relatively dry cloud systems. This may be seen in Table 11.

The null hypothesis for this test is that seeding has no effect on the number of individuals in the zero category. The alternate hypothesis is that seeding increases the number of zero precipitation hours. The value of chi-square for this test suggests the null hypothesis may be rejected in favor of the alternate hypothesis and there is a high probability that some zero precipitation hours on seeded days would be positive without seeding.

Table 11. Contingency table showing the number of positive and zero precipitation hours distributed according to seeded and non-seeded conditions for the Total Climax (623) sample, when 700 mb equivalent potential temperatures were 284K through 289K.

---

	Seeded	Non-seeded
positive precipitation hours	51	73
zero precipitation hours	296	195

chi-square = 14.8 with 1 degree of freedom

$$P(\chi^2 > 14.8) < .005$$


---

The average number of precipitation hours per experimental day for seeded conditions (3.53 hrs) is only about half that for non-seeded conditions (6.54 hrs). However, Student's t-test on the difference of these averages indicates one chance in six that this could occur by chance.

The above two tables demonstrate a high probability that seeding has a pronounced influence on the duration of precipitation. It is evident from Figure 37, the major effect of seeding warmer cloud systems is in overcoming cloud microstability and initiating precipitation, when it would not have occurred naturally.

#### 6. Cloud Microstability and Forecasting Precipitation From Cold Orographic Clouds

In investigating the nature of the seeding effect, evidence was found for the existence of cloud microstability at warmer cloud temperatures. Inefficiency of the natural cloud system mainly lies in not being able to overcome this cloud microstability. This suggests the

magnitude of the diffusional growth rate of ice in the cloud system controls the precipitation release in these clouds. Further indirect evidence of this is found in the Climax experimental data listed next:

Table 12. Distribution of non-seeded experimental days, experimental precipitation days and experimental zero precipitation days with the concurrent 500 mb temperature for the Total Climax (623) sample.

Temperature Category (°C)	No. of Exp. Days	No. of Precip. Days	No. of Zero Days	Percentage of Precip. Days to Exp. Days
-40 to -36	2	2	0	100.0
-35 to -31	17	16	1	94.2
-30 to -26	64	60	4	93.8
-25 to -21	129	103	26	79.8
-20 to -16	88	50	38	56.8
-15 to -11	21	7	14	33.3
Total or Average (321)		(238)	(83)	(73.9)

In table 12 the percentage of precipitation days to experimental days is really a measure of the accuracy in forecasting measurable precipitation by present day forecasting techniques. The experimental days of the Climax experiment were based upon a forecast of measurable precipitation at Leadville, Colorado, which lies within the target area.

The decline in forecast accuracy as cloud temperatures become warmer is startling. The Weather Bureau Forecast Center in Denver was over 90 percent accurate in their forecasts of measurable precipitation when 500 mb temperatures were -26C and colder. This declined steadily as 500 mb temperatures became warmer reaching only 33.3 percent for temperatures from -15C to -11C. It seems reasonable to assume that

the forecaster, using the usual forecast methods and procedures, found these events to be equally likely to produce measurable precipitation. It follows then, that the cause of the decline in forecast accuracy is probably due to the neglect of an important and temperature dependent factor. It is believed that current forecast procedures emphasize condensation rates and neglect ice growth rates, and the usual assumption that condensate will automatically be converted to precipitation does not hold for these warmer orographic cloud systems. As is seen in Table 12, as cloud temperatures become warmer, the probability decreases that cloud microstability will be overcome and a precipitation release obtained.

## CHAPTER VI

### OVERSEEDING AND THE INVALIDITY OF THE MODEL

In the development of the model equations, the possibility was pointed out that under certain meteorological conditions seeding might cause a decrease in precipitation on the mountain. In particular, this possibility seemed favored by cloud systems with very cold temperatures and very high wind speeds normal to the barrier. It was also pointed out subsequently, that the model precipitation and S.M.P. equations were not valid if cloud treatment brought about overseeding. These equations are based on considerations of cloud efficiency, which do not transfer into terms of precipitation efficiency under overseeded conditions. Losses due to ice crystal evaporation are no longer small compared to the total vapor supplied to the cloud system, and the assumption underlying the model equations is not valid.

Experimental evidence already presented suggests overseeding may occur at Climax during both of the above mentioned conditions. Tables 1, 2, 3 and 6 show negative seeding effects for the coldest and driest cloud systems and for highest wind speeds. Some of the p-values for these statistical tests were less than 5 percent. Table 11 also demonstrates a high probability that some zero precipitation hours on seeded days would have been positive without seeding for the coldest cloud systems. It is also seen in Table 13, a high probability exists that some zero precipitation hours on seeded days would have been positive without seeding for these highest wind speeds. Thus, there is strong

evidence that overseeding is very real, and a complex function of cloud temperatures and the speed of the wind flow normal to the barrier as suggested by Ludlam (1955).

Table 13. Contingency table showing the number of positive and zero precipitation hours distributed according to seeded and non-seeded conditions for the Total Climax (623) sample, when 700 mb wind speeds were 15 through 28 meters/sec.

---

	Seeded	Non-seeded
Positive precipitation hours	156	199
Zero precipitation hours	466	377

Chi-square = 16.8 with 1 degree of freedom

$$P(\chi^2 \geq 16.8) < .005$$


---

Overseeding is mainly a duration effect, for if present, snow crystals do not reach the mountain and precipitation ceases. This is demonstrated in Figure 37, which shows that decreases in daily precipitation due to seeding at the extremely cold cloud temperatures are totally a duration effect. In the development of the model, it was proposed that overseeding associated with extremely cold cloud temperatures might occur due to the reduction in crystal size and fall speeds as cloud supersaturation lowers in response to a growing excess of crystal concentration over the optimum. However, it is difficult to pin point at what crystal concentration the stage of overseeding is reached, since this is also a function of the wind speed normal to the barrier. Ludlam (1955) suggested excessive crystal concentrations by a factor of ten may not be harmful. This factor can be estimated for the Climax

cloud system, for conditions averaged over all wind speeds, by considering Figure 15. It is seen that the temperature range over which precipitation changes are essentially constant and near zero, covers about a five to six degree interval of cloud temperature. The ice nuclei temperature spectrum observed for seeded days at Climax and calculations of optimum crystal concentration, may be compared to evaluate this factor. Following this approach, it is estimated that crystal concentrations exceeded the optimum concentration by about a factor of 14 before precipitation efficiency at HAO was noticeably lowered.

It is emphasized however, that this factor was evaluated for conditions averaged over all wind speeds and should be smaller for higher wind speeds. This factor may, in fact, become indeterminate at extremely high wind speeds, if the concept of an optimum crystal concentration becomes invalid due to overseeding.

In designing operational programs, the case where overseeding is due mainly to the coldness of the cloud system (wind speeds are not a crucial factor) presents only a minor problem. Cloud efficiency becomes optimum before overseeding enters the picture, and one should not be seeding these cloud systems anyway. However, for extremely high wind speeds, it is conceivable that seeding may increase cloud efficiency, while causing a decrease in precipitation efficiency. It is this particular case that will require careful design considerations.

## CHAPTER VII

### ANALYSES OF WEATHER MODIFICATION POTENTIAL

#### 1. Natural Precipitation Efficiencies

Precipitation efficiencies can be discussed in terms of the amount of precipitation observed at the ground compared to the available rate of condensation defined in the model development. In Figures 39 and 40 it is seen, by comparing the areas under the natural precipitation curves to those under the available rate of condensation curves, that the natural precipitation efficiencies are 35 percent and 37 percent for the Climax I (251) and Climax II (372) samples respectively. These values of precipitation efficiencies are evaluated in the warmer cloud temperature region where the diffusional growth rate of ice has fallen below the available rate of condensation. It may also be noted in Figures 39 and 40, observed precipitation efficiencies are a little greater than given by the model precipitation equation, which assumed only diffusional growth of ice crystals. This difference in precipitation efficiency reaches a factor as high as 12 at 500 mb temperatures of  $-16^{\circ}\text{C}$  to  $-14^{\circ}\text{C}$  in both Climax samples. Since crystal replication indicates that accretional growth of ice crystals seldom attains the same magnitude as diffusional growth in the Climax cloud, an ice crystal multiplication factor between 6 and 12 may be present at these warmer cloud temperatures. This is in good agreement with Grant (1968), who found ice crystal multiplication of around 10 for several cases in this temperature range.

These values of natural precipitation efficiency indicate that snowfall increases of 170 percent to 185 percent would be realized at these warmer cloud temperatures if seeding converts all the available rate of condensation to snowfall on the mountain. These estimates do not include additional increases that might result from the existence of D.M.P.

## 2. Seeded Precipitation Efficiencies

In Figures 39 and 40 it is seen, by comparing the areas under the seeded precipitation curves to those under the available rate of condensation curves, that seeded precipitation efficiencies are 89 percent and 76 percent for the Climax I and Climax II samples respectively. These values of precipitation efficiency were computed over the same cloud temperature region for which the natural efficiencies were determined.

It should be emphasized at this point, this analysis considers only experimental precipitation days. When it is stated that 89 percent of the available rate of condensation was converted to snowfall for seeded conditions, this percentage refers only to those experimental days when a precipitation release was obtained. Those days, when a S.M.P. might have existed, but a precipitation release was not obtained, are not included in the analysis.

## 3. Analysis of Static and Dynamic Modification Potentials

The available rate of condensation curves shown in Figures 39 and 40 for seeded conditions are estimates derived with the assumption that seeding has no effect on the average rate of condensation in the cloud system. In the event that seeding produced a significant D.M.P., and

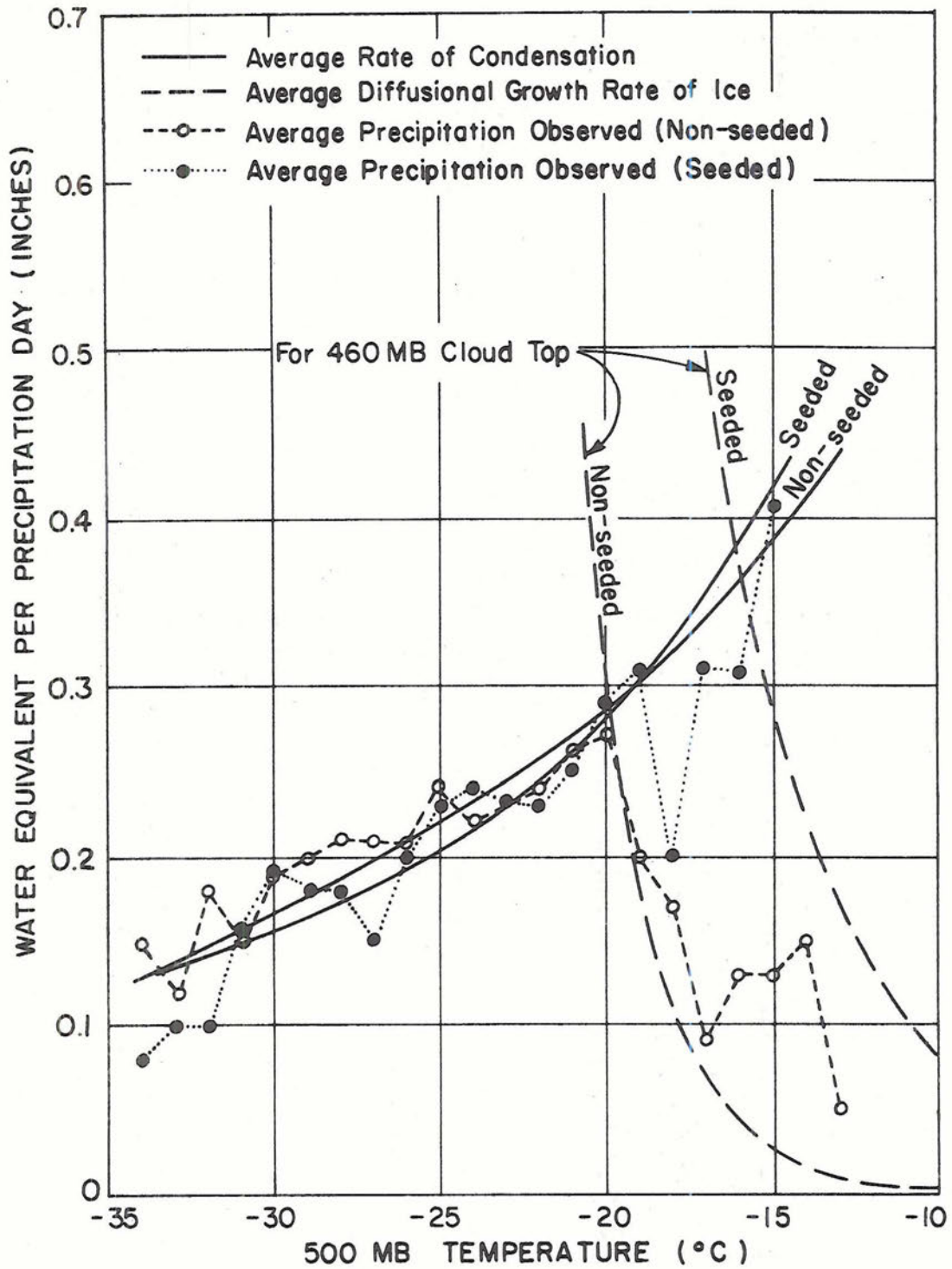


Figure 39. Distributions of seeded and non-seeded precipitation at HAO as a function of 500 mb temperature. Precipitation data are from Climax I (251) sample and values are a running mean over a two-degree temperature interval.

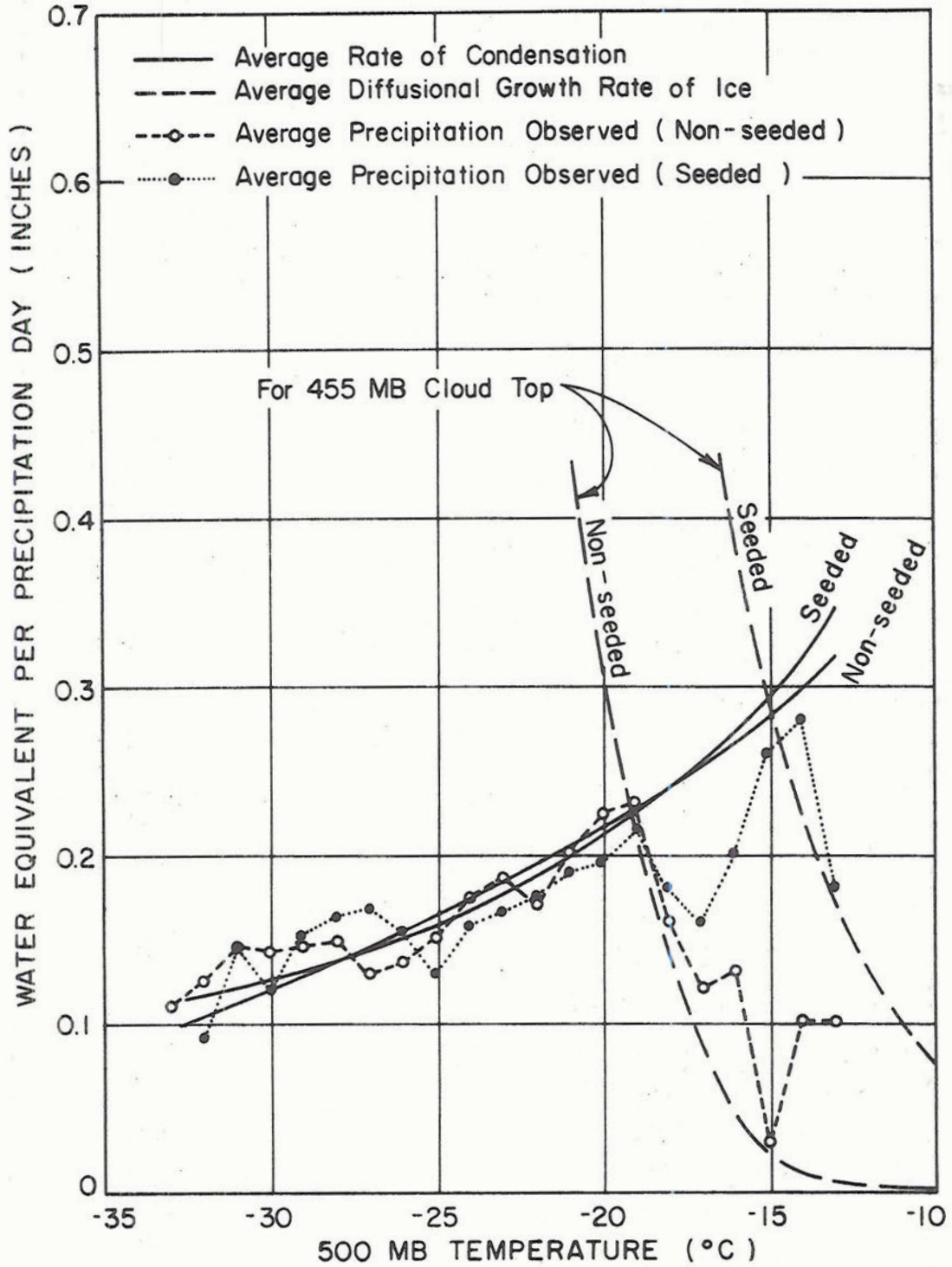


Figure 40. Distributions of seeded and non-seeded precipitation at HAO as a function of 500 mb temperature. Precipitation data are from Climax II (372) sample and values are a running mean over a two-degree temperature interval.

simultaneously all the S.M.P. was realized, seeded precipitation values should fall above the available rate of condensation curve. This is the only way in which a beneficial dynamic seeding effect can be detected in this type of analysis. However, a D.M.P. can exist in spite of the fact that seeded precipitation values are below the available rate of condensation curve, since these values integrate dynamic and static seeding effects and the efficiency of seeding itself.

It is seen from Figures 39 and 40 that precipitation values are generally near or just slightly below the available rate of condensation curves during seeded conditions. It is therefore not necessary to invoke a dynamic seeding effect to explain these results.

There are other reasons for believing dynamic seeding effects are small for the Climax cloud system. This cloud system is a relatively cold and dry one, since the mountain barrier producing it extends to near 14,000 ft msl and cloud bases are generally near 12,000 ft msl. Therefore, the additional latent heat of fusion, which is less than 14 percent the latent heat of vaporization, is released by only a small mass of water. From this argument, and from the results of the Climax experiment, it appears that dynamic seeding effects are secondary to static seeding effects in the Climax cloud system.

There is another point to be made concerning D.M.P. Any beneficial dynamic seeding effects that do exist, and which originate from changes in latent heat release, should occur mainly with warmer cloud systems where the diffusional ice process is naturally inefficient. In the colder cloud system essentially all the latent heat of sublimation is already released naturally, and seeding will not increase the amount released. For the warmer cloud systems however, where cloud water is

not converted to ice efficiently, seeding could increase the latent heat release by adding all or part of the latent heat of fusion. Under these conditions, D.M.P. would coexist with S.M.P., and meteorological conditions which delineated the availability of S.M.P. would also delineate the availability of total weather modification potential.

#### 4. Estimates of Water Augmentation

##### a. The Climax Area

It has been shown that significant increases in snowfall can be produced in the Climax area if meteorological conditions are favorable. It is of interest that these favorable conditions do not accompany a large percentage of the total snowfall at Climax. In Table 14 there are presented estimates of what seeding would accomplish in the Climax area for 1) a program where all events were seeded, and 2) a program where only favorable meteorological conditions were seeded. Percentage changes used in this computation are derived from mean daily precipitation observed for seeded and non-seeded days for the HAO site.

It is estimated that percentage increases in snowfall might attain 16 percent in the Climax area in a program of discriminatory seeding. This would represent 2.31 inches of additional water per winter season. These estimates of additional water to be added by cloud seeding were based on observed seeding results. In the next subsection, the weather modification potential model is employed, along with observed natural precipitation, to derive an estimate of what a discriminatory cloud seeding program at Wolf Creek Pass, Colorado would yield in terms of additional water.

Table 14. Estimated changes in precipitation at HAO for a seeded winter season with normal precipitation

---

ALL EVENTS ARE SEEDED

500 mb temperatures	Percentage Snowfall	Natural Snowfall (inches)	Percentage Change	Seeded Snowfall (inches)
-39.5C to -25.5C	33.5	4.75	-26	3.51
-25.5C to -20.5C	46.5	6.57	0	6.57
-20.5C to -10.5C	20.0	2.82	+82	5.13
	<u>100.0</u>	<u>14.14</u>		<u>15.21</u>

Total increase in snowfall is 1.07 inches or 7.5 percent

FAVORABLE EVENTS ARE SEEDED

-39.5C to -25.5C	33.5	4.75	0	4.75
-25.5C to -20.5C	46.5	6.57	0	6.57
-20.5C to -10.5C	20.0	2.82	+82	5.13
	<u>100.0</u>	<u>14.14</u>		<u>16.45</u>

Total increase in snowfall is 2.31 inches or 16 percent

---

b. The Wolf Creek Pass Area

The model precipitation equation was fitted to observed natural precipitation at Wolf Creek Pass. This precipitation was an average of that observed at Wolf Creek West and Summit recording gages. Figure 41 shows the results of fitting the model to this observed precipitation. It is immediately obvious that the strict diffusional model does not hold very well for the Wolf Creek cloud system at warmer cloud temperatures. However, there is no problem in determining the critical temperature where the diffusional ice growth process begins to lose efficiency. It is noted that the mean upward speed of this cloud system is greater than the Climax cloud and the time-averaged cloud top during

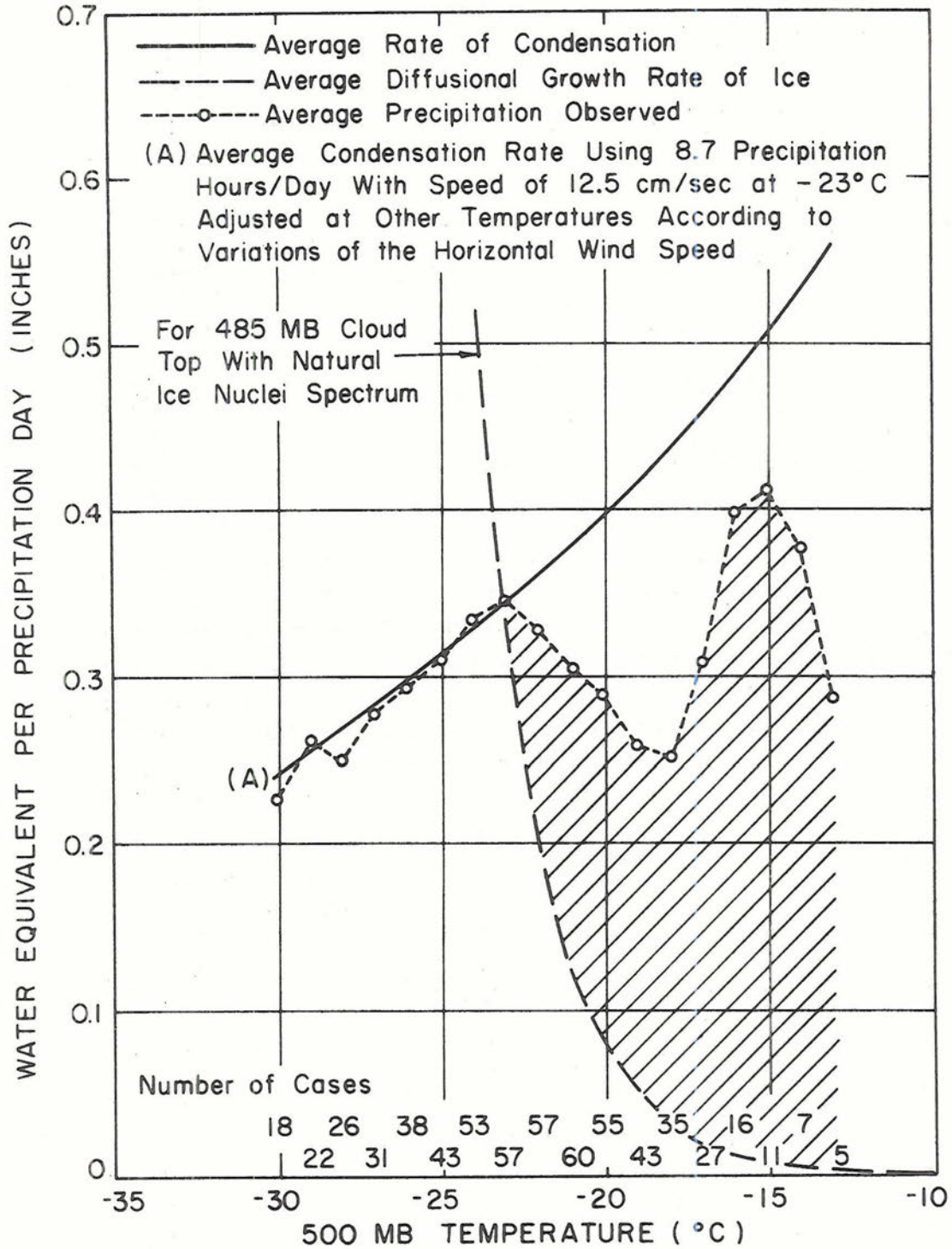


Figure 41. Distribution of non-seeded precipitation at Wolf Creek Pass as a function of 500 mb temperature compared to a theoretical distribution computed using the weather modification potential model. Precipitation data are from Wolf Creek (441) sample and values are a running mean over a four-degree temperature interval.

precipitation is about 25 mb lower. This appears consistent with the fact that the mountain barrier in the Wolf Creek Pass area is about 1400 ft lower than in the Climax area.

If the average diffusional growth rate of ice equation is used to estimate the additional water to be added by cloud seeding, the amount of the additional water would be overestimated. However, if the observed natural precipitation is employed instead, and compared to the available average rate of condensation, reasonable estimates of the additional water can be made. Table 15 shows these results.

Table 15. Estimated changes in precipitation at Wolf Creek Pass for a winter season with 24 inches of total precipitation and assuming discriminatory seeding

500 mb temperatures	Percentage Snowfall	Natural Snowfall (inches)	Percentage Change	Seeded Snowfall (inches)
-35.5C to -23.5C	36.4	8.74	0	8.74
-23.5C to -20.5C	28.8	6.91	+13	7.81
-20.5C to -16.5C	22.4	5.37	+52	8.15
-16.5C to -12.5C	8.4	2.02	+48	2.99
-12.5C to -10.5C	4.0	.96	+90	1.82
	<u>100.0</u>	<u>24.00</u>		<u>29.51</u>

Total increase in snowfall is 5.51 inches or 23 percent

The more substantial precipitation augmentation at Wolf Creek Pass stems from the lower and warmer cloud and the greater upward speed in the cloud system. These factors combine to produce a greater total precipitation during the winter season, and causes a greater percentage of the total precipitation to fall under favorable seeding conditions.

It is of interest that this estimate, of what a discriminatory seeding program would accomplish for the Wolf Creek Pass area, is based solely on observations taken during natural precipitation episodes. Application of the model allows one to estimate results prior to initiation of operational programs.

## CHAPTER VIII

### SUMMARY AND CONCLUSIONS

#### 1. Summary

##### a. Weather Modification Potential Model

A physical model of the cold orographic cloud system was formulated that stimulates precipitation during non-seeded and seeded conditions. Major assumptions in the model included 1) steady state conditions, 2) horizontal temperature advection is small, 3) the growth rate of ice in the cloud is specified by diffusional growth of ice crystals that activate from primary ice nuclei, 4) cloud base and top are constant in the horizontal and 5) the evaporative rate of ice crystals is small compared to the total vapor supply rate. Efficiency of the ice process in the model cloud is defined as the ratio of the rate of ice growth to the rate of vapor supplied in the cloud system. Full cloud efficiency is attained when this ratio reaches one. In the model precipitation efficiency approximates cloud efficiency if the rate of crystal evaporation is small compared to the vapor supply rate. The model is not physically valid therefore, for overseeded conditions. The model was parameterized in a time-averaged mode to make it compatible with experimental data available for testing, and parameters were evaluated for conditions representative of the Climax cloud system.

In the model the availability of static modification potential is mainly controlled by cloud top temperature. This quantity defines the concentration of growing crystals in the cloud system. The concentration of crystals in turn, largely controls cloud supersaturation which

ultimately determines whether there is a net growth of liquid droplets in the cloud system. If a net growth of liquid droplets is present in the cloud system, a static modification potential (S.M.P.) will exist, since this liquid water will be lost as precipitation, carried over the mountain and evaporated in the subsiding airstream in the mountain lee.

The availability of dynamic modification potential (D.M.P.) in the model is also mainly controlled by cloud top temperature. In fact, it coexists with S.M.P. This follows since in the absence of S.M.P., diffusional growth of crystals is efficient in converting the vapor supply to ice form. Latent heat of fusion is already being released in the cloud system and seeding will not increase this amount. However, if S.M.P. does exist, a certain fraction of the liquid water is not being converted to ice form, and seeding may then release the latent heat of fusion from this unconverted portion of liquid water. Cloud top temperature, by controlling ice crystal concentrations in the cloud, largely controls the availability of total weather modification potential.

In the model the cloud updraft speed exerts only a minor influence on the availability of weather modification potential. Doubling or tripling the updraft speed only displaces the availability of weather modification potential about 2 to 3 degrees C toward colder cloud systems. A nearly equivalent effect could be realized in the model by lowering cloud top only 20 to 25 mb. If weather modification potential is present from other considerations, doubling the updraft speed will at least double the magnitude of this potential, and may increase it a few times over. Thus, the updraft speed takes on considerable importance in defining the magnitude of weather modification potential present, once its availability is established.

Underlying model theory and physical observations indicated that accretional growth of crystals and probably ice crystal multiplication do not appreciably influence the availability of weather modification potential, only its magnitude. This follows since significant accretional growth depends upon the presence of cloud droplets with radii in excess of 7 or 8 microns. If diffusional growth of crystals is efficient in the cloud system, there is a small probability that a given droplet will attain the size necessary for its collection by a falling crystal. Thus, significant accretional growth does not appear in the cloud system until S.M.P. is present. Evidence also suggests that significant ice crystal multiplication occurs in conjunction with the accretional growth of at least a portion of the crystals in the cloud.

b. Testing the Model

It was found that the model precipitation equation could be fitted to observed natural precipitation reasonably well for the Climax cloud system. Model parameters associated with this fit had realistic values. Effects upon precipitation of accretional growth and ice crystal multiplication processes were subdued in the Climax cloud, so that the diffusional model performed satisfactorily. This was not the case for the Wolf Creek cloud system, where accretional growth and ice multiplication appear to assume more importance.

When testing the model precipitation equation for seeded conditions, observed precipitation continued to increase irregularly with the warmer cloud systems. This increase occurred over the temperature range, where ice nuclei observations indicated the natural precipitation process should become increasingly inefficient, but the seeded precipitation process would maintain efficiency. Within this temperature range, the

difference, between seeded and non-seeded precipitation, increased roughly exponentially, coincident with the exponential decline of diffusional ice growth in the natural cloud system.

Snowfall augmentation was enhanced when wind flow and topographic features combined to produce the most favorable orographic lifting. Positive seeding effects also increased with the wind speed over the mountain barrier up to a point. For wind speeds above this point, a high probability of overseeding was demonstrated, and the model is no longer physically valid. Snowfall augmentation also extended into somewhat colder cloud systems, when orographic uplifting and synoptic scale upward motions were frequently superimposed upon one another. The consistency of observed seeding effects among the three independent data samples, and with the model S.M.P. equation, was quite good.

In testing the model theory with observed crystal growth processes, evidence was found that seeding reduced the number of rimed crystals for all cloud temperatures. It was found in the natural and seeded cloud systems that accretional growth of crystals became significant as the diffusional growth rate of ice fell below the vapor supply rate. Evidence suggested that seeding displaced the onset of significant accretional growth in the cloud toward warmer cloud temperatures. This temperature displacement was approximately equal to the temperature interval that separates the natural and seeded diffusional ice growth rate equations. This behavior of crystal growth processes suggests that accretional growth of crystals is nature's way of attempting to maintain precipitation efficiency in cold orographic clouds, when the diffusional ice growth process no longer utilizes all of the vapor supplied to the cloud system.

### c. The Nature of the Seeding Effect

The investigation into the nature of the seeding effect revealed that seeding influences the duration of precipitation more than its intensity. The dominant effect of seeding warmer cloud systems was to bring about a precipitation release during many hours, when it would not have occurred naturally. A smaller beneficial effect was to increase precipitation rates during snowfall hours. Seeding also appeared to inhibit precipitation for cloud systems with very cold temperatures and high wind speeds.

## 2. Conclusions

### a. Cloud Microstability

The nature of the seeding effect suggests that a certain threshold of cloud microstability may exist in the cold orographic cloud. Unless the magnitude of the diffusional ice growth process, or nearly equivalently, the number of ice crystals exceeds a given value, a precipitation release will not be realized. The inefficiency of the cold orographic cloud lies mainly in not overcoming this threshold of cloud microstability. Conversely, the natural precipitation efficiency of cold orographic clouds is relatively high during hours of precipitation occurrence, and seeding has a relatively smaller beneficial effect during these hours.

### b. Experimental and Operational Program Designs

The Climax experimental results indicate that as operational or experimental sampling units become a smaller fraction of the average precipitation episode, and biased toward seeding during natural precipitation occurrence, the total weather modification potential available

will not be sampled nor realized. Seeding carried out only during natural precipitation occurrence will realize approximately the intensity change component of the total precipitation change available. In the case of the Climax area, an experiment conducted in this mode would probably have yielded percentage increases in snowfall conservative by a factor of four or five for the warmer cloud temperatures. Design of operational and experimental programs should place emphasis on "cloud seeding" and not precipitation seeding for best results.

c. Transfer of Climax Experimental Results to Other Barriers

The blind transfer of Climax experimental results to other orographic barriers would be unwise, if not meaningless. The natural precipitation observed as a function of cloud temperature at Wolf Creek Pass points out the folly of such an approach. The actual weather modification potential is quite sensitive to cloud top temperature and the microphysical processes that control accretional growth and ice crystal multiplication. These must be defined for individual barriers.

d. Water Augmentation

Important, artificially induced increments of water may be added to winter snowpacks over many of the mountain ranges in the western United States by intelligent and discriminatory operational cloud seeding programs. Further, it appears that reasonable estimates, of the additional artificial water available on orographic barriers, can be obtained prior to operational programs through well-designed field programs. The goal of such programs would be to measure over a sufficient period of time, quantities needed to solve the model equations and to define the magnitude of accretional growth and ice multiplication in the cloud systems. These estimates would provide valuable information

for decision making concerning the evolution of operational programs throughout the western United States and for designing these operational programs in the future.

e. Efficiency of Ground-based Seeding

The realization of 76 to 90 percent of the actual S.M.P. for the two Climax samples through seeding from ground generators indicates this delivery system was generally satisfactory in this instance. As pointed out previously however, these percentages apply only to those days in which a precipitation release was obtained. It is not known how much S.M.P. was not realized on days in which a precipitation release was not obtained. Some of these days were undoubtedly "clear sky" days.

The seeding rate of 20 gms AgI/hr appeared to be a good choice for the Climax cloud system and resulted in picking up most of the weather modification potential available on precipitation days. It is not known whether a higher seeding rate would have "triggered" more precipitation days during the very warmest experimental days, but this seems to be a possibility.

f. General Conclusions

The consistency between experimental results of the three independent data samples and the weather modification potential model comprise a verification of the basic tenets of cold orographic cloud seeding theory. The inconclusive results of broadcast seeding programs in the past are probably the net result of a wide spectrum of individual results. These range from precipitation suppression for the coldest cloud systems to significant increases and precipitation initiation for warmer cloud systems.

It is apparent that accretional growth and ice multiplication effects will have to be brought into the model for it to simulate satisfactorily the precipitation processes of some cold orographic clouds. This cannot be done using a mean term, as was possible for diffusional growth, since an analysis of this possibility indicated the deviation terms were considerably more important than the mean term in the case of accretional growth.

There is probably an optimum barrier height for cloud seeding results with present technology. For high orographic barriers, such as the Climax barrier (about 14,000 ft msl), cloud tops average around 20,000 ft msl and only about 20 percent of snowfall occurrence is under favorable conditions for seeding. At Wolf Creek Pass where the barrier is about 12,500 ft msl, about 60 percent of snowfall occurrence is under favorable seeding conditions. As lower mountain barriers are considered, the percent of snowfall occurrence under favorable conditions may perhaps, reach 80 to 90 percent. However, as even lower mountain barriers are considered, a point may be reached where cloud top temperatures are so warm that nucleating agents are ineffective a great deal of the time. Also, a point is reached where the mountain barrier no longer sustains a snow pack during the winter months. There is of course, a latitudinal temperature influence superimposed upon the mountain barrier effect discussed above.

### 3. Further Research

The reason for developing the physical model in a climatological mode was mainly so that it would be compatible with the huge amount of experimental field data that was available for comparison and

verification. In this mode it was also possible to establish statistical confidence in many of the results obtained. Work should continue toward deriving and improving more sophisticated numerical models which simulate the natural precipitation processes and their changes with seeding. These models may be either; sophisticated and probably time-dependent models for further research purposes, or models for controlling and evaluating operational programs, which will probably be no more complicated than is necessary to do an acceptable job.

Three main obstacles remain before really satisfactory models for use in cold orographic cloud seeding programs become a reality. These are 1) more realistic definition of the vertical motion field over the mountain barrier with synoptic scale influences included, 2) more realistic incorporation of the diffusion and transport processes by which seeding materials reach the cloud system, and 3) a more realistic incorporation of accretional growth and ice multiplication in the models. Undoubtedly, more basic research is required on some of these aspects before satisfactory solutions are obtained.

Research is especially needed on ice multiplication in cold orographic clouds. Evidence suggests it may be related to accretional growth within the cloud system but this is by no means established. It is of considerable interest that the natural precipitation process at Wolf Creek Pass is almost twice as efficient at the warmer cloud temperatures than was the Climax cloud system. Such differences in natural precipitation efficiencies are in need of investigation and explanation.

The extent of the downwind seeding effect during the Climax experiment is not well defined. Frequently, the major seeding effect was

located on Hoosier Pass at the eastern edge of the experimental area. Further work is now in progress to define the magnitude, and to locate geographically any downwind seeding effect.

The Climax experiment took on a new experimental design as of February 1, 1970. New features of this design include 1) elimination of the long distance generators at Reudi and Aspen, and 2) incorporation of a variable seeding output in discrete steps. The seeding output for the colder cloud systems has been reduced an order of magnitude and increased by a factor of four for the warmer cloud systems. The elimination of the long distance generators may shed light on the poor seeding effectiveness observed with westerly wind flows in prior years. The incorporation of variable seeding outputs is an attempt to seed more aptly according to the physical model.

## REFERENCES

- Bergeron, T., 1933: On the physics of clouds and precipitation. Proc. 5th Assembly U.G.G.I., Lisbon, 156-178.
- Bergeron, T., 1949: The problem of an artificial control of rainfall on the globe; I. General effects of ice-nuclei in clouds. Tellus, 1, 32-50.
- Braham, R.R., 1964: What is the role of ice in summer rain showers? J. Atmos. Sci., 21, 640-645.
- Braham, R.R., 1967: Cirrus cloud seeding as a trigger for storm development. J. Atmos. Sci., 24, 311-312.
- Braham, R.R., 1968: Meteorological bases for precipitation development. Bull. Amer. Meteor. Soc., 49, 343-353.
- Braham, R.R., and P. Spyers-Duran, 1967: Survival of cirrus crystals in clear air. J. Appl. Meteor., 6, 1053-1061.
- Brown, S., and G. Bertolin, 1969: Multiplication of ice crystals due to heavy riming. Unpublished Manuscript.
- Brown, S.R., 1970: The terminal velocities of ice crystals. Preprints of Conf. Cloud Physics, Fort Collins, 47-48.
- Brownscombe, J.L., and J. Hallet, 1967: Experimental and field studies of precipitation particles formed by the freezing of supercooled water. Quart. J. Roy. Meteor. Soc., 93, 455-473.
- Byers, H.R., 1965: Identification of ice nuclei in the atmosphere. Proc. Intern. Conf. on Cloud Physics, Tokyo, 126-130.
- Chappell, C.F., 1967: Cloud seeding opportunity recognition. Dept. of Atmos. Sci., Colorado State Univ., Atmos. Sci. Paper No. 118, 87 pp.
- Duran, B.S., and P.W. Mielke, Jr., 1968: Robustness of sum of squared ranks test. J. Amer. Statis. Assoc., 63, 338-344.
- Dye, J.E., and P.V. Hobbs, 1968: The influence of environmental parameters on the freezing and fragmentation of suspended water drops. J. Atmos. Sci., 25, 82-96.
- Elliott, R.F., 1966: Effects of seeding on the energy of systems. J. Appl. Meteor., Vol. 5, No. 5, 663-668.

- Fletcher, N.H., 1962: The Physics of Rain Clouds, Cambridge University Press, 122-127.
- Frössling, N., 1938: Über die Verdunstung fallender Tropfen. Gerl. Beitr. Geophys., 52, 170.
- Fukata, N., 1969: Experimental studies on the growth of small ice crystals. J. Atmos. Sci., 26, 522-531.
- Furman, R.W., 1967: Radar characteristics of wintertime storms in the Colorado Rockies. Dept. of Atmos. Sci., Colorado State Univ., Atmos. Sci. Paper No. 112, 53 pp.
- Grant, L.O., 1960: Colorado State University Climax study of the effect of cloud seeding on snowfall, General Information Booklet supplied to all participants (February).
- Grant, L.O., 1968: The role of ice nuclei in the formation of precipitation. Proc. Intern. Conf. Cloud Physics, Toronto, 26-30.
- Grant, L.O., and R.A. Schlessener, 1961: Snowfall and snowfall accumulation near Climax, Colorado. Proc. 29th Annual Meeting Western Snow Conf., Spokane, 53-64.
- Grant, L.O., and P.W. Mielke, Jr., 1967: A randomized cloud seeding experiment at Climax, Colorado, 1960-65. Proc. of the Fifth Berkeley Symposium on Math. Statis. and Prob., 5, 115-131.
- Grant, L.O., C.F. Chappell, and P.W. Mielke, Jr., 1968: The recognition of cloud seeding opportunity. Proc. First Nat. Conf. Weather Modification, Albany, 372-385.
- Grant, et al., 1969: An operational adaptation program of weather modification for the Colorado River Basin. Interim Report, Bureau of Reclamation Contract No. 14-06-D-6467, 98 pp.
- Hallet, J., 1965: Field and laboratory observations of ice crystal growth from the vapor. J. Atmos. Sci., 22, 64-69.
- Hobbs, P.V., 1969: Ice multiplication in clouds. J. Atmos. Sci., 26, 315-318.
- Hobbs, P.V., and A.J. Alkezweeny, 1968: The fragmentation of freezing water droplets in free fall. J. Atmos. Sci., 25, 881-888.
- Howell, W.E., 1949: The growth of cloud drops in uniformly cooled air. J. Meteor., 6, 134.
- Isono, K., 1955: On ice crystal nuclei and other substances found in snow crystals. J. Meteor., 12, 456-462.

- Jiusto, J.E., 1968: Snow crystal development in supercooled clouds. Proc. First Nat. Conf. Weather Modification, Albany, 287-295.
- Jiusto, J.E., and R.K. Schmidt, 1970: A model of supercooled cloud microphysics. Preprints Sec. Nat. Conf. Weather Modification, Santa Barbara, 41-44.
- Kline, D., 1963: Evidence of geographical differences in ice nuclei concentrations. Mon. Wea. Rev., 91, 681-686.
- Koenig, L.R., 1963: The glaciating behavior of small cumulonimbus clouds. J. Atmos. Sci., 20, 29-47.
- Koenig, L.R., 1968: Some observations suggesting ice multiplication in the atmosphere. J. Atmos. Sci., 25, 460-463.
- Koenig, L.R., 1968: Comments on atmospheric ice multiplication mechanisms. Proc. Intern. Conf. Cloud Physics, Toronto, 213-216.
- Kumai, M., 1951: Electron-microscope study of snow crystal nuclei., J. Meteor., 8, 151-156.
- Kuroiwa, D., 1955: Growth of snow crystals in supercooled cloud: On the role of minute water droplets. Low Temp. Sci. A, 14, 1-13.
- Leaf, C.F., 1962: Snow measurement in mountainous regions. Master's Thesis, Department of Civil Engineering, Colorado State University, Fort Collins, Colorado.
- Longham, E.J., and B.J. Mason, 1958: The heterogeneous and homogeneous nucleation of supercooled water. Proc. Roy. Soc., London A247, 483-504.
- Ludlam, F. H., 1955: Artificial snowfall from mountain clouds. Tellus, 7, 277-290.
- McDonald, J.E., 1963: Use of the electrostatic analogy in studies of ice crystal growth. Z. Angew. Math. Phys., 14, 610-619.
- Magono, C., and C.W. Lee, 1966: Meteorological classification of natural snow crystals. J. Fac. Sci., Hokkaido University, Series 7, Vol. 2, 321-335.
- Marshall, J.S., and M.P. Langleben, 1954: A theory of snow crystal habit and growth. J. Meteor., 11, 104-120.
- Mason, B.J., 1953: The growth of ice crystals in a supercooled water cloud. Quart. J.R. Meteor. Soc., 79, 104-112.

- Mason, B.J., 1956: The nucleation of supercooled water clouds. Sci. Progress, 175, 479-499.
- Mason, B.J., 1957: The Physics of Clouds. Oxford University Press, 481 pp.
- Mason, B.J., 1965: The nucleation and growth of ice crystals. Proc. Intern. Conf. Cloud Physics, Tokyo, 467-480.
- Mason, B.J., and J. Maybank, 1960: The fragmentation and electrification of freezing water drops. Quart. J. Roy. Meteor. Soc., 86, 176-186.
- Mason, B.J., G.W. Bryant, and A.P. Van den Heuvel, 1963: The growth habits and surface structure of ice crystals. Phil. Mag., 8, 505-526.
- Mauritz, J.D., and A.H. Auer, Jr., 1968: Ice crystal growth by diffusion and accretion. Proc. Intern. Conf. Cloud Physics, Toronto, 249-254.
- Mielke, Jr., P.W., 1967: Note on some squared rank tests with existing ties. Technometrics, Vol. 9, No. 2, 312-314.
- Mielke, Jr., P.W., L.O. Grant, and C.F. Chappell, 1970: Elevation and spatial variation in effects from wintertime orographic cloud seeding. J. Appl. Meteor., 9, 476-488.
- Mielke, Jr., P.W., L.O. Grant, and C.F. Chappell, 1970: Randomized orographic cloud seeding results for eight wintertime seasons at Climax, Colorado. Preprints Sec. Nat. Conf. Weather Modification, Santa Barbara, 66-69.
- Mossop, S.C., 1968: Comparison between concentrations of ice crystals in cloud and the concentration of ice nuclei. J. Rech. Atmos., 3, 119-124.
- Mossop, S.C., 1970: Concentrations of ice crystals in clouds. Bull. Amer. Met. Soc., Vol. 51, No. 6, 474-479.
- Mossop, S.C., A. Ono, and D.J. Hefferman, 1967: Studies of ice crystals in natural clouds. J. Rech. Atmos., 3, 45-64.
- Mossop, S.C., and A. Ono, 1969: Measurement of ice crystal concentration in clouds. J. Atmos. Sci., 26(1), 130-137.
- Reinking, R.F., 1970: Personal Communication.
- Renz, W.E., and J.B. Wong, 1952: Impaction of dust and smoke particles on surface and body collectors. Ind. Eng. Chem., 44, 1371.

- Rhea, J.O., and L.G. Davis, 1970: Statistical results of the Park Range winter orographic cloud seeding experiment. Preprints Sec. Nat. Conf. Weather Modification, Santa Barbara, 70-75.
- Roberts, P., and J. Hallet, 1968: A laboratory study of the ice nucleating properties of some mineral particles. Quart. J. Roy. Meteor. Soc., 94, 25-34.
- Schaefer, V.J., 1946: The production of ice crystals in a cloud of supercooled water droplets. Science, 104, 457.
- Schaefer, V.J., 1950: The occurrence of ice crystal nuclei in the free atmosphere. Project Cirrus Occas. Rept. No. 20, General Electric Laboratory, 27 pp.
- Schaefer, V.J., 1952: Formation of ice crystals in ordinary and nuclei free air. Ind. Eng. Chem., 44, 1300-1304.
- Scorer, R.S., 1949: Theory of waves in the lee of mountains. Quart. J. Roy. Meteor. Soc., 75, 41-56.
- Taha, M.A.H., 1964: Rank test for scale parameter for asymmetrical one-sided distributions. Publications de L' Institute de Statistiques de L' Université de Paris, 13, 169-180.
- Tazawa, S., and C. Mogono, 1966: Observation of snow clouds by S.C. sondes. Proc. Autumn Meeting, Meteor. Soc. Japan, 110-111.
- Todd, C.J., 1964: A system for computing ice-phase hydrometeor development. Atmospheric Research Group, Box 637, Altadena, California (ARG 64 Pa-121), 30 pp.
- Veal, D.L., A.H. Auer, Jr., and J.D. Maurwitz, 1969: Information Circular No. 59, Natural Resources Research Institute, University of Wyoming.
- Vonnegut, B., 1947: The nucleation of ice formation by silver iodide. J. Appl. Phys., 18, 593.
- Warner, J., and T. D. Newnham, 1958: Time lag in ice crystal nucleation in the atmosphere. Bull. Obs. Puy de Dome, 1, 1-10.
- Warnick, C.C., 1953: Experiments with windshields for precipitation gages. Transactions of the American Geophysical Union, 34, 379-398.
- Wegner, A., 1911: Thermodynamik der Atmosphere. Leipzig.
- Weickmann, H.K., J.E. Juisto, G. McVehil, R. Pilie, and J. Warburton, 1970: The Great Lakes project. Preprints Sec. Nat. Conf. Weather Modification, Santa Barbara, 34-40.

Weinstein, A.I., and D.M. Takeuchi, 1970: Observations of ice crystals in a cumulus cloud seeded by vertical fall pyrotechnics. J. Appl. Meteor., 9, 265-268.

Wilson, W.T., 1954: Analysis of winter precipitation observations in the cooperative snow investigations. Mon. Wea. Rev., 82, 183-199.

APPENDIXES

## APPENDIX A

### CONTRIBUTIONS OF MEAN AND DEVIATION TERMS

In order to estimate the importance of the deviation terms in (32), it is advantageous to consider correlations of the deviation quantities under various cloud system temperature distributions. Evaluation is accomplished for conditions representative of the Climax cloud system since the model will be compared with precipitation data observed in that area. The following assumptions and conditions are invoked as aids in estimating the magnitude of the various terms.

- (1) It is assumed that the orographic cloud system in the Climax area is generally embedded in the layer from 650 mb to 500 mb.
- (2) It is assumed that the stability of the cloud layer is neutral with respect to moist convection.
- (3) It is assumed that ice nuclei activate in the cloud system according to an activation spectrum observed at the High Altitude Observatory (HAO) during non-seeded experimental days of the Climax experiment (see Figure 6).
- (4) The averaging process is performed only in the vertical since  $F_1$ ,  $r$ ,  $F_T$  and  $N_c$  have variations mainly in the vertical. This is consistent with the assumption that horizontal temperature gradients may be neglected.

The method used to estimate the magnitudes of the terms in (32) was to divide the cloud segment into three vertical sections. Mean and deviation quantities were then estimated for the cloud segment and the

terms evaluated. Deviation terms were solved by summing the correlations over the three vertical sections.

The deviations of  $r$  and  $F_1$  will be negative in the upper portion and positive in the lower portion of the cloud segment since crystal radii increase downward from the top of the cloud system toward cloud base. However, the thermodynamic function,  $F_T$ , has a maximum value at around  $-16C$ , so the vertical distribution of its deviations will depend upon the location of the  $-16C$  level within the cloud system. The specific function utilized in this evaluation assumes a mean pressure of 600 mb. Initially, a one to one correspondence between ice nuclei and ice crystal concentrations is assumed. The vertical distribution of ice crystals in the cloud can therefore be estimated from the exponential temperature relationship for the activation of primary ice nuclei. This is accomplished by determining the vertical distribution of ice nuclei activating in the cloud, allowing them to fall downward through the cloud segment, and adding to them the additional ice nuclei that activate at the next lower level, etc. In this way one can sum over the vertical distribution of ice crystals to derive the mean concentration in the cloud and take departures from this mean to establish the deviation quantities.

#### 1. Colder Cloud Systems

Initially, a cloud system representative of the colder clouds observed at Climax is considered with cloud base and cloud top temperatures of  $-14C$  and  $-30C$ , respectively. The mean and deviation quantities for this cloud system are estimated to be:

$$\bar{N}_c = 109 \text{ crystals per liter}$$

$$\bar{r} = .0065 \text{ cm}$$

$$\bar{F}_T = 4.15(10^{-8}) \text{ gm/cm sec crystal}$$

$$\bar{F}_1 = 1.2$$

$$N_c' = -17 \text{ top, } +6 \text{ middle, and } +11 \text{ bottom}$$

$$r' = -.004 \text{ top, } 0 \text{ middle, and } +.004 \text{ bottom}$$

$$F_T' = -0.7(10^{-8}) \text{ top, } 0 \text{ middle, and } +0.7(10^{-8}) \text{ bottom}$$

$$F_1' = -0.2 \text{ top, } 0 \text{ middle, and } +0.2 \text{ bottom}$$

The appropriate terms in (32) are then evaluated to be:

$$8\bar{N}_c \bar{r} \bar{F}_T \bar{F}_1 = 28.2(10^{-8}) \text{ gm/sec liter}$$

$$8\bar{N}_c \bar{r} \bar{F}_T' \bar{F}_1' = 0.5(10^{-8}) \text{ gm/sec liter}$$

$$8\bar{r} \bar{F}_T \bar{F}_1' N_c' = 0.4(10^{-8}) \text{ gm/sec liter}$$

$$8\bar{F}_T \bar{F}_1 N_c' r' = 1.5(10^{-8}) \text{ gm/sec liter}$$

$$8\bar{F}_1 N_c r' F_T' = 2.0(10^{-8}) \text{ gm/sec liter}$$

$$8\bar{N}_c \bar{F}_T r' F_1' = 2.1(10^{-8}) \text{ gm/sec liter}$$

$$8\bar{r} \bar{F}_1 N_c' F_T' = 0.4(10^{-8}) \text{ gm/sec liter}$$

Total contribution of the deviation terms is equal to  $6.9(10^{-8})$  gm/sec liter.

This particular cloud temperature distribution gives rise to all positive values for the double correlation terms in (32). The triple and quadruple correlation terms may be neglected since they are extremely small.

It is seen that the combined effect of the deviation terms is about 24 percent of the mean term, and the average diffusional growth rate of ice in the cloud segment, when computed using the mean term only, is underestimated by about 20 percent.

## 2. Normal Cloud Systems

Next, a cloud system is considered with cloud base and cloud top temperatures about  $-8^{\circ}\text{C}$  and  $-24^{\circ}\text{C}$ , respectively. Under these conditions  $F_T$  reaches a maximum half way up in the cloud and therefore, will have negative deviations in the bottom and top thirds of the cloud segment. The mean and deviation quantities for this cloud system are estimated to be:

$$\overline{N_c} = 8 \text{ crystals per liter}$$

$$\overline{r} = .01 \text{ cm}$$

$$\overline{F_T} = 4.6(10^{-8}) \text{ gm/cm sec crystal}$$

$$\overline{F_1} = 1.2$$

$$N_c' = -1.5 \text{ top, } +0.5 \text{ middle, } +1.0 \text{ bottom}$$

$$r' = -.006 \text{ top, } 0 \text{ middle, } +.006 \text{ bottom}$$

$$F_T' = -.2(10^{-8}) \text{ top, } +.4(10^{-8}) \text{ middle, } -.2(10^{-8}) \text{ bottom}$$

$$F_1' = -.2 \text{ top, } 0 \text{ middle, } +.2 \text{ bottom}$$

The appropriate terms in (32) are then evaluated to be:

$$8\overline{N_c r F_T F_1} = 3.54(10^{-8}) \text{ gm/sec liter}$$

$$8\overline{N_c r F_T' F_1'} = 0 \text{ gm/sec liter}$$

$$8\overline{r F_T F_1' N_c'} = .06(10^{-8}) \text{ gm/sec liter}$$

$$8\overline{F_T F_1' N_c' r'} = .22(10^{-8}) \text{ gm/sec liter}$$

$$8\overline{F_1' N_c' r' F_T'} = 0 \text{ gm/sec liter}$$

$$8\overline{N_c F_T r' F_1'} = .24(10^{-8}) \text{ gm/sec liter}$$

$$8\overline{r F_1' N_c' F_T'} = .01(10^{-8}) \text{ gm/sec liter}$$

Total contribution of the deviation terms is equal to  $.53(10^{-8})$  gm/sec liter.

The triple and quadruple correlation terms are extremely small and are neglected. Two of the double correlation terms involving  $F_T'$  may

also be neglected since they give rise to positive correlations in the upper portion and negative correlations in the lower portion of the cloud system which cancel in the summation. It is seen that the combined effect of the deviation terms is about 15 percent of the mean term. The average diffusional growth rate of ice in the cloud segment would therefore be underestimated by about 13 percent if computed using the mean term only.

### 3. Warmer Cloud Systems Without Ice Crystal Multiplication

Finally, a relatively warm cloud system is considered with cloud base and cloud top temperatures around  $-2^{\circ}\text{C}$  and  $-16^{\circ}\text{C}$ , respectively. Under these conditions  $F_T$  attains a maximum at the top of the cloud system. The mean and deviation quantities for this cloud system are estimated to be:

$$\bar{N}_c = 0.28 \text{ crystals per liter}$$

$$\bar{r} = .015 \text{ cm}$$

$$\bar{F}_T = 3.60(10^{-8}) \text{ gm/cm sec crystal}$$

$$\bar{F}_1 = 1.3$$

$$N_c' = -.005 \text{ top, } +.002 \text{ middle, } +.003 \text{ bottom}$$

$$r' = -.01 \text{ top, } 0 \text{ middle, } +.01 \text{ bottom}$$

$$F_T' = +1.0(10^{-8}) \text{ top, } 0 \text{ middle, } -1.0(10^{-8}) \text{ bottom}$$

$$F_1' = -0.3 \text{ top, } 0 \text{ middle, } +0.3 \text{ bottom}$$

The appropriate terms in (32) are then evaluated to be:

$$8\bar{N}_c\bar{r}\bar{F}_T\bar{F}_1 = .157(10^{-8}) \text{ gm/sec liter}$$

$$8\bar{N}_c\bar{r}\bar{F}_T'F_1' = -.008(10^{-8}) \text{ gm/sec liter}$$

$$8r\bar{F}_T\bar{F}_1'N_c' = .0004(10^{-8}) \text{ gm/sec liter}$$

$$8F_T'F_1'N_c'r' = .001(10^{-8}) \text{ gm/sec liter}$$

$$\overline{8F_1 N_c r' F_T'} = -.020(10^{-8}) \text{ gm/sec liter}$$

$$\overline{8N_c F_T r' F_1'} = .014(10^{-8}) \text{ gm/sec liter}$$

$$\overline{8rF_1 N_c' F_T'} = -.0005(10^{-8}) \text{ gm/sec liter}$$

Total contribution of the deviation terms is equal to  $-.013(10^{-8})$  gm/sec liter. The triple and quadruple correlation terms are again neglected. The double correlation terms in this case tend to cancel one another but the final contribution of the deviation terms is about 8.3 percent of the mean term. The average diffusional growth rate of ice in the cloud segment in this case would be overestimated by about 7.6 percent when computed using the mean term only.

#### 4. Warmer Cloud Systems with Ice Crystal Multiplication

One more special case of warmer clouds should be considered. The observations of Grant (1968) indicate that ice crystal concentrations occasionally are about an order of magnitude larger than ice nuclei concentrations when 500 mb temperatures are around  $-15\text{C}$  in the Climax area. It is assumed again that cloud base and cloud top temperatures are around  $-2\text{C}$  and  $-16\text{C}$ , respectively, and that a tenfold increase in ice crystal concentration is present in the lower two-thirds of the cloud system. The mean and deviation quantities for this cloud system are then estimated to be:

$$\overline{N_c} = 2.1 \text{ crystals per liter}$$

$$\overline{r} = .015 \text{ cm}$$

$$\overline{F_T} = 3.60(10^{-8}) \text{ gm/cm sec crystal}$$

$$\overline{F_1} = 1.3$$

$$N_c' = -1.7 \text{ top, } +0.8 \text{ middle, } +0.9 \text{ bottom}$$

$$r' = -.01 \text{ top, } 0 \text{ middle, } +.01 \text{ bottom}$$

$$F_T' = +1.0 \text{ top, } 0 \text{ middle, } -1.0 \text{ bottom}$$

$$F_1' = -0.3 \text{ top, } 0 \text{ middle, } +0.3 \text{ bottom}$$

The appropriate terms in (32) are then evaluated and found to be:

$$8\overline{N_c r F_T F_1} = 1.17(10^{-8}) \text{ gm/sec liter}$$

$$8\overline{N_c r F_T' F_1'} = -.06(10^{-8}) \text{ gm/sec liter}$$

$$8\overline{r F_T F_1' N_c'} = +.11(10^{-8}) \text{ gm/sec liter}$$

$$8\overline{F_T F_1' N_c' r'} = +.26(10^{-8}) \text{ gm/sec liter}$$

$$8\overline{F_1' N_c' r' F_T'} = -.15(10^{-8}) \text{ gm/sec liter}$$

$$8\overline{N_c' F_T' r' F_1'} = +.12(10^{-8}) \text{ gm/sec liter}$$

$$8\overline{r F_1' N_c' F_1'} = -.11(10^{-8}) \text{ gm/sec liter}$$

Total contribution of the deviation terms is equal to  $+.17(10^{-8})$  gm/sec liter.

It is seen that the magnitudes of most deviation terms are 10 percent or more of the mean term. However, the various terms tend to compensate so that computation of the average diffusional growth rate with the mean term alone underestimates the growth rate by only 13 percent.

It appears that errors involved in computing the average diffusional growth rate of ice using only the mean term in (32), are not greater than the inherent uncertainty present in using the theoretical growth equation itself. A fortunate circumstance is that the computation is most accurate in the 500 mb temperature range from -24C to -16C. This is the transition range where meteorological conditions generally change from unfavorable to those that are favorable for augmenting snowfall by cloud seeding. Thus, the computation is most accurate in this

important transition range and to a first approximation (32) can be written

$$\overline{N_c \frac{dm}{dt}} = 8 \overline{N_c r F_T F_1}.$$

## APPENDIX B

### FITTING THE MODEL PRECIPITATION EQUATION TO OBSERVED PRECIPITATION

This appendix describes the procedure employed in fitting the weather modification potential model to observed precipitation. The development is presented in step by step fashion for the Climax I sample in order that the reader may follow the methodology and assumptions invoked during the analysis.

#### 1. Methodology of Analysis

- (a) The non-seeded precipitation data observed at HAO was used to generate precipitation as a function of 500 mb temperature with values computed using a running mean over a two degree temperature interval.
- (b) The non-seeded precipitation was inspected to determine the 500 mb temperature where precipitation efficiency began to decrease steadily and appreciably. This is clearly at -20C for the Climax I sample (Figure 11).
- (c) The average number of hours of precipitation per non-seeded precipitation day was then generated as a function of 500 mb temperature. This function is shown in Figure B1.
- (d) The precipitation values computed under (a), for 500 mb temperatures of -20C and colder, were then normalized to 10.1 hours. This was found to be the overall average hours of precipitation per precipitation day for non-seeded events with 500 mb temperatures -20C and colder.

- (e) The precipitation values determined under letter (d) plus the precipitation values computed under letter (a) (for 500 mb temperatures warmer than  $-20^{\circ}\text{C}$ ), were plotted as a function of 500 mb temperature. These are shown in Figure 11.
- (f) The average rate of crystal growth  $(dm/dt)_d = 8r\bar{F}_T\bar{F}_1$  was then computed for the Climax cloud system for a 500 mb temperature of  $-20^{\circ}\text{C}$ . Cloud base was taken to be 650 mb and cloud top is estimated at this point.
- (g) Using the 10.1 average hours of precipitation per precipitation day as a conversion factor, the average number of ice crystals per liter is solved for by equating the unseeded precipitation rate at  $-20^{\circ}\text{C}$  to the average rate of ice growth by diffusion. This gives  $\bar{N}_c$ .
- (h)  $\bar{N}_c$  is now used to determine the average cloud top temperature by (45), assuming  $(\bar{R}_c)_{ns}$  is one.
- (i) Since  $\bar{F}_T$  was initially computed using an estimated cloud top temperature, computations under letters (f) and (h) above must be iterated to obtain final values of the average rate of crystal growth and cloud top temperature. This final value of cloud top was found to be 460 mb, valid for a 500 mb temperature of  $-20^{\circ}\text{C}$ .
- (j) Assuming average cloud tops are nearly the same for warmer 500 mb temperatures, the average rate of ice growth in the cloud system can be computed as a function of the 500 mb temperature. This was accomplished by assuming a moist adiabatic lapse rate between 500 mb and the top of the cloud, and then solving for  $\bar{F}_T$  as a function of cloud system temperatures and  $\bar{N}_c$  as a

function of cloud top temperature. The computed average rate of ice growth as a function of 500 mb temperature is shown in Figure 11.

- (k) Assuming the Climax cloud system is embedded in the 650-460 mb layer on the average,  $\bar{\rho} \frac{\partial r_s}{\partial p}$  was computed as a function of the 500 mb temperature.
- (l) At a 500 mb temperature of -20C, the average rate of condensation was assumed equal to the observed non-seeded precipitation (equation 40). Using the 10.1 hours as a conversion factor again, the mean upward speed that explains this observed precipitation is computed to be 11 cm/sec.
- (m) With the mean upward speed determined at a 500 mb temperature of -20C, it was evaluated at other 500 mb temperatures by adjusting the mean upward speed by the ratio of the horizontal wind speed at the new temperature to that at -20C. This was done using values from the regression line of Figure 20. This was a crude attempt to take into account variations of the horizontal wind speed with cloud temperature and its effect upon mass flow rates over the barrier.
- (n) The average rate of condensation was then computed as a function of the 500 mb temperature using the values of mean upward speed computed in letter (m).

The above 14 steps represent a procedure for computing the average available rate of condensation and the average rate of ice growth by diffusion as a function of the 500 mb temperature. In essence, the model equation that describes the natural precipitation has been fitted to observed precipitation at HAO and in so doing, estimates of the cloud

top and mean upward speed in that portion of the Climax cloud system producing precipitation at HAO have been determined.

It is possible theoretically, to solve the model equation for seeded precipitation following again the 14 steps outlined previously. Practically, however, this is not the case. The problem arises that the 500 mb temperature, at which the diffusional ice growth process would be expected to lose efficiency occurs at the extreme end of the temperature distribution and cannot be identified. A somewhat less satisfactory procedure is therefore employed.

It is assumed that average cloud tops are again at 460 mb for seeded conditions. The mean upward speed, associated with non-seeded precipitation at a 500 mb temperature of  $-20^{\circ}\text{C}$ , is adjusted for differences in the duration conversion factor and horizontal wind speeds and becomes the mean upward speed for seeded conditions. After the mean upward speed for seeded precipitation is established for a 500 mb temperature of  $-20^{\circ}\text{C}$ , the average rate of condensation as a function of the 500 mb temperature is computed as before.

The assumption that seeded cloud tops are also at 460 mb is invoked from the randomization of events. This could be a serious restriction if seeding is responsible for bringing about changes in cloud tops (a dynamic effect). However, if there is a substantial dynamic effect, it might still be indicated in the analysis by the appearance of seeded precipitation values greater than the available rate of condensation, since this is computed assuming no dynamic seeding effect.

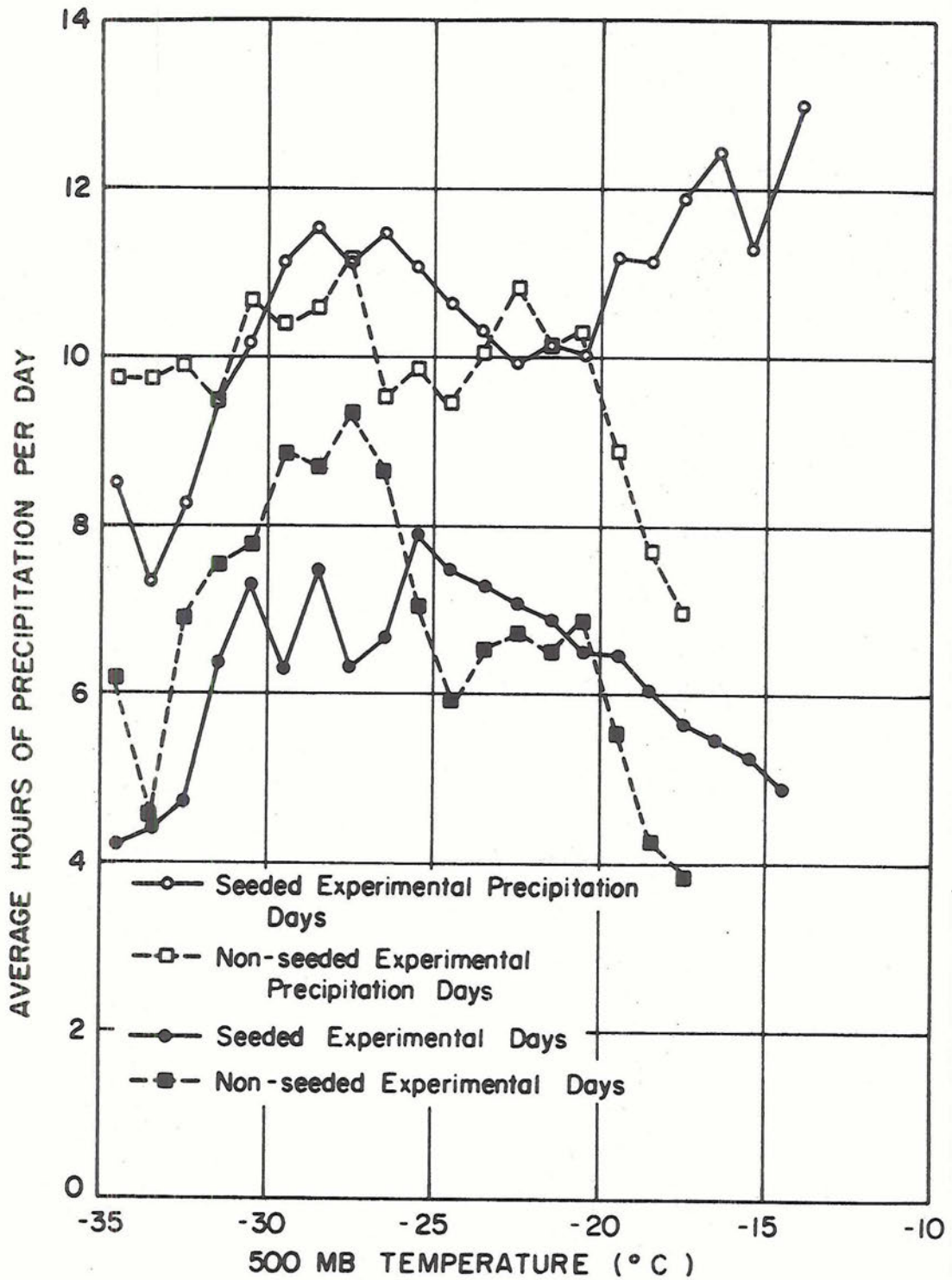


Figure B1. Average number of hours of precipitation per day recorded at Climax 2NW gage during Climax I (251) experimental days and experimental precipitation days as a function of 500 mb temperature. Values were computed using a running average over a three-degree temperature interval.

## APPENDIX C

### CLIMAX AND WOLF CREEK EXPERIMENTS

#### 1. The Climax Experiment

A study of the precipitation processes which accompany central Colorado mountain snowfall was begun in 1959 by Colorado State University. An important part of this investigation included a study of the possibilities of beneficially modifying important phases of the natural precipitation process. In this section, pertinent information on the Climax experiment is summarized in order to aid in interpretation of experimental results.

##### a. Design of Experiment

The basic features incorporated in the Climax experiment are summarized as follows:

- (1) Randomization is employed in obtaining the seeded and non-seeded samples. The randomization is restricted to the extent that large blocks (20 to 40) have the same number of seeded and non-seeded cases.
- (2) The experimental time unit is 24 hours. This compromise minimizes variation in the physical parameters during an event. It is still long enough to lower the "noise" level to reasonable values when establishing correlations with upwind precipitation controls, and minimizes uncertainties of seeding in the area near the start and end of the experimental period.

- (3) Eight standard Weather Bureau stations located southwest, west northwest and north of the experimental site are available for use as control stations. These were used as controls since the terrain upwind of the target is unsuitable for establishment of special control stations. The eight stations used as control, along with their azimuth and distance in miles from Climax, are Winter Park (032/42), Shoshone (283/54), Fraser (029/46), Grand Lake 6SSW (017/58), Crested Butte (230/52), Aspen (257/34), Marvine (302/83) and Eagle (303/37). The eight stations explain a little over 58 percent of the total precipitation variance at the Weather Bureau gage at Climax.
- (4) The criteria of an experimental day is that at least .01 inches of precipitation be forecasted during a 24-hour sampling unit at Leadville, Colorado, accompanied by a 500 mb wind direction between 210 degrees and 360 degrees inclusive. This forecast is prepared by the United States Weather Bureau in Denver. The forecasters have no access to the seeding decision.

b. Operation Procedures

- (1) While the 24-hour time unit has been conserved, two changes have been made in the start of the experimental period since the experiment began. During the spring of 1960 the experimental day began at 1600 MST. This occasionally exposed nighttime snowfall to daytime melting and evaporation off observation snowboards. Beginning with

the 1960-61 winter season the experimental period was altered to begin at 0800 MST. This time corresponds to the low point of a pronounced diurnal variation in precipitation occurrence. The experimental interval was changed slightly for the 1961-62 season, and subsequently has begun at 0900.

- (2) Generators at Minturn, Redcliff, south of Tennessee Pass, and west of Leadville are turned on 30 minutes prior to the start of the experimental day. They are run continuously until operations are terminated 30 minutes prior to the end of the period. The procedure is identical for generators at Aspen and Reudi except a one-hour lead time is employed. Specific units used are changed during the interval as specified by the Weather Bureau wind forecast.
- (3) A Colorado State University modified Skyfire, needle-type ground generator is used for seeding. These generators have been extensively calibrated in the Colorado State University cloud chamber to establish the temperature activation characteristics of the particles produced. A seeding rate of about 20 grams of silver iodide per hour is used. Figure C1 shows the output of effective ice nuclei from these generators. The output is compared with Fletcher's (1962) theoretical curve and other efficient silver iodide generators. The modified Skyfire generator produces about  $10^{14}$  particles per gm AgI effective at  $-12^{\circ}\text{C}$  and  $4(10^{15})$  particles per gm AgI effective at  $-20^{\circ}\text{C}$ .

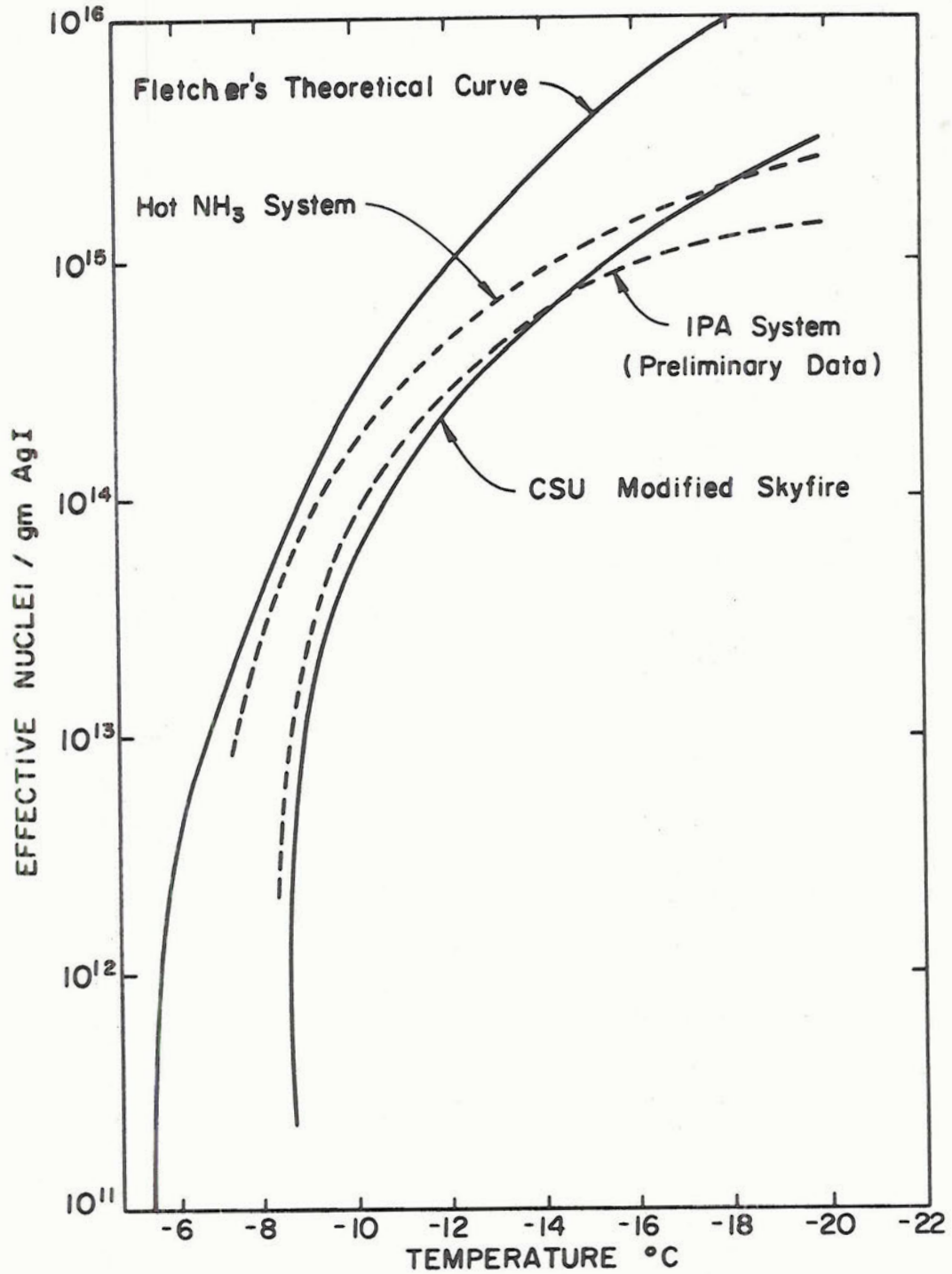


Figure C1. Seeding output as a function of temperature for generator used in the Climax experiment (Effective particles/gm AgI).



- (4) Precipitation data from 65 snowfall observation sites are read daily and available for analyses. Their locations are shown in Figure C3. It can be noted that 26 sites are located over Fremont Pass from Leadville to Frisco at about 1 mile intervals. There are 18 sites located along the highway over Hoosier Pass from Alma to Breckenridge, and 20 sites are located along the highway over Vail Pass from Wheeler Junction to Minturn. Most of these observations are taken with snowboards which compare favorably with snowfall observations from shielded 8-inch precipitation gages (Warnick, 1953; Wilson, 1954; Grant and Schleusener, 1961; Leaf, 1962). Due to drifting and blowing snow, buried snowboards, inaccessible highways, etc., it was not possible to read all 65 sites on each experimental day. It is not believed that the missing days are biased between seeded and non-seeded days except as adverse observational conditions may have resulted from the seeding operations themselves. During later years of the experiment non-recording precipitation gages were included at most snowboard sites which cut down on the amount of missing data. Also, three recording gages were added on Hoosier Pass and three more on Fremont Pass to improve the observing network.
- (5) Many physical observations were taken which are related to this study. Ice nuclei observations were made on most days. Intermittent observations were made of snow crystals reaching the ground on seeded and non-seeded days,



Other physical observations included ice crystal replications, cloud photography, radar photography and rawinsonde data during the last few years.

c. Topography of Experimental Area

The experimental area is located along the continental divide of central Colorado. Figure C2 shows the important topographical features of the region. The primary target (summit of Fremont Pass) lies along an expanse of the Continental Divide, which is oriented east-west for about 18 miles across the region.

Three passes, Tennessee (10,424 ft msl), Fremont (11,318 ft msl) and Hoosier (11,542 ft msl) traverse this east-west section of the divide separated by distances of about 8 miles. These passes are kept open all winter despite snow accumulations of several feet by early spring. Thus, the area is accessible throughout the winter and daily observations can usually be taken. Elevations in the experimental area vary mainly from 8,000 feet to 12,000 feet with a few peaks reaching over 14,000 feet. Timberline is at approximately 11,500 feet and the area is covered extensively by coniferous forests.

The Sawatch Mountain Range, lying 15 to 20 miles southwest through west northwest of Climax, is a formidable barrier. This range generally exceeds 12,000 feet with several peaks over 13,500, and includes the combination of Mt. Elbert and Mt. Massive which rise over 14,400 feet just 20 miles southwest of the target.

The Gore Range rises abruptly just east of Climax and reaches elevations over 14,000 feet within 3 miles of the primary target.

Large scale uplifting occurs over the experimental area as upper wind currents are forced over the high mountain ranges of the region.

## d. Relationship of Generator Sites to Primary Target

Six generators were employed in the design. The locations of these generators with respect to the primary target are shown in Figure C3. The azimuth and distance of each generator from the primary target is shown in Table Cl.

Table Cl. Location of Climax seeding generators with respect to the primary target

Location	Azimuth and Distance from Target (degrees/nautical miles)
Minturn, Colorado	320/16
Redcliff, Colorado	316/11
South of Tennessee Pass	250/07
West of Leadville, Colorado	218/11
Aspen, Colorado	249/31
Reudi, Colorado	267/29

The generator designated as Reudi was moved slightly during the experiment. At the beginning of the experiment it was located at Reudi. It remained there until March, 1966, when it was relocated at Meredith (about 3 miles east of the original site) due to the filling of a new reservoir. However, on April 25, 1967, this generator was moved back to another location in Reudi.

The generator designated as Aspen was also moved slightly during the experiment. Until February 27, 1967, the actual location of this generator was about 4 miles north northwest of Aspen. It was then relocated at Aspen.

The generator designated west of Leadville was also moved slightly during the experiment. It was initially located at the Fish Hatchery west of Leadville and remained there until the beginning of the 1964-65 winter season. At this time it was moved to Cavelli Ranch about 3/4 of a mile northeast of the Fish Hatchery due to operator availability. On December 19, 1968, it was moved back to the Fish Hatchery.

The generator sites at Aspen and Reudi lie west southwest and west of the target about 30 nautical miles. Particles released by these units are forced to ascend the western slope of the Sawatch Range, 15 to 20 miles west of the target.

Four generator sites are within 7 to 16 nautical miles of the target. These are located in the high valley which separates the Sawatch and Gore Ranges. They extend from southwest through north northwest of the target.

The Chicago Ridge separates the generator south of Tennessee Pass from the primary target. This short range reaches 12,000 feet only 3 to 5 miles west of the target.

The particles emanating from the generator west of Leadville are subject to gradual orographic lifting as they approach the target. The upwind fetch from this generator is limited by the Mt. Elbert-Mt. Massive combination.

The nuclei generated at Minturn and Redcliff are embedded in an orographic stream having a long, continuous fetch toward the target. This northwesterly flow appears to be most similar to an idealized orographic current.

Table C2. Climatological data for Climax, Colorado, for the period  
November through April

---

Based on records from November 1953 to April 1960  
(Grant and Schleusener, 1961)

Mean temperature	18.6F
Mean precipitation	14.14 inches
Average number of days with precipitation	85
Median number of days with precipitation	88

---

Based on records from November 1956 to April 1964  
Seeded precipitation data included after March 1960

Daily Precipitation (inches)	Cumulative Frequency (percentage)
.06	35
.11	50
.15	60
.21	70
.26	80
.30	85
.36	90
.43	95
.57	98
.63	99
.72	99.5
.95	100.0

---

Based on records from November 1956 to April 1964  
Seeded precipitation data included After March 1960

Daily Precipitation Range (inches)	Relative Frequency (percentage)
.04 to .40	80
.03 to .50	90
.02 to .65	99
.01 to .95	100

---

e. Climatology of the Experimental Area

During the winter months (November through April) the target area is effected by traveling cyclones which occasionally penetrate this long-wave ridge position. These occur more frequently during the late winter and early spring months. An important role of these storms is to bring moisture inland to the mountain barriers. Through the winter period cloud temperatures are within the range where ice nuclei can be expected to play an important part in the formation of precipitation. Table C2 describes the important characteristics of the snow season at Climax, Colorado. The large number of days having measurable precipitation (almost one-half of the total possible) provided a great opportunity to assemble experimental events rapidly. The many days of light amounts result from the orographic origin of most precipitation. Table C2 shows that one-half of all measurable precipitation days yield amounts of .11 inches or less, while 90 percent of such days result in .36 inches or less.

Table C2 also indicates that the range of daily precipitation amounts for 80 percent of all cases remains within one order of magnitude. This is a highly desirable feature for statistical analysis. It is also noted that the total range of measurable snowfall has remained within two orders of magnitude during the eight year period of record.

A pronounced diurnal variation in precipitation is in evidence at Climax. Figure C4 shows that the probability of snowfall occurrence between 0200 MST and 0500 MST is about twice that between 0800 MST and 1400 MST. The minimum in snowfall frequency occurs between 1100 MST and 1300 MST with a gradual, slightly irregular increase in frequency during the afternoon and evening. After midnight the frequency rises sharply

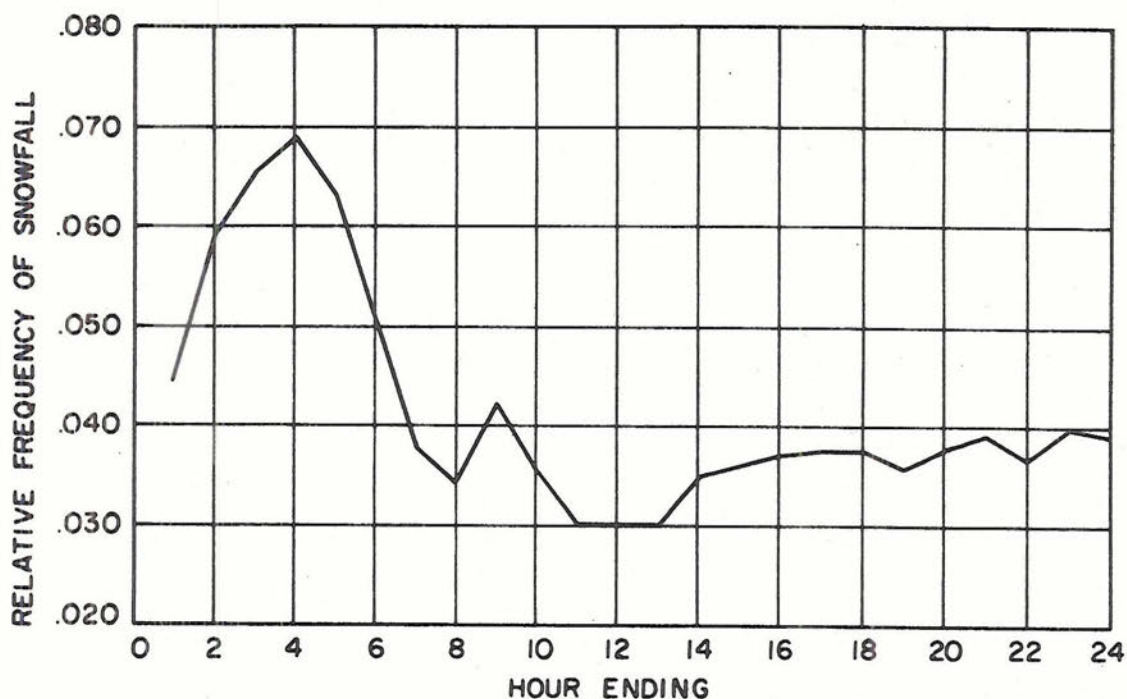


Figure C4. Diurnal distribution of precipitation observed at Climax 2NW recording gage. Data are from the period November through April for the years 1953 through 1968.

to a peak at 0400 MST. The 24-hour sampling unit chosen for the Climax experiment encompasses this important diurnal variation.

The snowpack which accumulates in the mountains around Climax during the winter season is due mainly to many hours of snowfall at small intensities. This can be noted from Figure C5 which shows over 90 percent of the hourly occurrences of precipitation are at intensities of .04 inches or less and the average over all hours is only slightly greater than .02 inches.

Figures C6 and C7 show the distribution of snowfall at the High Altitude Observatory (HAO) with respect to 500 mb temperature and 700 mb equivalent potential temperatures respectively. It is seen that 83 percent of the snow at HAO occurs at 500 mb temperatures colder than  $-20^{\circ}\text{C}$  and 70 percent of the snow occurs between  $-29^{\circ}\text{C}$  and  $-20^{\circ}\text{C}$ . Also,

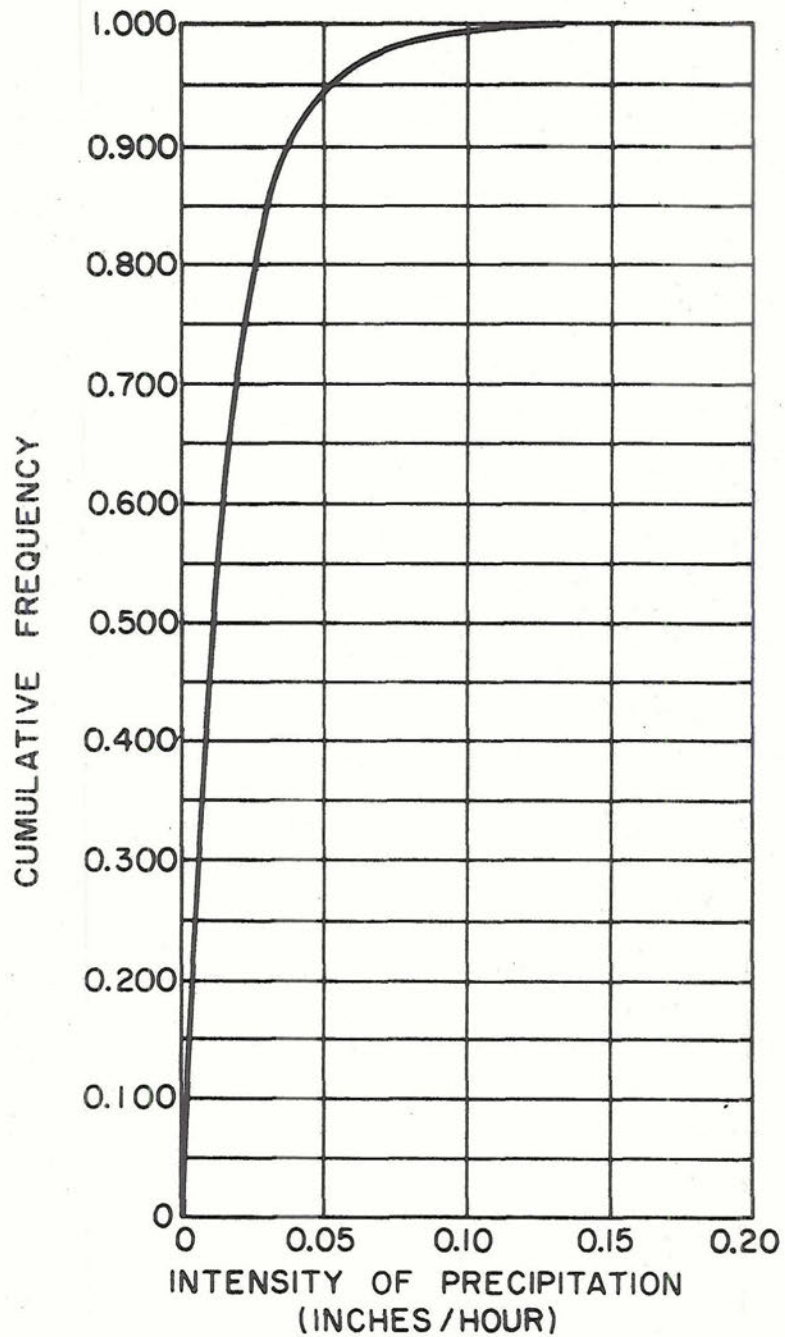


Figure C5. Cumulative frequency of snowfall at Climax 2NW recording gage as a function of hourly precipitation intensity. Data are from the period November through April for the years 1953 through 1968.

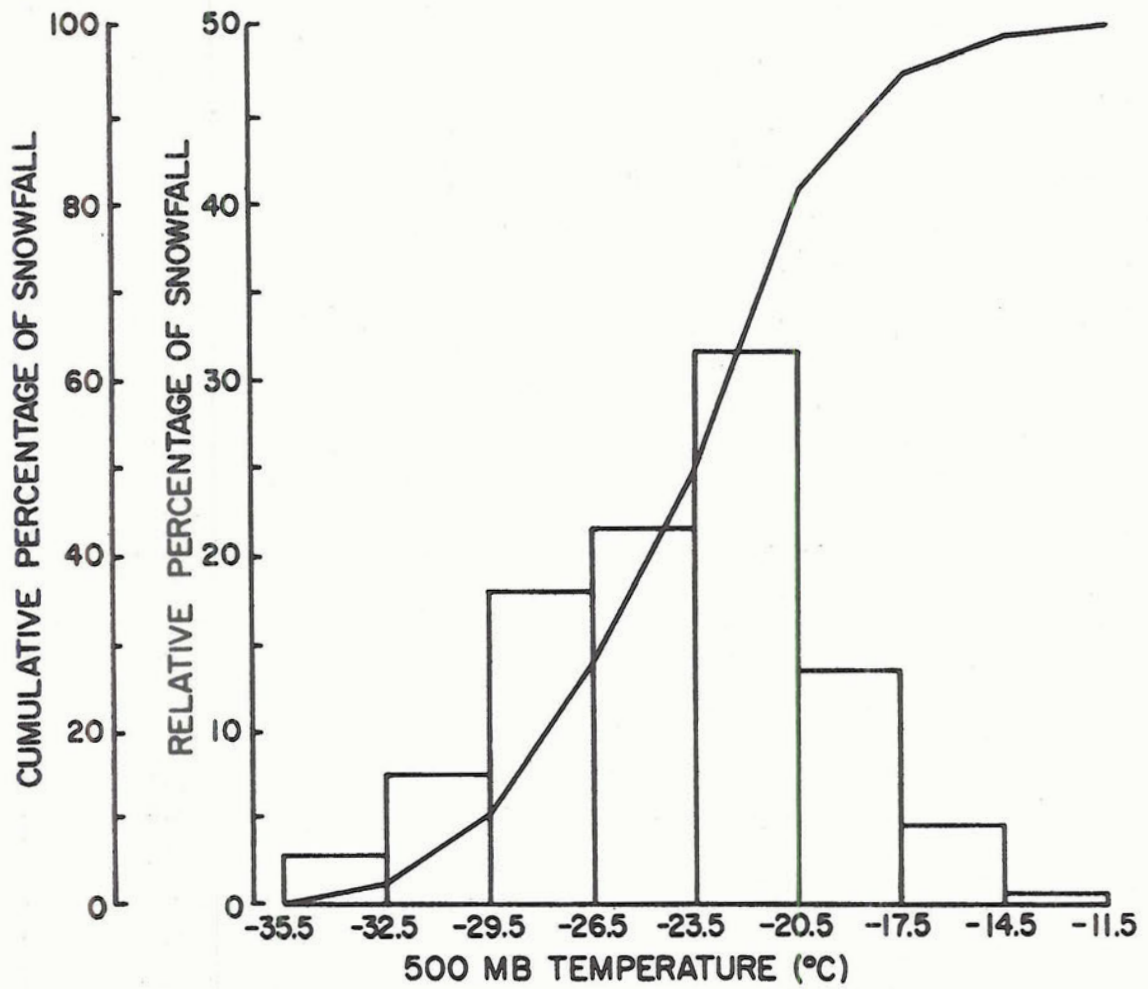


Figure C6. Relative and cumulative percentage of snowfall at HAO as a function of 500 mb temperature.

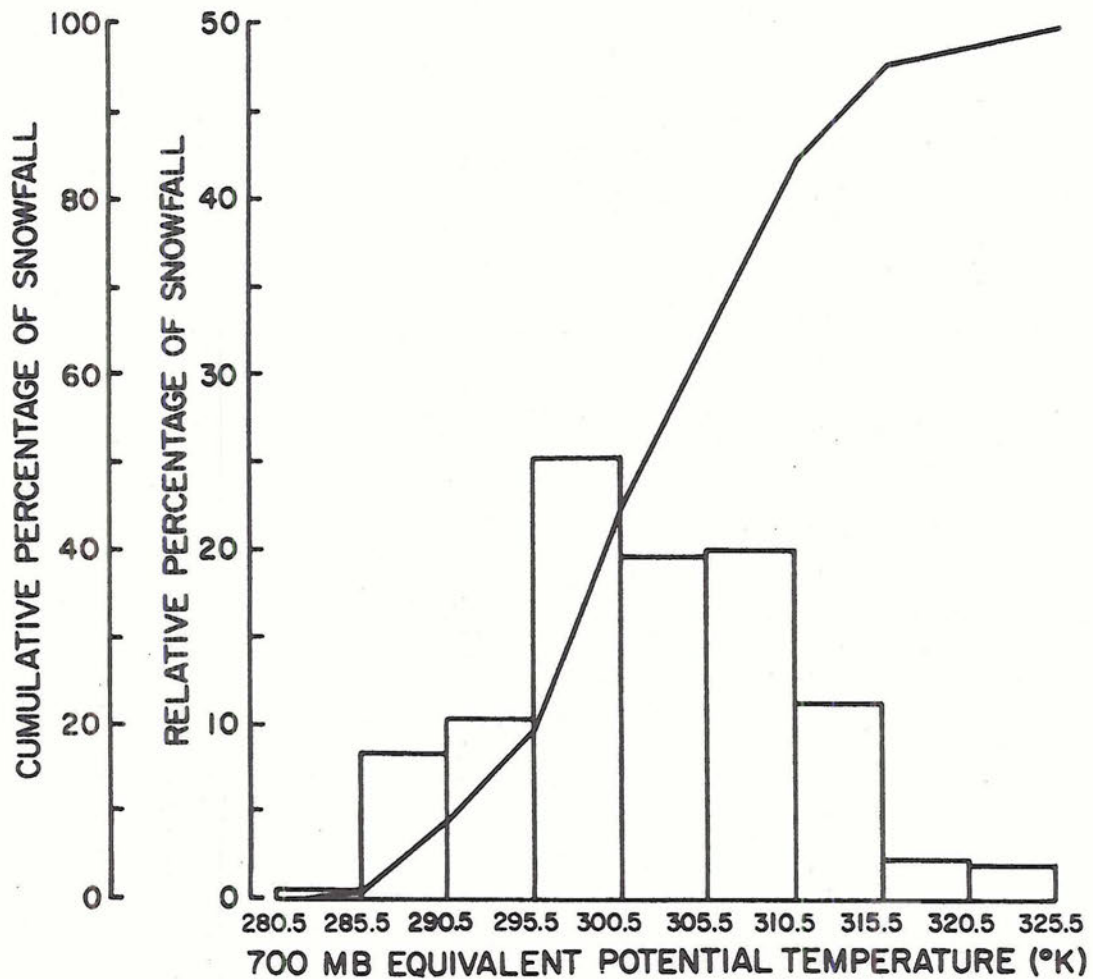


Figure C7. Relative and cumulative percentage of snowfall at HAO as a function of 700 mb equivalent potential temperature.

75 percent of the snow at HAO occurs with 700 mb equivalent potential temperatures colder than 308K with 64 percent occurring between 295K and 310K.

## 2. The Wolf Creek Pass Experiment

The Wolf Creek Pass experiment was inherently an operational program whose basic objective was to augment snowfall over an area of the San Juan Mountain Massif centered at the summit of Wolf Creek Pass. In order to secure useful data from this operational program, three recording precipitation gages were installed on the pass. Hourly precipitation amounts are available near the summit and on the west and east sides of the pass.

### a. Design of Experiment

The basic features incorporated in the Wolf Creek Pass design are summarized below:

- (1) Randomization is employed in obtaining the seeded and non-seeded samples. The randomization is restricted to entire winter seasons. This resulted in the winter seasons of 1964-65, 1966-67 and 1968-69 being seeded periods while the winter seasons of 1965-66, 1967-68 and 1969-70 were left unseeded. The last unseeded year is not included in the sample used in this study because of time considerations.
- (2) The experimental time unit is the 24-hour time period beginning at 0900 MST.
- (3) Seven standard Weather Bureau stations located south, southwest and west of the experimental site are available for use as control stations. The locations of these

stations are shown in Figure C8. These stations were chosen by a step-wise multiple regression program which shows that the seven stations explain 50 to 58 percent of the total precipitation variance at the three recording precipitation gages on the pass.

- (4) The criteria of an experimental day is that at least .01 inches of precipitation occurred during a 24-hour sampling unit at one or more of the recording precipitation gages on Wolf Creek Pass, or at the control station.
- (5) The generator operations were controlled by a private meteorological group from Denver (Water Resources Development Corp.) during the winter season of 1964-65, and by Colorado State University personnel during the winter season of 1966-67 and 1968-69. Arc and Coke type generators were employed during the 1964-65 season and C.S.U. modified Skyfire generators were used the last two seeded years. Seeding rates of the Arc and Coke type generators were about 1 gm AgI/hr and 16 gm AgI/hr, respectively. The modified Skyfire generators employed a seeding rate of about 20 gm AgI/hr. Generator sites did change during the experiment and are shown in C8. A discussion of the topography and a precipitation climatology of the Wolf Creek Pass area is presented by Grant et al., (1969) and is not repeated here.

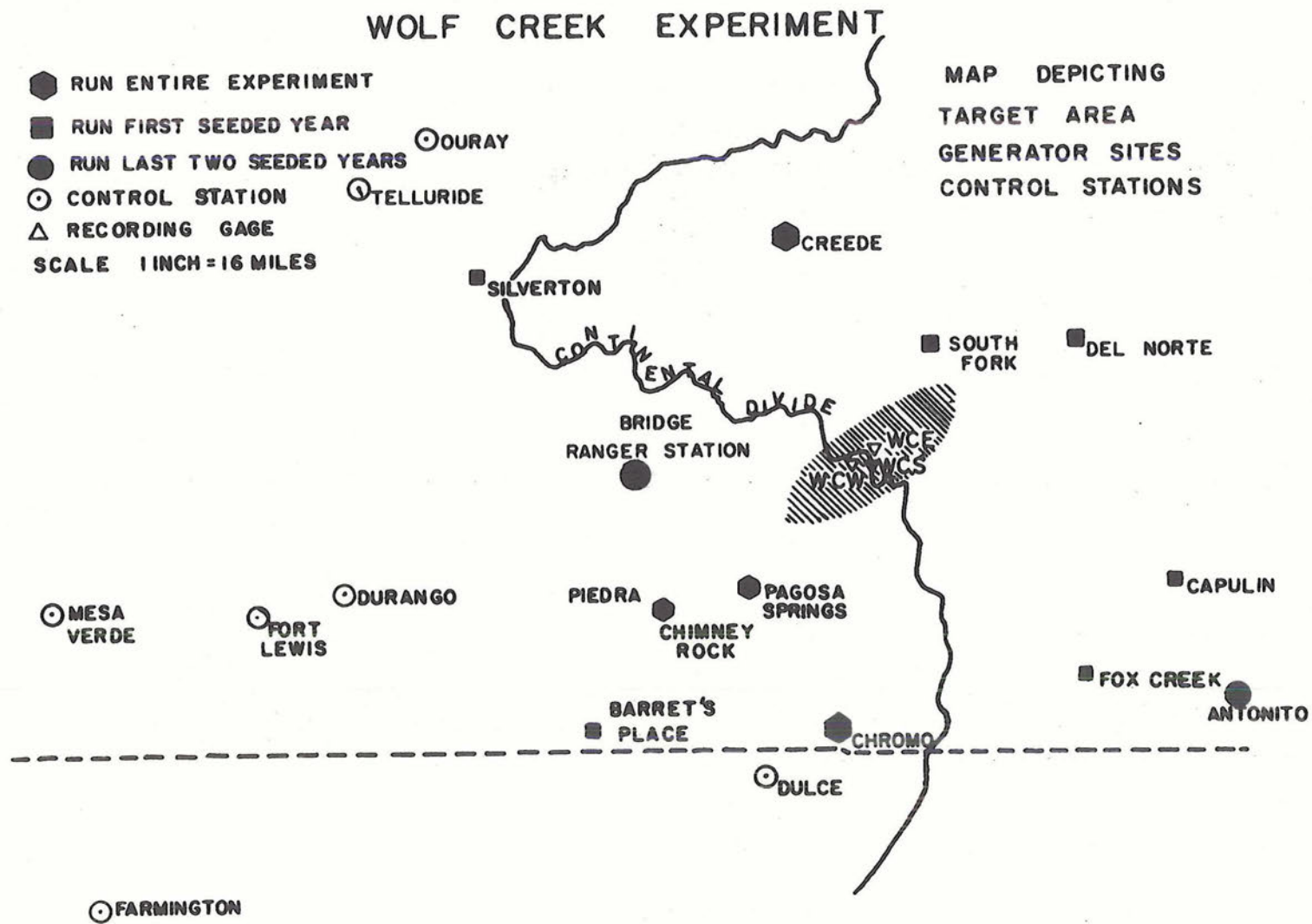


Figure C8. Wolf Creek Pass Experimental Area

## APPENDIX D

### METEOROLOGICAL ANALYSIS PROGRAMS

#### 1. Climax Program

##### a. Interpolation Scheme

A linear, distance weighted interpolation scheme was used to derive meteorological data for the Climax area. The interpolation equation was of the form

$$X_{\text{cmx}} = (.62)X_{\text{den}} + (.38)X_{\text{gjt}} \quad (\text{D-1})$$

where  $X$  denotes the meteorological quantity being interpolated and  $X_{\text{den}}$  and  $X_{\text{gjt}}$  represent the observed value of the quantity at Denver, Colorado, and Grand Junction, Colorado, respectively. This relationship was used to interpolate all meteorological quantities except for relative humidities at pressures of 600 mb or higher. The wind data was decomposed into  $u$  and  $v$  components before interpolation.

It was decided to use the observed Grand Junction relative humidity as representative of Climax at pressures of 600 mb or higher. The reason is the continental divide is generally 12,000 feet or higher between Grand Junction and Denver and frequently creates a discontinuity in the vertical motion field at the 700 mb level. This is especially true during wintertime orographic storms. This can produce humidities near saturation west of the divide and quite low immediately east of the divide. A distance weighted interpolation would result in humidities below those actually existing upstream from the divide near the experimental site.

### b. Analysis Procedures

Since orographic clouds at Climax are normally embedded within the 700 mb and 500 mb layer, meteorological data at these two pressure levels were used to derive several parameters. These parameters describe aspects of the orographic precipitation process and are used to investigate the dependency of seeding effects upon existing meteorological conditions.

The following analysis program was computerized and used to calculate the meteorological parameters.

#### 1) Input to Analysis Program

- (1) 700 mb temperature,  $T_7$
- (2) 700 mb pressure,  $P_7$
- (3) 700 mb relative humidity,  $RH_7$
- (4) 700 mb wind direction,  $\theta_7$
- (5) 700 mb wind speed,  $V_7$
- (6) 500 mb temperature,  $T_5$
- (7) 500 mb pressure,  $P_5$
- (8) 500 mb relative humidity,  $RH_5$
- (9) 500 mb wind direction,  $\theta_5$
- (10) 500 mb wind speed,  $V_5$

#### 2) Computations

- (1) Compute saturation vapor pressure over water

$$\ln e_s = \ln 6.11 + aT/(T+b)\ln 10 \quad (D-2)$$

where  $e_s$  is saturation vapor pressure in mb,  $T$  the temperature in degrees C,  $a = 7.5$ , and  $b = 237.3$ .

- (2) Compute vapor pressure over water

$$e = (RH)e_s/100 \quad (D-3)$$

where  $e$  is vapor pressure in mb and  $RH$  is relative humidity in percent.

- (3) Compute dew point temperature

$$T_d = K(237.3)/(7.5-K) \quad (D-4)$$

where  $K = (\ln e - \ln 6.11)/\ln 10$  and  $T_d$  is dew point temperature in degrees C.

- (4) Compute condensation level pressure

A parcel of air at 700 mb is taken to be representative of the mixed sub-cloud layer and is lifted adiabatically to saturation.

Equation D-2 is differentiated logarithmically to yield

$$de/e = [(\ln 10)(7.5)(237.3)/(T_d + 237.3)^2]dT_d \quad (D-5)$$

For unsaturated adiabatic changes  $de/e = dP/P$  so

$$dT_d/dP = (T_{d7} + 237.3)^2/2.66(10^6) \quad (D-6)$$

where  $dT_d/dP$  is in degrees C/mb and the relation holds best at pressures near 650 mb.

The dew point temperature of the lifted parcel at the condensation level is given by

$$T_{dc} = T_{d7} + (P_c - 700)dT_d/dP \quad (D-7)$$

or

$$T_{dc} = T_{d7} - (700 - P_c)[(T_{d7} + 237.3)^2/2.66(10^6)] \quad (D-8)$$

The temperature of the lifted parcel at the condensation level is given by

$$T_c = T_7 + (P_c - 700)dT/dP \quad (D-9)$$

and  $dT/dp$  can be determined from Poisson's equation for an unsaturated process by differentiating the equation logarithmically while holding potential temperature constant. The following relations hold with good approximation at pressures near 650 mb.

$$dT/dP = .00044(T_7 + 273.2) \quad (D-10)$$

$$T_c = T_7 + [.00044(273.2 + T_7)](P_c - 700) \quad (D-11)$$

where  $dT/dP$  is in degrees C/mb.

At the condensation level, dew point temperature and temperature are equal and (D-8) and (D-11) may be equated to yield a solution for the condensation level in mb.

$$P_c = 700 + (T_7 - T_{d7})/[T_{d7} + 237.3]^2/2.66(10^6) - .00044(273.2 + T_7)] \quad (D-12)$$

(5) Compute condensation level temperature

Condensation level temperature can be computed using Poisson's equation or

$$T_c = (T_7 + 273.2)(P_c/700)^{.286} - 273.2 \quad (D-13)$$

(6) Compute potential temperature

$$\theta = (T + 273.2)(1000/P)^{.286} \quad (D-14)$$

- (7) Compute specific humidity and mixing ratio

$$q = .622e/(P - .378e) \quad (D-15)$$

$$w = q/(1 - q) \quad (D-16)$$

where  $q$  and  $w$  are in gm/gm.

- (8) Compute equivalent potential temperature at 700 mb and 500 mb

$$\theta_{e7} = \theta_7(1 + .622w_7)^{.286} \exp[L_s w_7 / (.241)(T_c + 273.2)] \quad (D-17)$$

where  $L_s = 597.3 - .566T_c$

$$\theta_{e5} = \theta_5(1 + .622w_5)^{.286} \exp[L_s w_5 / (.241)(T_c + 273.2)] \quad (D-18)$$

- (9) Compute lifted temperature at 500 mb

The lifted temperature of a parcel at 500 mb can be expressed as a function of the equivalent potential temperature through the following cubic equation.

$$T_L = -244.556055 - .046086 \theta_{e7} + .005197 \theta_{e7}^2 - .000009 \theta_{e7}^3 \quad (D-19)$$

where  $T_L$  is in degrees C and subscript "L" refers to conditions of the lifted parcel after reaching the 500 mb level.

- (10) Compute potential condensate in the 700 to 500 mb layer

$$W_a = (w_7 - w_L)(10^3) \quad (D-20)$$

where  $w_L = .622e_{sL}/(P_5 - e_{sL})$

$$\ln e_{sL} = \ln 6.11 + [7.5T_L / (T_L + 237.3)] \ln 10$$

and  $W_a$  is in gm/kgm.

(11) Compute vertical gradient of potential condensate below 500 mb

$$C = (10^2)W_a / (P_c - P_5) \text{ for } P_c \geq 520 \text{ mb}$$

$$C = 0 \quad \text{for } P_c < 520 \text{ mb} \quad (\text{D-21})$$

where C is in gm/kgm(100 mb) and is arbitrarily assigned to zero for  $P_c < 520$  mb to insure computational stability.

(12) Compute convective stability index

$$\text{LSI} = \theta_{e5} - \theta_{e7} \quad (\text{D-22})$$

where LSI is in degrees C

(13) Compute mean temperature advection in the 700 to 500 mb layer

First, compute the magnitude of the observed vector wind shear in the 700 to 500 mb layer.

$$V_T = [(u_5 - u_7)^2 + (v_5 - v_7)^2]^{1/2} \quad (\text{D-23})$$

Then temperature advection in degrees C/12 hours is given by

$$\text{TA} = (.041)V_5 V_T \sin(\theta_{VT} - \theta_5) \quad (\text{D-24})$$

where  $V_5$  is 500 mb wind speed in mps,  $V_T$  the thermal wind speed in mps,  $\theta_{VT}$  the meteorological angle of the thermal wind, and  $\theta_5$  the meteorological angle of the 500 mb wind.

The constant in (D-24) contains the coriolis parameter for a latitude of 39.4 degrees and the specific gas constant for dry air.

## 2. Wolf Creek Pass Program

### a. Interpolation scheme

A linear, distance weighted interpolation scheme was also used to derive meteorological data for the Wolf Creek Pass area. The

interpolation equation was of the form

$$X_{wcp} = (.204)X_{den} + (.365)X_{gjt} + (.255)X_{abq} + (.176)X_{inw} \quad (D-25)$$

where X again denotes the meteorological quantity being interpolated. This relationship was used to interpolate all meteorological quantities except for relative humidities at pressures of 600 mb or higher.

For relative humidities at pressures of 600 mb or higher the interpolation equation was changed to

$$X_{wcp} = (.435)X_{gjt} + (.348)X_{abq} + (.217)X_{inw} \quad (D-26)$$

The removal of the Denver data from the interpolation of low level humidities was for the same reasons discussed previously under the Climax program.

b. Analysis Procedures

Analysis procedures for the Wolf Creek Pass data were identical to those outlined under the Climax program.